공학박사학위논문

Rational Design of Flexible Thermoelectric Generators Based on Nano-carbon Materials

나노탄소재료를 기반으로 한
유연 열전 소자의 설계

2017년 2월

서울대학교 대학원
재료공학부
최 재 유

Abstract

Rational Design of Flexible Thermoelectric Generators Based on Nano-carbon Materials

Jaeyoo Choi
Department of Materials Science and Engineering
The Graduate School
Seoul National University

This research was performed in purpose of rationally designing flexible thermoelectric generator based on nano-carbon materials. Thermoelectric (TE) materials, harvesting electrical energy directly from temperature gradients, have attracted tremendous attention due to their potentials for realizing next-generation power generators and waste-heat-recovery systems. For several decades, many attempts have been made to improve the TE materials efficiency, now TE generators based on semiconductors are commercially used in various applications including an automobile and aerospace industries. Recently, following the trend of consumer electronics, there is a strong demand for TE devices to provide new function other than simply converting heat energy to electricity. In particular, use as a flexible power generator that can supply continuous power to wearable smart devices has been highlighted and many

researches are ongoing to make this technology a reality using various TE materials.

Inorganic semiconductors with narrow band-gap for a large thermopower, especially, the bismuth-tellurium-antimony-selenium (Bi-Te-Sb-Se) alloy family have been widely investigated. However, despite their high TE performances, the mechanical endurance of TE modules based on inorganic semiconductors cannot be guaranteed owing to their brittleness, and with their energy-intensive process, exquisite or large-area flexible TE device are inconceivable. As possible candidate for flexible TE materials, organic materials including conducting polymers and their hybrid composites have been recently investigated because of their unique advantages including facile processability, scalability, and flexibility as well as low cost and weight. However, most of their performance could not satisfy the needs, yet. Although the performance of flexible TE materials have significantly improved, they are generally sensitive to humidity in ambient conditions, resulting limited practical applications. Therefore, we should spontaneously consider many factors including performance, flexibility, mechanical and chemical stability, and processability to develop TE materials for flexible TE generator. In addition, both N and P type TE materials are necessary for efficient TE generator, and proper module design and fabrication process of TE generator should also be considered.

Nano-carbon materials having great mechanical, chemical, electrical properties have been studied as promising TE materials to meet these requirements, but its use was limited to supplement electrical conductivity as fillers in composite system, systematic study to enhance the TE performance themselves have been lacked. The reason is that even if the electrical conductivity was improved by such as chemical doping, its thermopower was reduced because those two factors lie in a trade-off relation, leading to less effective improvement in TE performance. To solve these fundamental problems and dramatically enhance the TE performance of nano-carbon materials, effective way is to control the mobility of carriers, and not the carrier concentration. This was derived from the theoretical relationship between the carrier concentration and mobility. Based on these backgrounds, this research is systemically studied on what rational design of flexible TE materials is needed to enhance the fundamental TE performance of nano-carbon materials.

Chapter 1 provides a general introduction of TE generators, especially in needs of flexible generator for wearable electronic device. Theoretical considerations based on thermal and electrical viewpoint are also summarized. The state-of-the art of researches on flexible TE generators and their limitations are discussed. On the basis of them, the aims, strategies, and scopes of this work are presented.

Chapter 2 introduces apparatus for measuring the TE performances of materials and generators. It is consisted of two parts which are evaluation system of TE

properties of materials and power measuring system for TE generator. The design of our hand-made equipment is explained and the advantages of it are presented.

Chapters 3 discuss about the TE performance of manufactured carbon nanotube (CNT) films and yarn with different degree of orientation. Highly oriented CNT yarn with superior mobility shows greatly enhanced electrical conductivity, whilst maintaining relatively high thermopower. This results in drastic improvement of TE performance. It was demonstrated that the mobility engineering of nano-carbon materials is an effective strategy to enhance the TE performance of them.

Chapter 4 and 5 focus on hybridization of nano-carbon and inorganic materials for the simultaneous enhancement of both electrical conductivity and thermopower. These works have started to overcome the performance limitation of carbon materials from trade-off relation between the electrical conductivity and thermopower. Binary and ternary nano-carbon / inorganic hybrid system by controlling the work function of nano-carbons are designed, and synergetic enhancement of TE performance by effective energy filtering at heterojunctions is demonstrated. By the energy filtering, the whole mobility of composite materials is slightly decreased, but TE performance of it could be improved by enhanced energy transport efficiency of carrier. It was demonstrated that these materials design is also effective way to achieve high TE performance in terms of effective mobility engineering at hybrid interfaces.

Chapter 6 introduces novel design and high performance of flexible TE generators based on nano-carbon. While flexible TE materials show excellent TE properties, facile module fabrication and high power density of generator are also important for practical applications. For the effective design of TE generator, high current mobility of circuit leads to reduced thermal energy loss which maximize the power generation of TE module. Thus, to minimize the contact resistance, novel design of TE generators without metal electrodes was developed, and that electric power was actually generated from body heat was demonstrated.

In conclusion, this study has significant meaning in engineering research, because not only high performance nano-carbon based TE materials and modules was rationally designed, but also commercialization potential was realized by successfully fabricating prototype module. Furthermore, carrier mobility engineering strategies employed in this research can be a good guideline for researchers aiming to achieve high performance flexible TE generator.

Keywords: flexible thermoelectric generator, carbon nanotube, graphene, tellurium nanowire, hybrid composite, energy filtering

Student Number: 2013-30188

Contents

List of Tables

List of Figures

PART I. Fundamental backgrounds

Chapter 1. Introduction

1.1 General introduction of thermoelectric generator

1.1.1 Overview of the thermoelectrics

A worldwide over-dependence on fossil fuels for energy needs has led to an urgent need for alternative energy and novel energy conversion technologies.[1] As one of the possible candidates, thermoelectric (TE) materials, which can convert wasted heat into useful electrical energy (Seebeck effect) or provide both active cooling and heating from the electricity (Peltier effect) have been highlighted recently.[2] It is because close to 60% of energy produced in the world is wasted in the form of heat. (Fig. 1.1) Home heating, automotive exhaust, and industrial processes all generate an enormous amount of unused waste heat.[3] Therefore, TE power generation is a promising technical field that have a huge potential that can reduce industrial cost and increase energy efficiency.

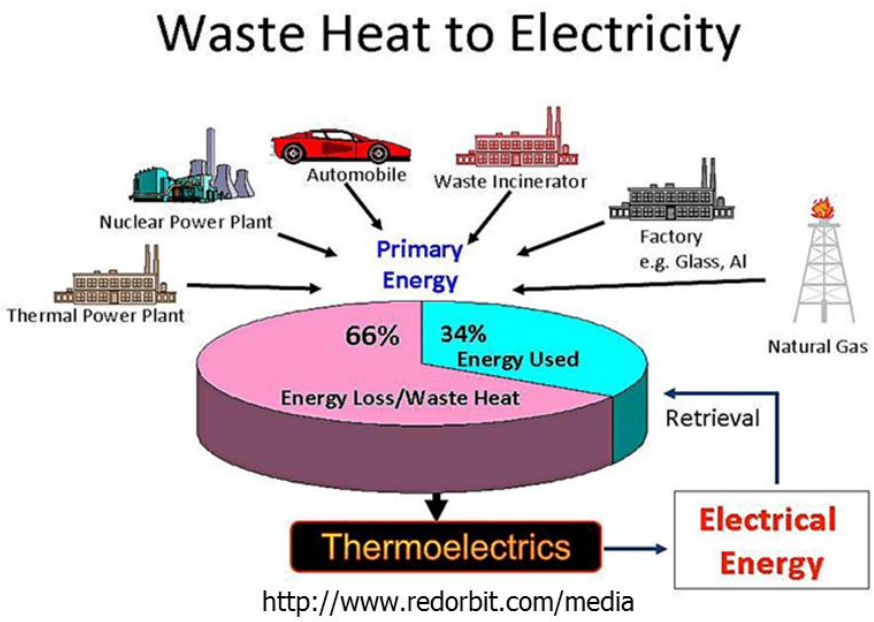

Fig. 1.1. Potential applications of thermoelectric generators for waste heat recovery

The TE effect arise because the charge carriers in TE materials are free to move, while carrying charge as well as heat. When thermal gradient is applied to TE materials, carriers spontaneously flow from a hot region to a cold region, thereby current can be produced by the carriers. Conversely, if current is applied, exothermic and endothermic reactions can occur at metallic junctions. Fig. 1.2 shows a progression of a TE device starting with a pair of n- and p-type materials known as a TE couple.[4] When several couples are connected together electrically in series and thermally in parallel, this is known as a TE module. Several modules interfaced with heat exchangers coupled to a heat source and heat sink constitute a TE generator as shown in Fig 1.3.[3] Practical TE generators are made of multiple pairs of *p*-type and *n*-type semiconductor legs. Putting many elements electrically in series and thermally in parallel increases the operating voltage of the module while reducing its electrical current. Such an arrangement minimizes parasitic losses from the series electrical resistance of the wires and interconnects.[5]

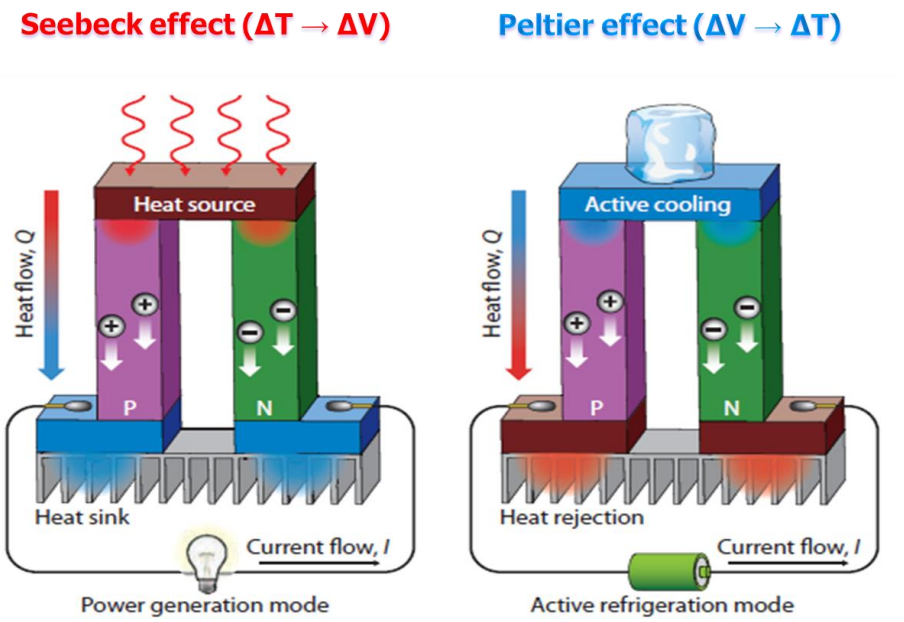

Fig. 1.2. Principle concept of thermoelectric energy transport[4]

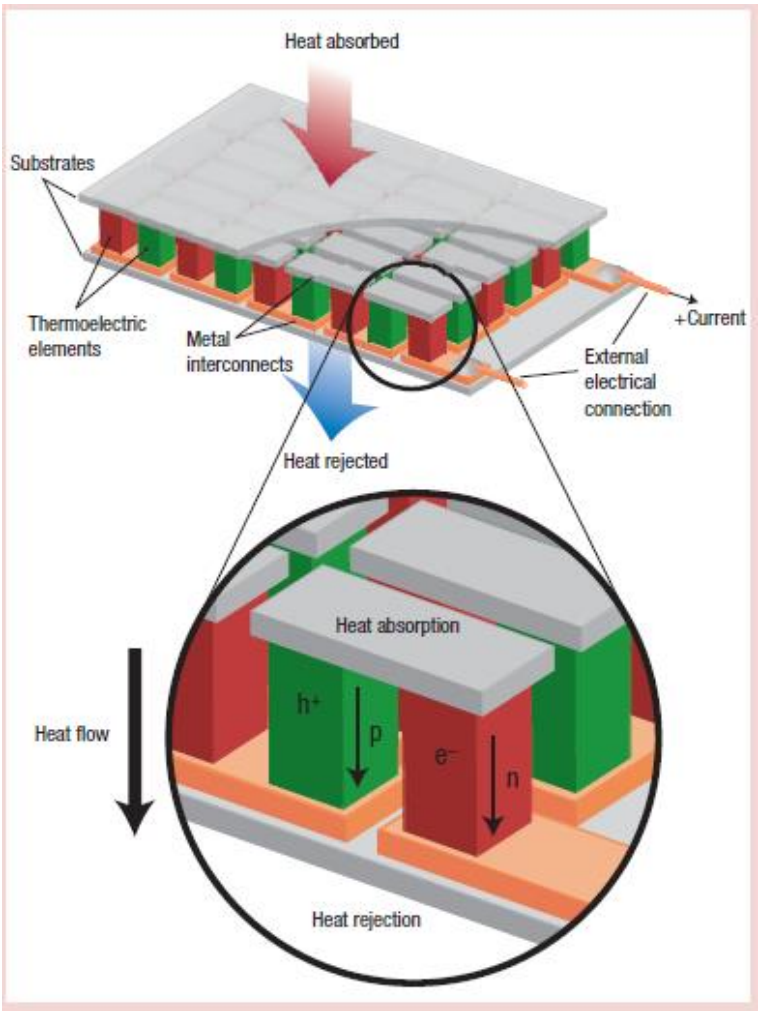

Fig. 1.3. Typical design of thermoelectric module[3]

1.1.2 Historical review of thermoelectric materials

In the 1950s and early 1960s, many new TE materials such as Bi_2Te_3, PbTe and SiGe were discovered and investigated.[6, 7] Especially, the high potential of Bi_2Te_3 as a thermoelectric material was discovered by H. J. Goldsmid and coworkers in the U.K.[8], and this material system still remains the basis for the thermoelectric industry up to the present time. In this period, the leading approach for increasing TE performance was to control doping conditions and form solid-solutions. This was an effective way of reducing the lattice thermal conductivity via point defect scattering of phonons.[9] Although significant reductions in the lattice thermal conductivity were achieved, there were also concurrent reductions in the charge carrier mobility, thus limiting the overall figure of merit ZT enhancement.[6] For a 30 year period since the 1960s, research activity in the field of thermoelectricity has been greatly reduced, and only modest progress was made in improving the performance of TE materials.[6] In 1990s, the study of TE materials had once again became activate, in part due to the demonstration of enhancement in the TE figure of merit of a low-dimensional materials.[10] Low dimensionality allows certain materials such as bismuth, which are poor TE materials in 3D bulk, to become good one, in principle, in 2D quantum-well or 1D quantum-wire structures.[11, 12] After 2000s, owing to improvement of nano-material science and nano-structuring techniques, novel TE materials with high performance such as skutterudites,

clathrates, and quantum dot superlattice have been reported.[13, 14] (Fig 1.4.) General N, P type TE materials and their performances are also shown in Fig. 1.5.[3]

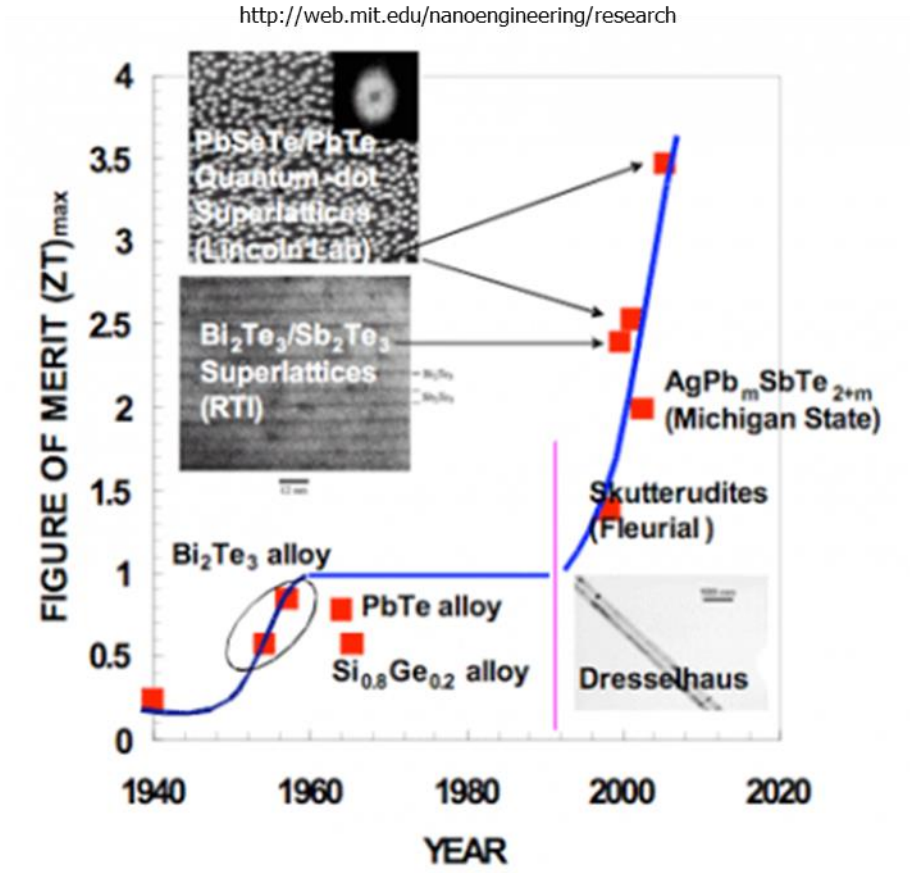

Fig. 1.4. Historical review on the development of TE materials

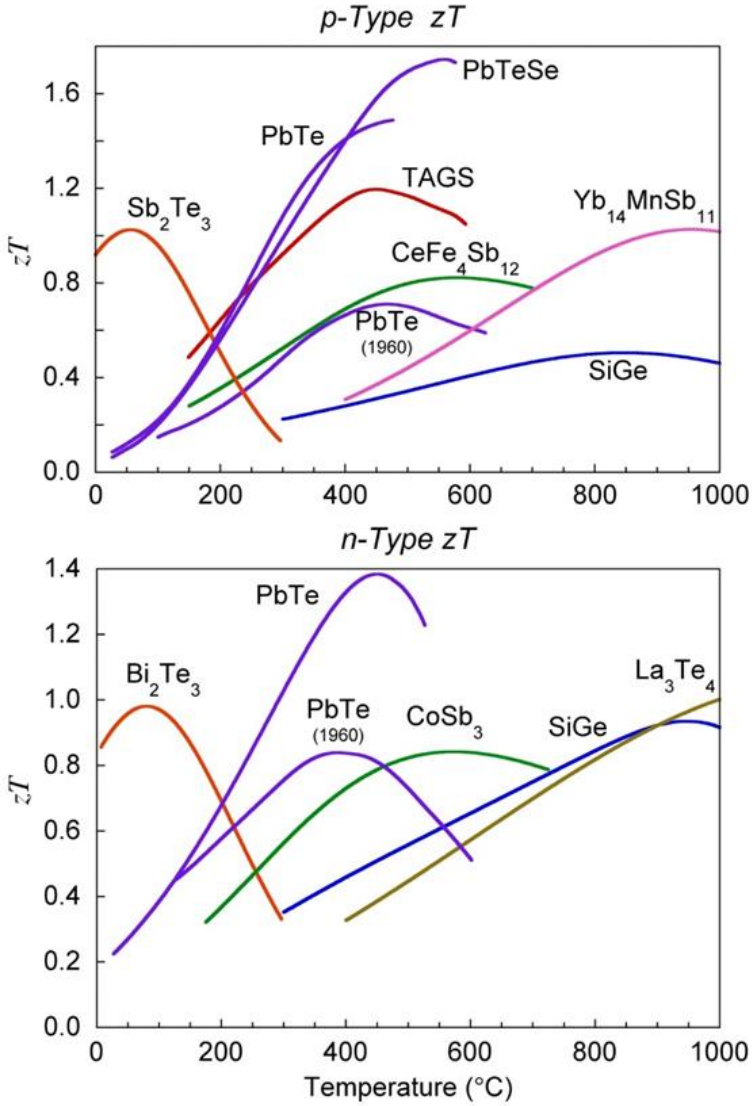

Fig. 1. 5. General P- and N-type TE materials and their TE performance as a function of temperature[3]

However, although above low-dimensional structures have demonstrated high preliminary ZTs, they are unsuitable for high temperature applications that require long-term thermal and mechanical stability as well as effective, practical coupling to existing heat sources and heat sinks.[9] Additionally, scale-up to kilogram quantities could also be very challenging in order to fabricate the required macro-sized devices. Another pressing issue is finding alternative TE materials to semiconductors such as Bi and Te. Inorganic conductors and semiconductors are no doubt efficient TE materials, but they are associated with issues like high cost of production, scarcity of materials, and toxicity.[15] (Fig. 1.6) Therefore, recently, organic TE materials including conducting polymers, nano-carbons and their hybrid materials have been emerged as potential alternatives.[16]

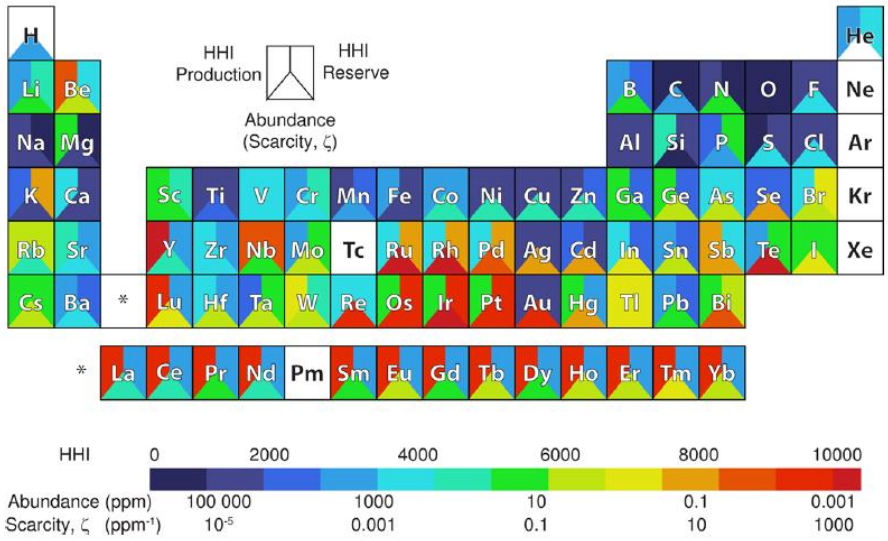

Fig. 1.6. Illustration of scarcity of inorganic materials for TE application[15]

1.1.3 Challenging thermoelectric application: flexible power generator

Devices based upon the TE effect can be used for a variety of applications. Fig. 1.7 shows the history of typical applications of TE power generation.[17] However, due to their moderate energy conversion efficiency and relatively high cost, they have been used mainly in specialized military and space applications.[18] Radioisotope thermal generators for deep-space satellites and remote power generation for unmanned system are typical examples. Another main stream of TE application is vehicle exhaust waste heat recovery system.[1] (Fig. 1.8) TE generator could converts four to five percent of the escaping heat to 500-750 watts of electricity. This increases fuel economy by one to five percent, through reducing the amount of fuel burned to power the car's electrical components, such as the headlights. As the needs of fuel efficient hybrid cars and electric powered vehicles increases, the potentials of TE generators will be also drastically increased.[19]

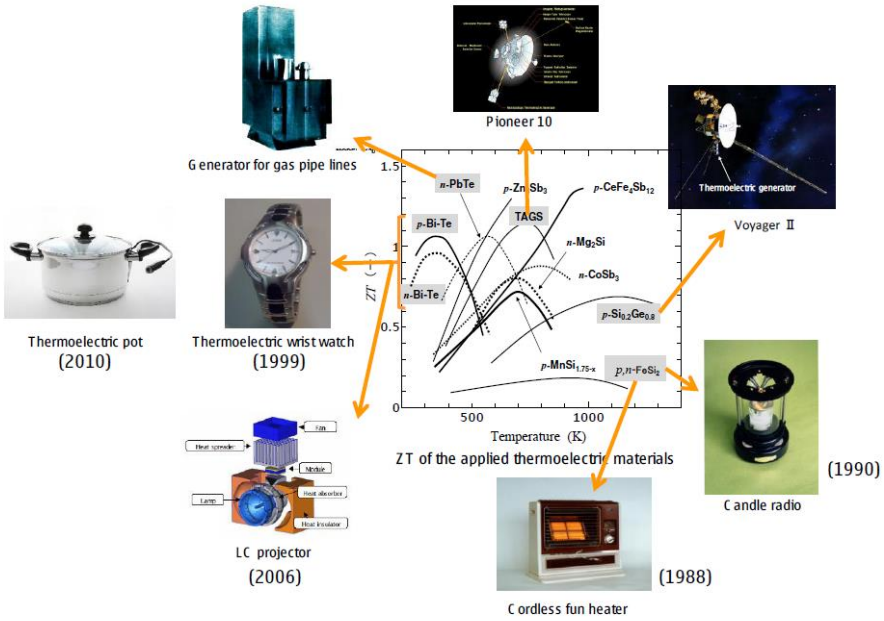

Fig. 1.7. History of various commercialized TE generators[17]

Fig. 1.8. Leading application: TE generator applied in automobile for waste heat recovery

Following the trend of consumer electronics, there is a strong demand for flexible or wearable electric devices. (Fig. 1.9) Naturally, flexible or wearable power supply has been required together because previous general power sources such as battery were not flexible and lack portability.[20] Among various candidates, TE generators have been recently highlighted for use as a flexible power generator that can supply continuous power using body heat. It has many advantages that not only body heat is steady and large but also waste heat recovery is green growth that conform to future-oriented issues. However, due to the complicated curvature of the human body, typical TE generators may not be suitable for applying to human body because of the rigid components.[21] In addition, TE generators should be tightly attached on the skin for efficient energy harvesting. Therefore, development of novel flexible TE generators must be an interesting and challenging issue. If efficient flexible TE generators are commercialized, it would be ideal for implantable microsystems because it can supply the electrical energy without the need of replacement battery or for wearable technologies that can be used for long-term health monitoring.[22]

Fig. 1. 9. Challenging demand for flexible and wearable electrical devices

1.2 Fundamental backgrounds of thermoelectrics

1.2.1 Theoretical considerations for thermoelectric properties of material

The TE performance of materials is evaluated by a dimensionless figure of merit (ZT), which is given by

$$\mathrm{ZT} = \frac{S^2\sigma}{K}T$$

where S, σ, T, and κ are the Seebeck coefficient (also called the thermopower), electrical conductivity, absolute temperature, and thermal conductivity, respectively.

The challenge to create high ZT thermoelectric materials lies in achieving simultaneously high electronic conductivity (σ), high thermoelectric power (S) and low thermal conductivity (k). These parameters are determined by the details of the electronic structure and scattering of charge carriers (electrons or holes), and thus are not independently controllable. (Fig. 1.10) The quantity $S^2\sigma$ is called the power factor (PF) and is the general key to achieving high performance. A large PF means that a large voltage and a high current are generated. The thermal conductivity k has contributions from carrier and lattice vibrations. The thermal conductivity must be low as a large ΔT must be maintained.

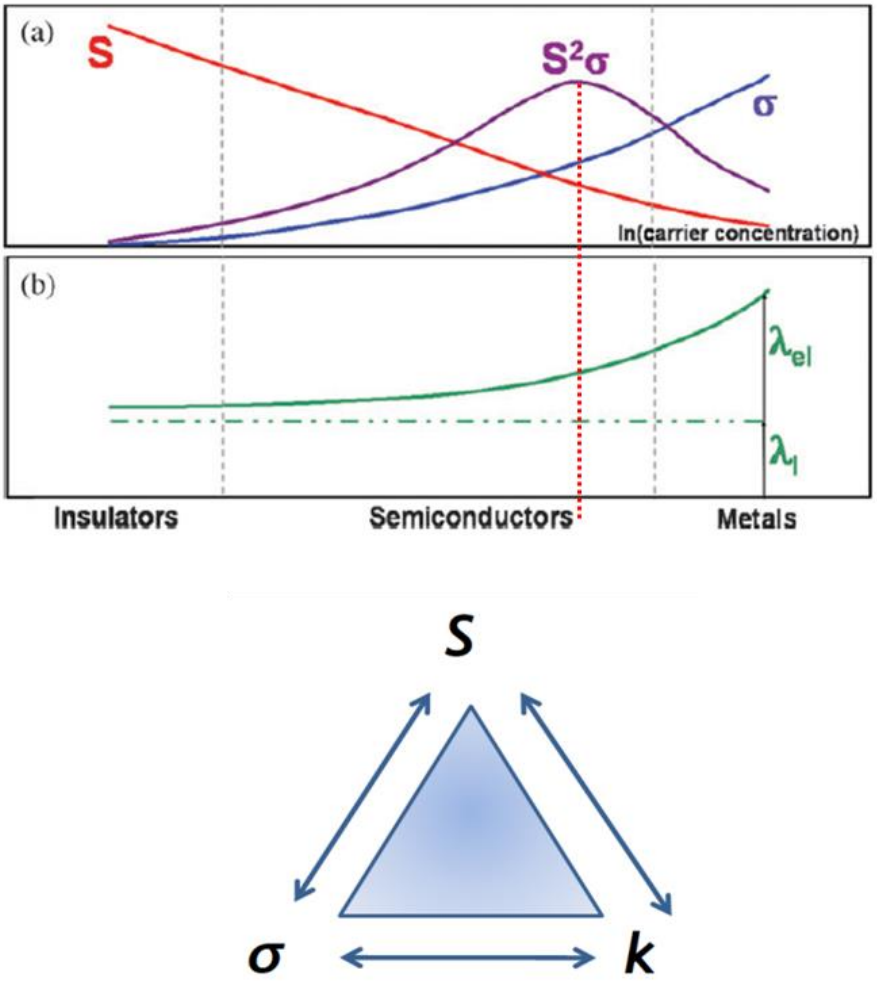

Fig. 1.10. Trade-off relations of thermopower, electrical conductivity, and thermal conducivity

There are two possible approaches aimed at increasing ZT: either the power factor is maximized and/or the thermal conductivity is minimized. However, as mentioned above, we should simultaneously consider many factors because these factors are not independently controllable. The complicated relation between many factors are summarized in Fig. 1.11. Based on this relation, theoretical considerations for high ZT are further discussed.

To ensure that the Seebeck coefficient is large, there should only be a single type of carrier. Mixed n-type and p-type conduction will lead to both charge carriers moving to the cold end, cancelling out the induced Seebeck voltages. Low carrier concentration insulators and even semiconductors have large Seebeck coefficients. However, low carrier concentration also results in low electrical conductivity. The interrelationship between carrier concentration and Seebeck coefficient can be seen from relatively simple models of electron transport. For metals or degenerate semiconductors (parabolic band, energy-independent scattering approximation) the Seebeck coefficient and electrical conductivity is given by:

$$S = \frac{8\pi^2 {K_B}^2}{3eh^2} \cdot m^* \cdot T \cdot \left(\frac{\pi}{3n}\right)^{2/3}$$

$$\sigma = n \cdot e \cdot \mu$$

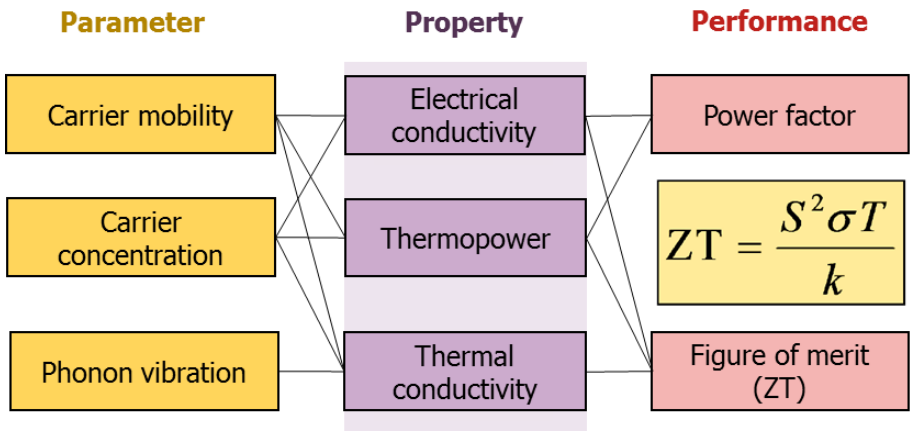

Fig. 1.11. Interdependence of factors considered for TE material design

where K_B, h, n, m* and T is the Boltzmann constant, Plank constant, carrier concentration, effective mass of the carrier and absolute temperature, respectively. The electrical conductivity (σ) and electrical resistivity (ρ) are related to n through the carrier mobility μ

Thermal conductivity in TE materials comes from two sources: (1) electrons and holes transporting heat (K_e) and (2) phonons travelling through the lattice (K_l). Most of the electronic term (K_e) is directly related to the electrical conductivity through the Wiedemann–Franz law.

$$K = K_e + K_l$$

$$K_e = L \cdot \sigma \cdot T = n \cdot e \cdot \mu \cdot L \cdot T$$

where L is the Lorenz factor, 2.4×10^{-8} J^2 K^{-2} C^{-2} for free electrons.

Additionally, before the deep discussion in this research, the well-known fundamental concepts on TE property of material need to be introduced. Low-dimensional systems can reduce lattice thermal conductivity K_l without too high loss in mobility, and the Seebeck coefficient in low-dimensional systems at a given carrier concentration is expected to be greater than that of 3D systems because of two reasons which are size-quantization effect and electron energy filtering. More detail discussions will be provided in later chapters.

1.2.2 Theoretical considerations for thermoelectric performance of module

As shown in Fig. 2, heat supplied to the hot side cause carrier diffusion to the cold side and it also carries electrical charge as well. The higher charge concentration on cold side build an internal electrical field that resist further diffusion, which is the origin of the seebeck voltage. In addition to the heat transfer due to charge flow, heat also flows from the hot side to the cold side due to thermal conduction and joule heating. In summary, the net heating in TE power generation is described by,

$$Q_H = \left(S_p - S_n\right) \cdot \mathrm{I} \cdot T_H + K(T_H - T_C) - \frac{1}{2} \cdot I^2 \cdot R$$

where S_p and S_n are the Seebeck coefficient of the P and N type TE material, I is the generated current, R is the electrical resistance of the two TE legs, and K is thermal conductance of TE material. In this principle a pair of module (Fig. 1.12), power output is given by $\mathrm{W} = I^2 \cdot R_L$, where R_L is the external resistance of the output circuit and output current is given by $\mathrm{I} = \frac{(S_p - S_n)(T_h - T_c)}{R + R_L}$. The thermal efficiency of module is defined as the ratio of the power output per heat supplied, therefore defined as,

$$\eta = \frac{W}{Q_H} = \frac{I^2 \cdot R_L}{(S_p - S_n) \cdot \mathrm{I} \cdot T_H + K(T_H - T_C) - \frac{1}{2} I^2 \cdot R}$$

Maximum thermal efficiency can be obtained when $R_L = R$ and determined by setting $\frac{d\eta}{dR_L} = 0$, therefore, the maximum TE efficiency is defined by

combining the Carnot efficiency ($\Delta T/T_{hot}$) and the figure of merit ZT as shown in Equation.

$$\eta = \frac{\Delta T}{T_h} \cdot \frac{\sqrt{1+zT_{avg}}-1}{\sqrt{1+zT_{avg}}+\frac{T_c}{T_h}}$$

This equation indicates that increasing efficiency requires both high ZT values and a large temperature gradient across the thermoelectric materials.

From this fundamental backgrounds, both enhancing the TE performance of materials and reducing the circuit resistance of module are key issues for high TE power and efficiency. However, because of the complicated relation between many factors are summarized in Fig. 1.13, we should carefully design and engineer the TE generator.

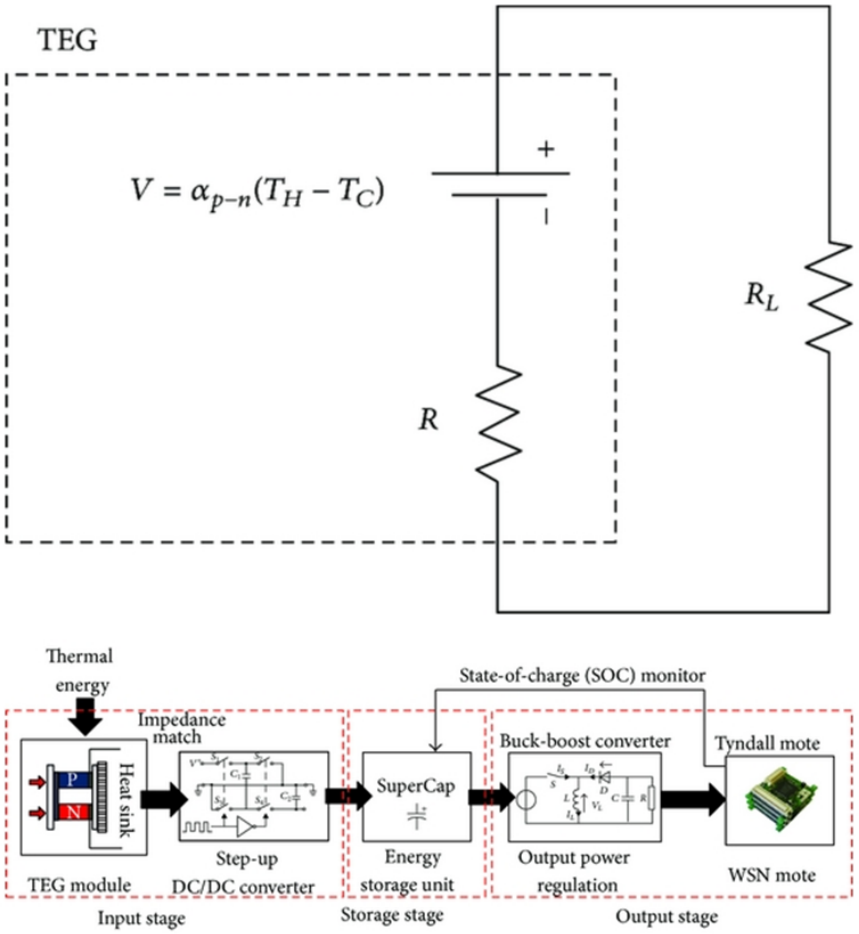

Fig. 1. 12. Illustration of typical TE circuit for power generation

(Wang *et. al.* International Journal of Distributed Sensor Networks, 2013)

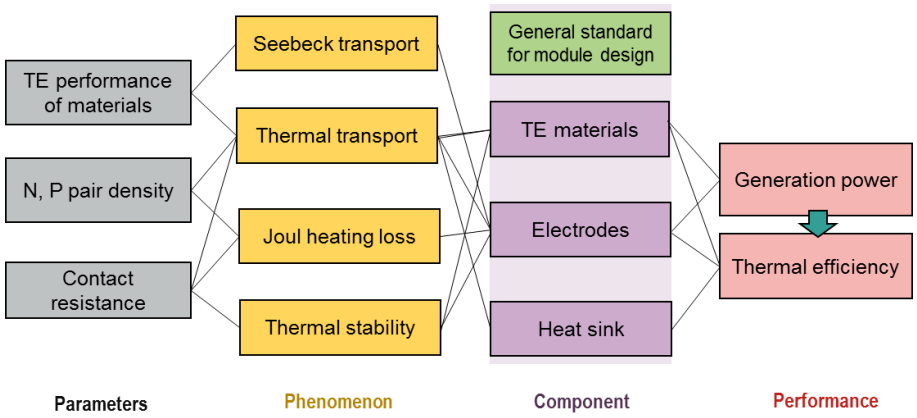

Fig. 1.13. Interdependence of factors considered for TE module design

1.3 State-of-the-art researches on flexible thermoelectric generator

1.3.1 Based on organic materials

Carbon-based π-conjugated materials such as conducting polymers and small molecules, carbon nanotubes and graphenes, and their hybrids have attracted as potential candidates for flexible TE applications.[23] The TE properties of conducting polymers such as polyacetylenes, polyanilines, polypyrroles, polyphenylenevinylenes, polythiophenes, polycarbazoles, and metallated polymers have all been extensively studied. The value of σ and S span a very broad range: from 10^{-5} to 60000 S/cm and 10 to 1000 μ V/K, respectively.[24] Especially, poly(3,4-ethylenedioxythiophene) doped with poly(styrenesulfonic acid) (PEDOT:PSS) is the most commonly studied and commercially available conducting polymer that has been widely applied as hole-transporting interfacial materials and conducting electrodes for various organic electronic devices due to their convenient solution processibility and good stability.[25] In addition, it was found that by adding small amounts of dimethyl sulfoxide (DMSO) or ethylene glycol (EG) as processing solvent for PEDOT:PSS film, the σ can be increased by around one order of magnitude while S is only slightly reduced.[26] As a result, an optimized ZT of 0.01 could be achieved at 300 K. Some papers demonstrated the prototype flexible TE generators based on PEDOT:PSS. The module composed of hundreds of PEDOT:PSS/Ag junctions

is reported by Søndergaard et al.[27], and Park et al. reported a flexible PEDOT electrodes with large thermoelectric power factors by solution casting polymerization.[28]

Since the first discovery by Iijima about two decades ago[29], carbon nanotubes (CNTs) have attracted tremendous attention due to their superior electric, thermal, and mechanical properties, and many potential applications such as flexible electronics and energy conversion and storage devices have been explored.[30] In general, these studies indicated that CNT is not an ideal material for TE applications because of its low S and high κ. In spite of their high σ, the optimal ZT value for CNT is only in the range of 0.001 to 0.01, which is much lower than that of the best available TE materials.[31] Several strategies have been employed to improve TE property of CNT-based materials: (1) the use of conducting polymer/CNT composite to take advantage of the high σ of CNT and low κ of the polymer matrix, (2) to use a polymer-CNT composite consists of a segregated CNT network within the polymer matrix, and (3) to alter the intrinsic charge transport and thermal transport of CNTs through structural modification.[31] Many flexible TE generators based on CNT films and inks are also reported. Yu et al. reported film type modules based on CNT and its segregated network,[32, 33] while Toshima et. al. reported organic hybrid materials made of nanoparticle/CNT/Vinyl polymer.[34] Japan AIST & Fujifilm Co. introduced one-leg modules with p-type CNTs organic mixtures which achieved ZTs of 0.15.[17] These modules were fabricated by printing the ink

including the organic mixtures on thin plastic films. Some remarkable results of flexible TE materials and generators are summarized in Table 1.1.

Organic Materials	***S***	**σ**	***Max.* $S^2\sigma$**	**Max. ZT**	***Ref.***
Sample	($\mu V \cdot K^{-1}$)	($S \cdot cm^{-1}$)	($\mu W \cdot m^{-1} \cdot K^{-2}$)	-	-
Single materials					
PEDOT:PSS	40~600	2~2000	324	0.25	Bubnova (2011)
SWCNT film	40	700	100	0.02	Toshima (2015)
Polyacetylene	25	3×10^4	2000	0.60	Dubey (2011)
SWCNT yarn	50	2×10^3	2800	-	Zhang (2016)
Hybrid materials					
Bi_2Te_3/Additives	140	1.0×10^3	324	0.30	Cho (2015)
SWCNT/PEDOT	30	1.4×10^3	160	0.24	Yu (2013)
PANI/Graphene/ PEDOT/DWCNT	120	1.9×10^3	2710	0.10	Grulan (2016)
TeNW/PEDOT	150	1.4×10^2	200	0.21	Yee (2012)

Table 1.1. TE properties of promising organic and hybrid TE materials

1.3.2 Based on inorganic materials with organic additives

TE systems based on organic/inorganic composites can potentially benefit from combined advantages of low κ of organic materials and high *S* and σ of inorganic materials while mitigating their associated obstacles.[31] By mixing solution-processible high *S* inorganic nanocrystals with conducting polymer, it may improve the overall TE properties of the nanocomposites. Highly conducting PEDOT:PSS is one of the promising candidate for nanocomposite TE materials.[35] As a typical study, porous composite films with ball-milled particles of either p-type or n-type Bi_2Te_3 infiltrated with PEDOT:PSS was reported.[36] Furthermore, in-situ synthesis of inorganic nanocrystals in a conducting polymer containing solution represents a simple method to produce nanocomposite ink that can be directly cast at low temperature for making TE films. This method has been demonstrated in the Tellurium/PEDOT:PSS film via aqueous solution process.[37, 38]

A leading research based on inorganic materials with organic additives is the development of glass fabric-based TE generator that is extremely light and flexible by Cho et. al. from KAIST, Korea. They synthesized liquid-like pastes of n-type (Bi_2Te_3) and p-type (Sb_2Te_3) TE materials and printed them onto a glass fabric using a screen printing technique.[39] Franciosoa et al. have utilized same n- and p-type materials to fabricate modules on flexible substrate.[40]

1.3.3 Limitations and challenging issues

As a leading TE candidate, inorganic semiconductors, bismuth-tellurium-antimony-selenium (Bi-Te-Sb-Se) alloy family have been widely investigated. In order to make flexible TE generator, some organic additives are used with them and generally printed onto flexible substrate. However, despite of their high TE performances, the mechanical endurance of TE modules based on inorganic semiconductors cannot be guaranteed owing to their brittleness, and with their energy-intensive process, exquisite or large-area flexible TE device are inconceivable.

As another candidate, organic materials including conducting polymers, carbon nanotubes, graphene and their hybrid composites have been recently investigated because of their unique advantages including facile processability, scalability, and flexibility as well as low cost and weight. However, most of their performance could not satisfy the needs, yet. Although the performance of flexible TE materials have significantly improved, they are generally sensitive to humidity in ambient conditions, therefore, the development of environmentally stable conducting polymers and dopants that can be easily processed from solution is critical for applying conducting polymers to practical TE applications. The development of efficient and stable n-type organic TE materials and n-dopants is also a significant challenging issue.

In addition, for practical applications, many requirements including modular design, flexibility, portability, and facile fabrication must be considered. (Fig. 1.14) While many previous reports on flexible TE materials show excellent TE properties, these studies do not move past characterization of the TE properties and lack facile module fabrication and performance. Therefore, researches on both TE properties of material and module including components and fabrication techniques are strongly required.

Flexible TE material		Process	*Power Density* ($\mu W \cdot cm^{-2}$) at $\Delta T = 40$ K	limitation	*Ref.*
P-type	**N-type**				
PEDOT-Tos	TTF-TCNQ	Inkjet Printing	0.48	Stability Low performance	Bubnova (2011)
-	n-PETT/ CNT/PVC	Inkjet Printing	0.62	Single component Low performance	Toshima (2015)
PANI/Graphene/ PEDOT/DWCNT	-	LBL film	0.36	Difficult fabrication Low performance	Grulan (2016)
Bi_2Te_3	Sb_2Te_3	Screen Printing	168	Scarcity of materials Difficult fabrication	Cho (2015)

Table 1.2. Performance of reported flexible TE generators and their limitations

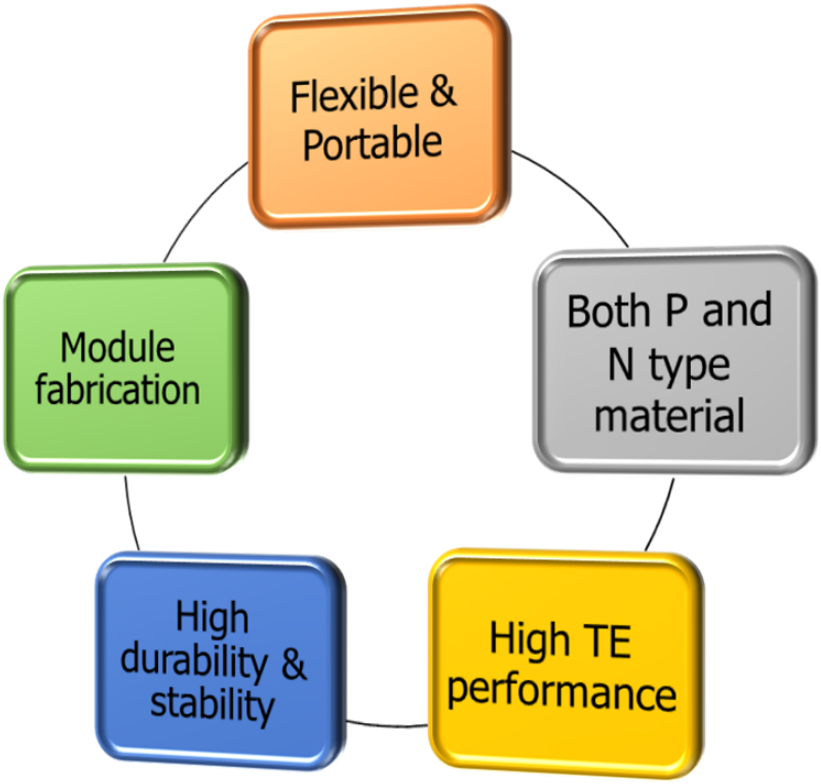

Fig. 1.14. Illustration of needs properties for flexible TE generators

1.3.4 Strategies to overcome limitations

Nano-carbon materials having great mechanical, chemical, electrical properties have been studied as promising TE materials to meet these requirements, but its use was limited to supplement electrical conductivity as fillers in composite system, systematic study to enhance the TE performance themselves have been lacked. The main reason is that even if the electrical conductivity was improved by such as chemical doping, its thermopower was reduced because those two factors lie in a trade-off relation, leading to less effective improvement in TE performance. To solve these fundamental problems and dramatically enhance the TE performance of nano-carbon materials, effective way is to control the mobility of carriers, and not the carrier concentration. This was derived from the below theoretical relationship between the carrier concentration and mobility.

$$S = \frac{8\pi^2 {K_B}^2}{3eh^2} \cdot m^* \cdot T \cdot \left(\frac{\pi}{3n}\right)^{2/3}$$

$$\sigma = n \cdot e \cdot \mu$$

Now we meet a new question, how can we obtain high TE performance by mobility engineering? Approach to enhance the mobility of materials without serious decrease of carrier concentration could be an effective way. Furthermore, sometimes in case of hybrid composite, specific mobility engineering such as energy filtering also could be a good strategy for enhancing TE performance.

1.4 Aim and scope of this research

1.4.1 Rational design of high-performance flexible thermoelectric materials based on nano-carbon materials

Although many mechanical and chemical advantages of nano-carbons exist, their TE performances are limited yet. In order to use as a flexible TE material, TE performance of nano-carbon should be enhanced. For this goal, initial approaches are controlling the alignment of carbon nanotube (CNT) for mobility engineering.

In addition, intrinsic low thermopower of nano-carbons is a critical obstacle for TE applications.[44] Enhancing the electrical conductivity of TE material could contribute to power factor enhancement, but cannot ensure the high ZT and seebeck voltage of module. Therefore, hybridization of nano-cabons and inorganic materials with high thermopower is one of the facile approaches to obtain both high thermopower of TE material and high seebeck voltage of TE generator. In fact, researches on hybridization of various materials have been widely reported,[45] but promising results are lacking because morphological and compositional controls of hybrid materials are difficult and TE properties of hybrid materials are sensitive to them. In addition, most of their TE properties generally lie in a trade-off relation between electrical conductivity and thermopower. Despite of strong fundamental interest, only a few papers reported a simultaneous enhancement of both electrical conductivity and

thermopower by carrier energy filtering at hybrid interfaces.[46] Therefore, systematic study on TE enhancement by carrier energy filtering is meaningful for fundamental research as well as practical use of flexible TE material.

1.4.1.1 By controlling the alignment of carbon nanotubes for mobility engineering

TE properties of CNT were already well-studied in many previous works due to their extraordinary electrical and mechanical properties. Also, owing to the improvement on separation technique of semiconducting and metallic CNTs, many researches on controlling and optimizing the TE performance of CNT are ongoing.[41, 42] However, because their results still couldn't satisfy the needs or limitations from the fundamental study, novel approach to get high TE performance is still required. The alignment of CNTs is one of the effective way to enhance the electrical conductivity of CNT, therefore, experimental and fundamental study on TE performance of aligned CNT must be an interesting issue.

1.4.1.2 By controlling the work function of Te nanowire/SWCNT binary hybrid for effective mobility engineering at hybrid interfaces

Hybridization of Te nanowire which have high thermopower and SWCNT which have high electrical conductivity is expected to be ideal combination for high performance. However, its TE properties are sensitively affected by

mechanical and chemical natures of each component. Furthermore, since simple mixing cannot guarantee high TE performance, it is important to find optimal conditions for ideal hybridization. From the previous works, the work function of two component material is a critical issue for synergetic TE enhancement by carrier energy filtering.[47] As a proof of concept, a simple SWCNT-doped inorganic semiconductor hybrid film is prepared, with a rationally engineered SWCNT work function, to systematically tune the energy filtering at the carbon-inorganic semiconductor interface.

1.4.1.3 By designing the work functions of Te nanowire / PEDOT:PSS / graphene ternary hybrid for effective mobility engineering at hybrid interfaces

Based on similar fundamental backgrounds above, the ternary hybrid paper of reduced graphene oxide (rGO) / PEDOT:PSS / Te nanowire (TeNW) is rationally designed. It consists of two heterojunctions at rGO/PEDOT:PSS and PEDOT:PSS/TeNW, and demonstrates that the two interfaces could act as energy filters to scatter low-energy carriers. TE hybrids with two heterojunctions with controlled interfacial energy barriers could show a significantly increased σ without a major decrease in S, thus leading to an enhanced power factor, which could be attributed to the double energy filtering at two junctions.

1.4.2 Rational design of high-performance flexible thermoelectric generators based on nano-carbon materials

Although simultaneous enhancement of thermopower and electrical conductivity is achieved by energy filtering and it results in a drastic enhancement of TE properties of hybrid material, facile fabrication of TE generator and its TE performance including power density, flexibility, mechanical and chemical stability are very important for practical use as flexible TE generator. It is realized that as-prepared hybrid films showing enhanced TE performance were not desirable for precise module fabrication. For practical use as a flexible TE generator, novel module design is required with development of processable TE material. Of course, high performance and flexibility of generator are still maintained as priority objective.

Applying previous module design to nano-carbons seem to be less-effective approach for high performance TE generator because it was based on rigid semiconducting materials. For instance, metal electrodes used in general TE module design are less compatible to most of organic materials including nano-carbons, which causes power decrease of TE generators due to increase of the contact resistance. Efficient module design could enhance low TE performance of materials, for example, increasing power density by using lightweight materials and close packed fabrication, and/or enhancing power generation by expanding the number of pairs. Therefore, study on efficient TE module design

is also meaningful and essential for flexible TE generator, comparable to development of TE materials.

1.4.2.1 By designing all-carbon nanotube thermoelectric generators without metal electrodes

Flexible and ultralight TE generator based on highly aligned carbon nanotube film and yarn with excellent TE performance are designed. This noble TE generator is innovative in that carbon materials have multi-functions in the same device. The nano-carbons were alternatively doped into n- and p-types and regions between the doped regions were used as electrodes to minimize the circuit resistance, thereby forming novel all-carbon TE generators without additional metal deposition.

1.5 References

1. Bell LE. Cooling, heating, generating power, and recovering waste heat with thermoelectric systems. *Science* **321**, 1457-1461 (2008).
2. Chu S*, et al.* Opportunities and challenges for a sustainable energy future. *Nature* **488**, 294-303 (2012).
3. Snyder GJ*, et al.* Complex thermoelectric materials. *Nat. Mater.* **7**, 105-114 (2008).
4. Li J-F*, et al.* High-performance nanostructured thermoelectric materials. *NPG Asia Mater* **2**, 152-158 (2010).
5. Shakouri A. Recent Developments in Semiconductor Thermoelectric Physics and Materials. *Annual Review of Materials Research* **41**, 399-431 (2011).
6. Dresselhaus MS*, et al.* Low-dimensional thermoelectric materials. *Phys. Solid State* **41**, 679-682 (1999).
7. Sootsman JR*, et al.* New and old concepts in thermoelectric materials. *Angew. Chem. Int. Ed. Engl.* **48**, 8616-8639 (2009).
8. Goldsmid HJ*, et al.* The use of semiconductors in thermoelectric refrigeration. *British Journal of Applied Physics* **5**, 386 (1954).
9. Bux SK*, et al.* Nanostructured materials for thermoelectric applications. *Chem Commun (Camb)* **46**, 8311-8324 (2010).

10. Dresselhaus MS, *et al.* New Directions for Low-Dimensional Thermoelectric Materials. *Adv. Mater.* **19**, 1043-1053 (2007).

11. Hicks L, *et al.* Thermoelectric figure of merit of a one-dimensional conductor. *Phys. Rev. B* **47**, 16631-16634 (1993).

12. Hicks L, *et al.* Effect of quantum-well structures on the thermoelectric figure of merit. *Phys. Rev. B* **47**, 12727-12731 (1993).

13. Liu W, *et al.* Recent advances in thermoelectric nanocomposites. *Nano Energy* **1**, 42-56 (2012).

14. Minnich AJ, *et al.* Bulk nanostructured thermoelectric materials: current research and future prospects. *Energy & Environ. Sci.* **2**, 466-479 (2009).

15. Yee SK, *et al.* $ per W metrics for thermoelectric power generation: beyond ZT. *Energy & Environ. Sci.* **6**, 2561-2571 (2013).

16. Dubey N, *et al.* Conducting polymers: Efficient thermoelectric materials. *J. Polym. Sci., Part B: Polym. Phys.* **49**, 467-475 (2011).

17. Shinohara Y. The State of the Art on Thermoelectric Devices in Japan. *Materials Today: Proceedings* **2**, 877-885 (2015).

18. Zebarjadi M, *et al.* Perspectives on thermoelectrics: from fundamentals to device applications. *Energy & Environ. Sci.* **5**, 5147-5162 (2012).

19. Yang J. Potential applications of thermoelectric waste heat recovery in the automotive industry. 24th International Conference on

Thermoelectrics, IEEE; 2005. p. 170-174.

20. Zhou G, *et al.* Progress in flexible lithium batteries and future prospects. *Energy & Environ. Sci.* **7**, 1307-1338 (2014).

21. Jo S, *et al.* Flexible thermoelectric generator for human body heat energy harvesting. *Electron. Lett* **48**, 1013-1015 (2012).

22. Park G, *et al.* Energy harvesting for structural health monitoring sensor networks. *Journal of Infrastructure Systems* **14**, 64-79 (2008).

23. He M, *et al.* Towards high-performance polymer-based thermoelectric materials. *Energy & Environ. Sci.* **6**, 1352-1361 (2013).

24. Yang J, *et al.* Rational Design of Advanced Thermoelectric Materials. *Adv. Energy Mater.* **3**, 549-565 (2013).

25. Bubnova O, *et al.* Optimization of the thermoelectric figure of merit in the conducting polymer poly(3,4-ethylenedioxythiophene). *Nat. Mater.* **10**, 429-433 (2011).

26. Kim GH, *et al.* Engineered doping of organic semiconductors for enhanced thermoelectric efficiency. *Nat. Mater.* **12**, 719-723 (2013).

27. Søndergaard RR, *et al.* Practical evaluation of organic polymer thermoelectrics by large-area R2R processing on flexible substrates. *Energy Science & Engineering* **1**, 81-88 (2013).

28. Park T, *et al.* Flexible PEDOT electrodes with large thermoelectric power factors to generate electricity by the touch of fingertips.

Energy & Environ. Sci. **6**, 788-792 (2013).

29. Iijima S. Helical microtubules of graphitic carbon. *Nature* **354**, 56-58 (1991).
30. Baughman RH*, et al.* Carbon nanotubes--the route toward applications. *Science* **297**, 787-792 (2002).
31. Yang J*, et al.* Rational Design of Advanced Thermoelectric Materials. *Adv. Energy Mater.* **3**, 549-565 (2013).
32. Yu C*, et al.* Light-Weight Flexible Carbon Nanotube Based Organic Composites with Large Thermoelectric Power Factors. *Acs Nano* **5**, 7885-7892 (2011).
33. Kim SL*, et al.* Flexible Power Fabrics Made of Carbon Nanotubes for Harvesting Thermoelectricity. *Acs Nano* **8**, 2377-2386 (2014).
34. Toshima N*, et al.* Novel Hybrid Organic Thermoelectric Materials:Three-Component Hybrid Films Consisting of a Nanoparticle Polymer Complex, Carbon Nanotubes, and Vinyl Polymer. *Adv. Mater.* **27**, 2246-2251 (2015).
35. Chabinyc M. Thermoelectric polymers: Behind organics thermopower. *Nat. Mater.* **13**, 119-121 (2014).
36. Zhang B*, et al.* Promising thermoelectric properties of commercial PEDOT: PSS materials and their Bi_2Te_3 powder composites. *ACS applied materials & interfaces* **2**, 3170-3178 (2010).
37. Coates NE*, et al.* Effect of interfacial properties on polymer-

nanocrystal thermoelectric transport. *Adv. Mater.* **25**, 1629-1633 (2013).

38. See KC*, et al.* Water-processable polymer-nanocrystal hybrids for thermoelectrics. *Nano Lett.* **10**, 4664-4667 (2010).

39. Kim SJ*, et al.* A wearable thermoelectric generator fabricated on a glass fabric. *Energy & Environ. Sci.* **7**, 1959-1965 (2014).

40. Francioso L*, et al.* Flexible thermoelectric generator for ambient assisted living wearable biometric sensors. *J. Power Sources* **196**, 3239-3243 (2011).

41. Avery AD*, et al.* Tailored semiconducting carbon nanotube networks with enhanced thermoelectric properties. *Nature Energy* **1**, 16033 (2016).

42. Hone J*, et al.* Thermoelectric Power of Single-Walled Carbon Nanotubes. *Phys. Rev. Lett.* **80**, 1042-1045 (1998).

43. Novoselov K*, et al.* Two-dimensional gas of massless Dirac fermions in graphene. *Nature* **438**, 197-200 (2005).

44. Bubnova O*, et al.* Towards polymer-based organic thermoelectric generators. *Energy & Environ. Sci.* **5**, 9345-9362 (2012).

45. Du Y*, et al.* Research progress on polymer–inorganic thermoelectric nanocomposite materials. *Prog. Polym. Sci.* **37**, 820-841 (2012).

46. He M*, et al.* Thermopower enhancement in conducting polymer nanocomposites via carrier energy scattering at the organic–

inorganic semiconductor interface. *Energy & Environ. Sci.* **5**, 8351-8358 (2012).

47. Sofo JO*, et al.* Optimum band gap of a thermoelectric material. *Phys. Rev. B* **49**, 4565-4570 (1994).

Chapter 2. Experimental apparatus for thermoelectric research

2.1 Electrical conductivity and thermopower measurement

For all kinds of experimental research, ensuring the reliability of experimental results is most important to in-depth discussion. That is why most researchers depend on well-known and generally commercialized measuring equipment. However, in some cases of research with specific aim and scope, measurement system need to be altered to a more appropriate form. General equipment for measuring TE properties of materials is ZEM series made by ULVAC. Even though it has verified reliability, it was designed for measuring inorganic semiconductors which are generally brittle and bulky. Therefore, it could be undesirable for flexible TE materials, modified method and apparatus are required.

In this research, distinguished probe stations are designed to measure the TE properties of flexible films and yarn type materials. The in-plane σ and *S* of the samples were simultaneously measured using a four-point probe SEEPEL TE measurement system (TEP 600, Seepel instrument), which is shown in Fig. 2.1. It consisted of probe station part, temperature controller, current source meter (Kethely 2400), voltage acquirement system (Keithely 2700), and control

program installed desktop. Four probes are horizontally placed in a line with 4 mm gaps, which measure the in-plane current and voltage of sample when temperature differences applied in both ends of sample. Temperature could be precisely controlled by feedback process using a pair of R-type thermocouple and a pair of Pt wire probes. Before all measurement, thermal EMPs are calculated to determine the thermal equilibrium of sample and it is automatically reflected in the measured data.

The electrical conductivity is calculated from measured voltages at each three different applied currents. Correlation factors from sample width and length are also considered, which means that reliable TE properties of specific shape of sample such as a rectangular film and yarns could be measured.

For seebeck coefficient calculation, the probes measured potential differences arising from temperature differences between the two ends of the sample (0.5, 1.5 and 2.5 °C at one end, and −0.5, −1.5 and −2.5 °C at the other) and calculated the *S*. These were considered reliable when the linear correlation (R^2) of the measured potential differences was higher than 0.9999. In addition, TE properties of sample could be measured at range of room temperature to nearly 500 K, because probe station part is protected by inner quartz tube and outer ceramic furnace. After tight sealing by screw, nitrogen gas is purged to prevent the oxidation of sample at high temperature.

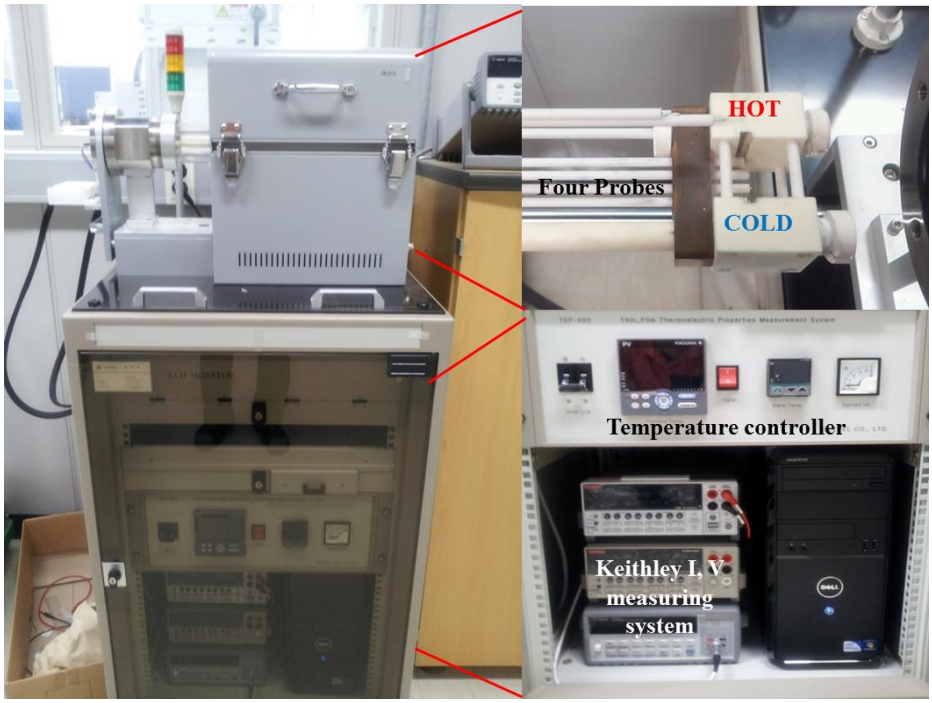

Fig. 2.1. Photograph of electrical conductivity and seebeck coefficient measuring system

2.2 Power measurement of thermoelectric generator

Measuring power of module is based on similar principles in the measurement of material, but requires novel design of measurement system. Scale of generator, degree and type of thermal source should be considered and electrical circuit should also be properly organized.

In this research, power measurement system in Fig. 2.2 is designed for vertical type of thermal gradients, which is desirable for applying in flexible TE generators. Such through-plane type of module could generate more power than in-plane type of module due to efficient energy transport mechanism, could be widely applied in real life. For instance, wearable TE generators using temperature differences in body heat and air are generally through-plane type. It is the common type of design even in conventional TE generator based on inorganic materials. To make vertical temperature gradients, four commercial Peltier modules are used. By applying a current, a pair of Peltier modules at the bottom side are cooled and opposite a pair of Peltier modules at the top side are heated. The temperatures at each side are controlled by degree of applied currents and measured by temperature sensors. Heat sinks and fans are equipped to maintain the stable temperature gradient. When temperature gradient is induced, open Seebeck voltage of module is measured by Keithely 2700 acquirement system. To calculated optimal power of module, reverse

currents are applied, which means that external resistance are intentionally loaded to TE circuit.

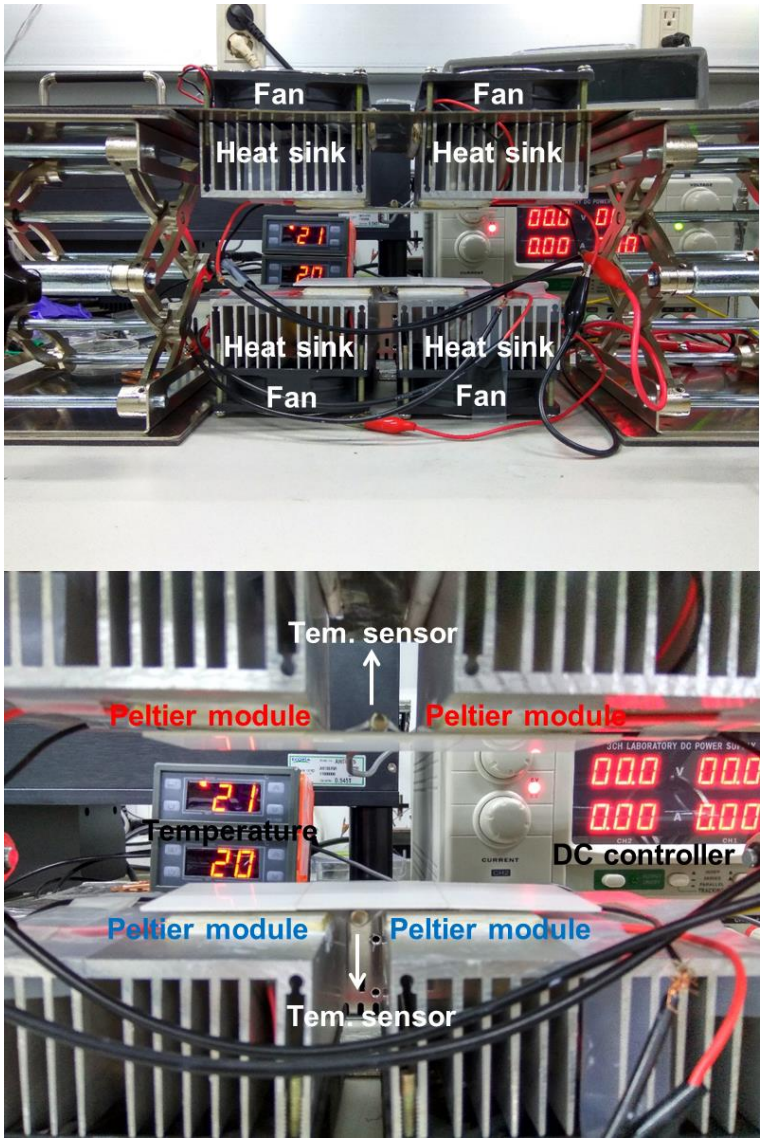

Fig. 2.2. Photograph of TE module power measuring system

PART II. Rational design of high-performance flexible thermoelectric materials based on nano-carbon materials

Chapter 3. Controlling the alignment of carbon nanotubes for mobility engineering

3.1 Research backgrounds

Organic polymers[1-3], nano-carbons[4-7], and their hybrid materials[8-12] have been investigated as possible alternatives for flexible TE materials due to their well-known advantages including flexibility, light-weight, low cost, easy processability, and scalability.[13] Although the TE performance of flexible materials has been significantly enhanced, their high performance is generally related to the extremely high electrical conductivity of organic polymers such as PEDOT:PSS.[1,14,15] However, flexible TE materials based on PEDOT:PSS are sensitive to humidity in ambient conditions, leading to a limitation for their practical applications. As another possible candidate, the carbon nanotube yarn (CNTY) has great potential for use in flexible TE materials because of its high electrical conductivity and controllable Seebeck coefficient (or thermopower).[16] In addition, it has excellent mechanical properties such as a low density of ~1 g/cm^3, approximately seven times lower than that of bulk Bi_2Te_3 (7.86 g/cm^3). Its carrier type and carrier concentration can be easily tuned as well by simple chemical doping, thereby allowing for its use in many flexible/or wearable TE applications. In this chapter, the high alignment and

optimized doping of CNTY resulted in enhanced TE properties, indicating its powerful potential as a flexible TE material.

3.2 Experimental

3.2.1 Synthesis of carbon nanotubes

CNTY was synthesized by a floating catalyst method as previously reported.[17] Ferrocene, thiophene, and methane were used as a catalyst precursor, promoter, and carbon source for CNT synthesis at 1200 ℃, respectively. CNTs are highly integrated into aerogel-like forms in a reactor. These aerogel forms can be continuously withdrawn from the reactor at the bottom without length limitations. The CNT film was prepared as an aerogel directly wound on a roller and r-CNTY was obtained by vertically rolling a CNT film. CNTY was directly fabricated on a roller and composed of hundreds of thread passing through a water bath after synthesis. (Fig 3.1)

3.2.2 Controlling the alignment of carbon nanotubes

To demonstrate the effect of CNT alignment on electrical conductivity, we systemically controlled the directional alignment of CNT bundles in four different samples (Fig. 2): (a) vacuum filtered film of commercial CNT (c-CNTF), (b) as-synthesized CNT film (a-CNTF), (c) CNT yarn by rolling up a-CNTF (r-CNTY), and (d) CNTY by direct spinning of a-CNTF (CNTY).

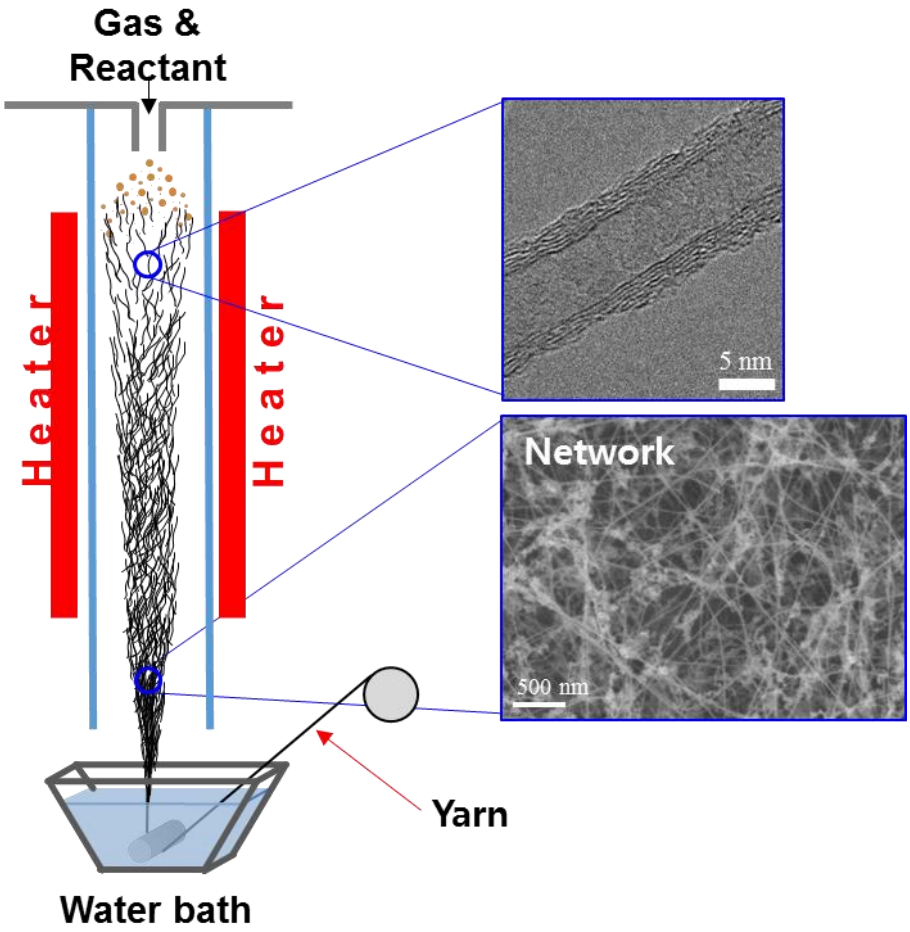

Fig. 3.1. Schematic illustration of CNT yarn synthesis

3.2.3 Solution based chemical doping of carbon nanotubes

For the doping process, the doping conditions were optimized by tuning the dopant concentration. The CNTY was p-doped with a $FeCl_3$ ethanol solution (Sigma-Aldrich, 2 mM) for 30 min, followed by well drying in ambient conditions. Additionally, the CNTY was n-doped with a polyethyleneimine ethanol solution (PEI (MW = 600), Sigma-Aldrich, 8 mM) for 30 min.

3.2.4 Characterizations

The microstructural morphology of the synthesized CNTY was investigated using high-resolution TEM (HR-TEM, JEOL, JEM-2100F) and field-emission SEM (FE-SEM, ZEISS, MERLIN Compact). Raman spectroscopy (RAMANplus, Nanophoton) with a 532 nm laser also was used to determine the crystallinity of the CNTs. The mechanical properties of the CNTY were measured with a tensile stage (Linkam, TST350) at a strain rate of 3 $mm \cdot min^{-1}$ and gauge length of 10 mm.

The TE properties of the as-prepared samples deposited on glass substrates with dimensions of 2 × 1 cm^2 were analyzed by measuring electrical conductivity (σ) and thermopower (S) at room temperature. The in-plane resistance (R) and S of the samples were simultaneously measured using a four-point probe TE measurement system (TEP 600, Seepel instrument), and the average values of at least ten measurements were taken. The σ of CNTY was calculated by a well-known follow equation. (assuming a spherical CNTY cross-sectional area.)

$$\sigma = \frac{1}{\rho} = \frac{l}{R \cdot A} \qquad (1)$$

Here, R, l and A are the measured electrical resistance (Ω), length (m) and cross-sectional area (m^2) of CNTY, respectively. The diameter of the CNTY was obtained by a micrometer (Mitutoyo, 1 μm in accuracy) with a mean of at least five measurements.

3.3 Results and discussion

3.3.1 Preparation of aligned carbon nanotube yarn

The CNTY was continuously produced by direct spinning after synthesis. Thousands of individual double walled-CNTs with a diameter of 5 nm compose a CNTY of 30 μm in diameter as shown in the scanning electron microscopy (SEM) and transmission electron microscopy (TEM) images in Fig. 3.2 and 3.3. Highly-integrated CNTYs have a low density of ~1.0 g/cm^3 and high specific strength of ~1 GPa/(g·cm^3), enough to support a 5 kg weight. Furthermore, the CNTY has excellent specific electrical conductivity, in the order of 10^3 S·cm^2/g, which is comparable to some metals. The superior electrical conductivity of CNTY could be due to the high degree of internal alignment and high longitudinal carrier mobility it affords. Fig. 3.4 shows SEM images of four different samples, which indicate that the CNTY features the best alignment. Additionally, the polarized Raman intensity factor ($I_{G\parallel}/I_{G\perp}$, the ratio of G peak intensity parallel to the Raman laser to one in the perpendicular direction) of CNTY is 3.8, stating that the degree of CNTY alignment here is the highest among the samples.[18]

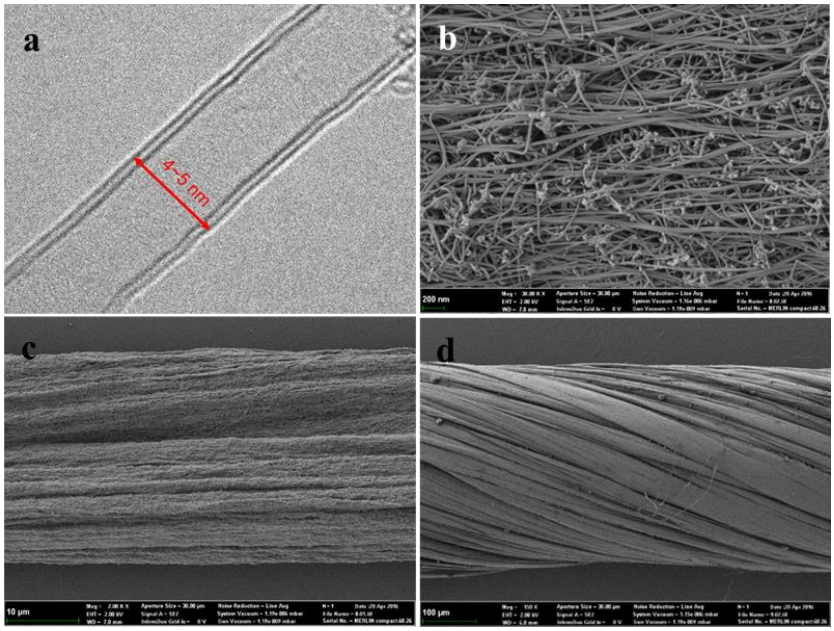

Fig. 3.2. (a) HR-TEM image and (b, c, d) FE-SEM images of CNT yarn

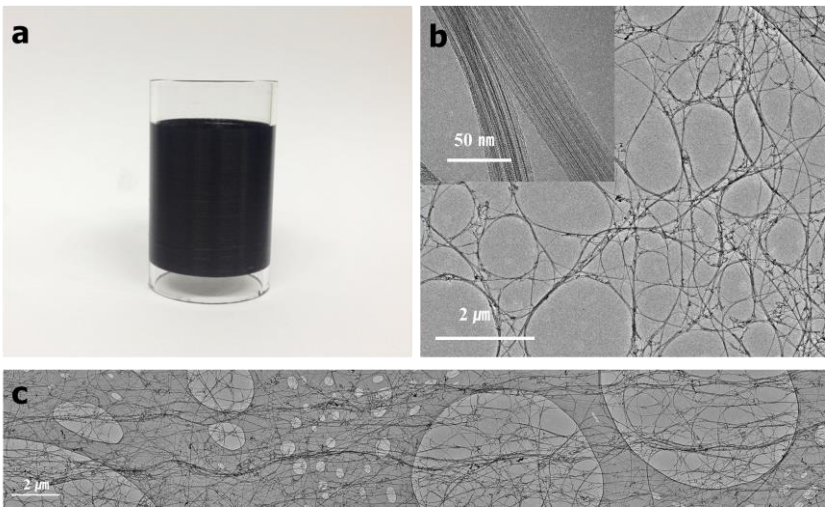

Fig. 3.3. Photograph of the CNTY wound on (a) vial (b, c) HR-TEM images of CNTY.

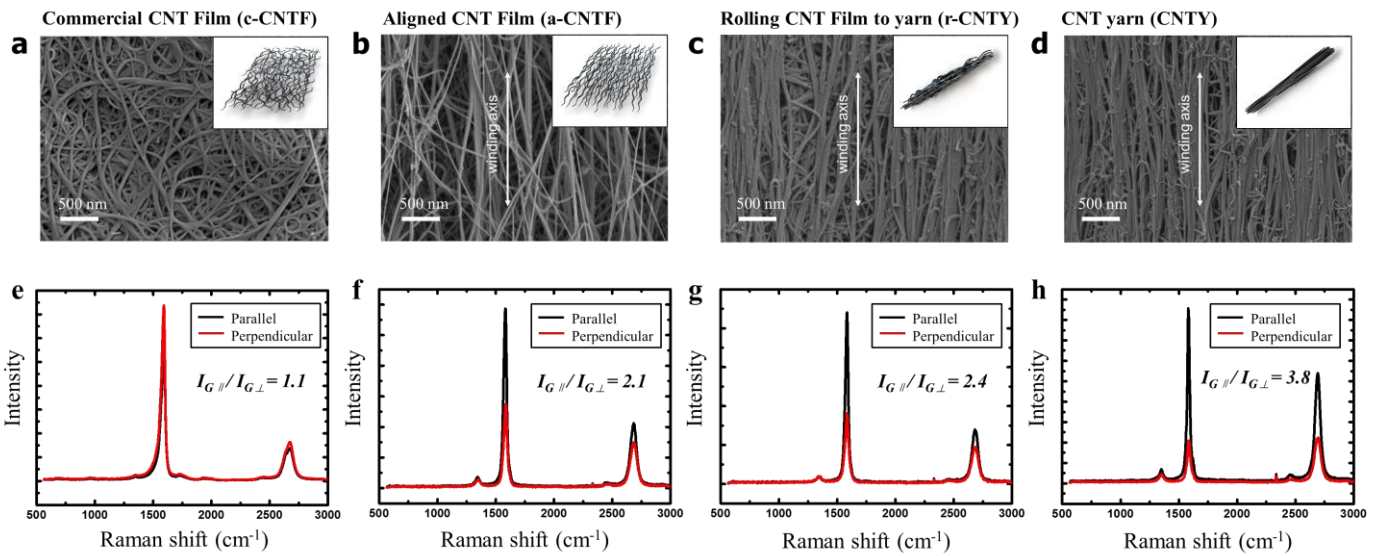

Fig. 3.4. FE-SEM image and morphological schematic of (a) c-CNTF, (b) a-CNTF, (c) r-CNTY, (d) CNTY. And Raman spectra (e)~(h).

3.3.2 Power factor enhancement of aligned carbon nanotube yarn

Table 3.1 summarizes the TE properties of these four samples. As the CNT alignment increases, the electrical conductivity (σ) drastically increases from 876 to 3147 S/cm. In contrast, the thermopower (S) is relatively unchanged, thus significantly increasing the power factor ($S^2\sigma$). According to the Drude model, the thermopower is inversely proportional to the carrier concentration but is unrelated to the carrier mobility.[19] As shown in Hall measurement data of c-CNTF and a-CNTF (Table 3.2), the carrier mobility increases without a main increase in the carrier concentration when the degree of alignment increases. These results indicate that the enhanced electrical conductivity without a major decrease in the thermopower is mainly due to an increase of carrier mobility derived from the highly-aligned structure.

Thermoelectric properties	c-CNTF	a-CNTF	r-CNTY	CNTY
Density (g/cm^3)	0.42	0.51	0.85	0.90
Electrical conductivity (S/cm)	876	1340	1949	3147
Thermopower (μV/K)	39	35	46	50
Power factor ($\mu W/m \cdot K^2$)	133	164	421	801

Table 3.1. Thermoelectric properties of various types of CNTs as a function of alignment degrees

Transport parameters	Pristine c-CNTF	Pristine a-CNTF	p-doped a-CNTF	n-doped a-CNTF
Electrical conductivity (S/cm)	876	1340	2272	1045
Thermopower (μV/K)	39	35	41	-58
Power factor ($\mu W/(m \cdot K^2)$)	133	164	378	357
Carrier concentration ($10^{22}/cm^3$)	1.14	1.01	1.80	-1.08
Carrier Mobility ($cm^2/(v \cdot s)$)	0.48	0.88	0.75	0.72

Table 3.2. Transport parameters of the pristine c-CNTF, pristine a-CNTF, p-doped a-CNTF, and n-doped a-CNTF.

3.3.3 Electrical conductivity enhancement by chemical doping

For practical use of CNTY in TE applications, the TE properties of CNTY after n- and p-doping are important (doping conditions are shown in Fig. 3.5). Figure 3.6 shows the electrical conductivity, thermopower, and power factor of doped CNT samples. The electrical conductivity of a-CNTF increases from 1340 to 2272 S/cm after p-doping but slightly decreases after n-doping. Nevertheless, the thermopower of a-CNTF slightly increases after doping. To further clarify this effect, we characterized the carrier properties of doped a-CNTF (Table 3.2). The a-CNTF shows an increase in carrier concentration by p-doping without a critical decrease in carrier mobility, thus leading to enhanced electrical conductivity with slightly increased thermopower by effective doping of a-CNTF. It is interesting to note that doped a-CNTF shows a higher thermopower than the pristine sample despite the increased electrical conductivity. This could be explained by the effects of the Fe catalyst used as a seed in the synthesis of a-CNTF. As shown in Fig. 3.7, the amount of Fe in the purified CNTY is 1.7 wt% and Fe can act as an n-dopant (because the CNTY and a-CNTF are synthesized using the same procedure, they contain the same amount of Fe catalyst).[20] While the as-synthesized CNTY shows p-type characteristics with thermopower of 4 μV/K, the CNTY synthesized with more Fe catalyst and the CNTY purified with 1 M HCl (used in all experiments) show thermopower values of -31 and 50 μV/K, respectively (Table 3.4). These indicate that purified CNTY may show lower

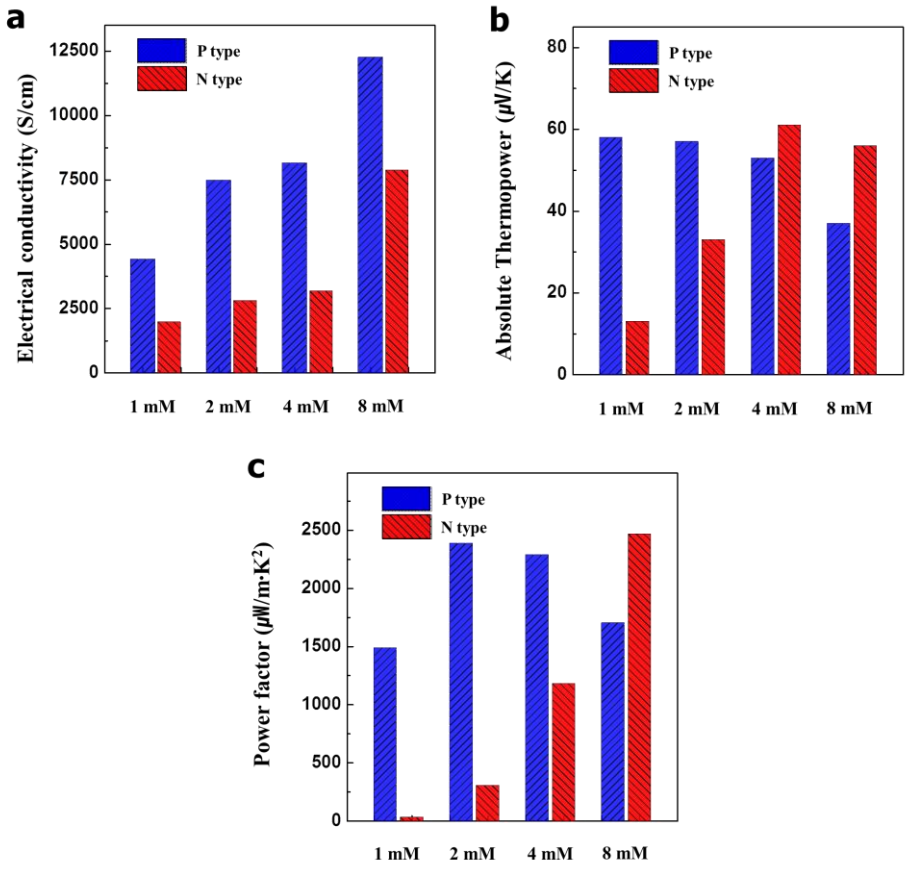

Fig. 3.5. TE properties of CNTY as a function of doping concentration of solution

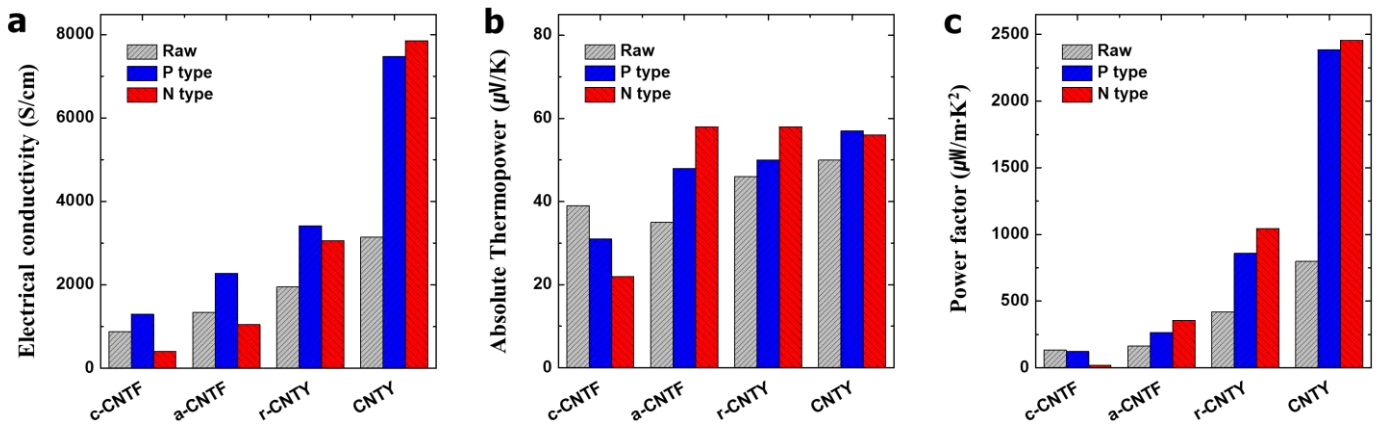

Fig. 3.6. (a) electrical conductivity, (b) absolute thermopower, and (c) power factor of various types of CNTs with N and P type doping

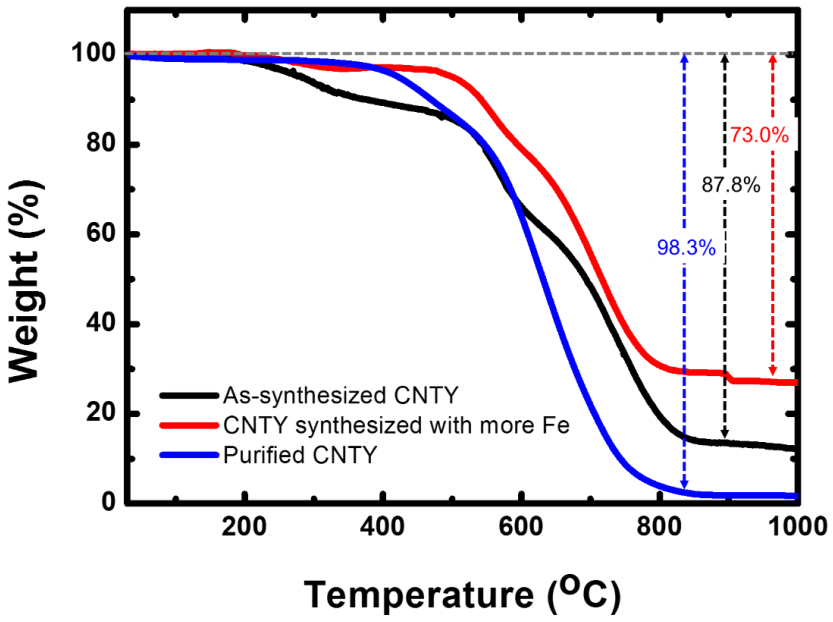

Fig. 3.7. TGA spectra of the CNTY as a function of Fe catalyst contents

Thermoelectric properties	**As-synthesized CNTY**	**CNTY synthesized with more Fe**	**Purified CNTY**
Electrical conductivity (S/cm)	4381	2790	3147
Thermopower (μV/K)	4	-31	50
Power factor (μW/(m·K^2))	6	273	801

Table 3.4 TE properties of CNTY as a function of Fe catalyst contents

thermopower than the intrinsic CNTY without any residual Fe, because Fe acts as an n-dopant. Therefore, the effective doping of CNTY can optimize the charge carriers and consequently increase the thermopower and electrical conductivity, resulting in significantly enhanced power factors of 2387 and 2456 μW/(m·K^2) by p- and n-doping, respectively. These values are some of the highest power factors reported for flexible TE materials such as PEDOT:PSS, CNTs, and their composites.[10,12,16]

3.4 Conclusions

In conclusion, the high alignment of CNTY resulted in the enhanced electrical conductivity without a major decrease in the thermopower, which is mainly due to an increase of carrier mobility derived from the highly-aligned structure. In addition, the effective doping of CNTY can optimize the charge carriers and consequently increase the thermopower and electrical conductivity, resulting in significantly enhanced power factors.

3.5 References

1. Kim G. H.*, et al.* Engineered doping of organic semiconductors for enhanced thermoelectric efficiency. *Nat. Mater.* **12**, 719-723 (2013).
2. Bubnova O.*, et al.* Towards polymer-based organic thermoelectric generators. *Energy & Environ. Sci.* **5**, 9345-9362 (2012).
3. He M.*, et al.* Towards high-performance polymer-based thermoelectric materials. *Energy & Environ. Sci.* **6**, 1352-1361 (2013).
4. Meng C.*, et al.* A promising approach to enhanced thermoelectric properties using carbon nanotube networks. *Adv. Mater.* **22**, 535-539 (2010).
5. Xiao N.*, et al.* Enhanced Thermopower of Graphene Films with Oxygen Plasma Treatment. *ACS Nano* **5**, 2749-2755 (2011).
6. Kim S. L.*, et al.* Flexible Power Fabrics Made of Carbon Nanotubes for Harvesting Thermoelectricity. *ACS Nano* **8**, 2377-2386 (2014).
7. Avery A. D.*, et al.* Tailored semiconducting carbon nanotube networks with enhanced thermoelectric properties. *Nature Energy* **1**, 16033 (2016).
8. Du Y.*, et al.* Research progress on polymer–inorganic thermoelectric nanocomposite materials. *Prog. Polym. Sci.* **37**, 820-

841 (2012).

9. Zhang K.*, et al.* Enhancing thermoelectric properties of organic composites through hierarchical nanostructures. *Sci. Rep.* **3**, 3448 (2013).

10. Toshima N.*, et al.* Novel Hybrid Organic Thermoelectric Materials:Three-Component Hybrid Films Consisting of a Nanoparticle Polymer Complex, Carbon Nanotubes, and Vinyl Polymer. *Adv. Mater.* **27**, 2246-2251 (2015).

11. Coates N. E.*, et al.* Effect of interfacial properties on polymer-nanocrystal thermoelectric transport. *Adv. Mater.* **25**, 1629-1633 (2013).

12. Cho C.*, et al.* Outstanding Low Temperature Thermoelectric Power Factor from Completely Organic Thin Films Enabled by Multidimensional Conjugated Nanomaterials. *Adv. Energy. Mater.* **6**, 1502168 (2016).

13. Chabinyc M. Thermoelectric polymers: Behind organics' thermopower. *Nat. Mater.* **13**, 119-121 (2014).

14. Bubnova O.*, et al.* Optimization of the thermoelectric figure of merit in the conducting polymer poly(3,4-ethylenedioxythiophene). *Nat. Mater.* **10**, 429-433 (2011).

15. Huang J.*, et al.* Investigation of the Effects of Doping and Post-Deposition Treatments on the Conductivity, Morphology, and Work

Function of Poly(3,4-ethylenedioxythiophene)/Poly(styrene sulfonate) Films. *Adv. Funct. Mater.* **15**, 290-296 (2005).

16. Zhou W. B.*, et al.* Ultrahigh-Power-Factor Carbon Nanotubes and an Ingenious Strategy for Thermoelectric Performance Evaluation. *Small* **12**, 3407-3415 (2016).
17. Jung Y.*, et al.* Effect of polymer infiltration on structure and properties of carbon nanotube yarns. *Carbon* **88**, 60-69 (2015).
18. Koziol K.*, et al.* High-performance carbon nanotube fiber. *Science* **318**, 1892-1895 (2007).
19. Snyder G. J.*, et al.* Complex thermoelectric materials. *Nat. Mater.* **7**, 105-114 (2008).
20. Pi K.*, et al.* Electronic doping and scattering by transition metals on graphene. *Phys. Rev. B* **80**, 075406 (2009).

Chapter 4. Controlling the work function of Te nanowire / SWCNT binary hybrid for effective mobility engineering at hybrid interfaces

4.1 Research backgrounds

Thermoelectric (TE) materials are very effective in harvesting electricity from heat sources or cooling/heating devices without moving parts.[1] Their energy conversion efficiency is evaluated by a dimensionless figure of merit (ZT), given by

$$ZT = (S^2\sigma)\, T/\kappa \qquad (1)$$

where S, σ, T, and κ are the Seebeck coefficient (also called the thermopower), electrical conductivity, absolute temperature, and thermal conductivity, respectively. Equation 1 shows that high ZTs are achieved with high S and σ and low κ. Inorganic semiconductors and their alloys are perhaps the most commonly used TE materials because their high-quality crystalline structures allow effective and large-scale energy transport.[2-4] Three fundamental concepts are currently being investigated to improve the performance of inorganic TE materials: (1) the quantum confinement effect, whereby sharp increases in the

electronic density of states can lead to increased thermopower; (2) the energy filtering effect, whereby energy-dependent scattering of charge carriers can increase the thermopower without a major decrease in the electrical conductivity; and (3) phonon scattering, whereby nanostructures limit the mean free paths of phonons but not of electrons, reducing the lattice thermal conductivity without affecting the electrical conductivity.[5-8] Recently, the phonon scattering and energy filtering effect have been exploited via the introduction of superlattices, nanoinclusions, and composites, to significantly improve the performance of inorganic TE materials.[9-12] However, these inorganic nanostructures have some drawbacks. Indeed, the scarcity and fragility of the raw materials and the expensive fabrication processes that are required limit the more general commercial use of inorganic TE materials, notably for flexible/or wearable power conversion devices.[13-14] Flexibility is also crucial to cover and adhere closely to the heat sources that emit low thermal radiation in the practical applications at the temperature range lower than 400 K.

Flexible TE materials have already been investigated to overcome the limitations of inorganic semiconductors. Early studies focused on the TE properties of homogeneous organic materials such as polymers[15-17] or carbons[18-21] not only because of their unique electronic properties, but also because of their low-cost, light-weight, and flexibility. More recently, hybrid systems designed to exploit the advantages of each component have led to enhanced TE

performances.[22] For example, a carbon nanotube/poly(vinyl acetate) (PVAc) hybrid with ZT = 0.006 at room temperature (RT)[23], a single-walled carbon nanotube (SWCNT) / PEDOT:PSS hybrid with ZT = 0.02 at RT[24], and a MWCNT/polyvinylidene fluoride composite with ZT = 0.02 at RT[25] have been reported. Elsewhere, the potential of flexible inorganic semiconductor/polymer composites, Bi_2Te_3/PEDOT:PSS notably, has also been investigated.[26-27] Interestingly, a few studies have reported hybrid materials with significantly enhanced TE performances, which are ascribed to the possibility of efficient energy filtering introduced in the inorganic TE area. Yu et al prepared carbon nanotube/PEDOT:PSS/PVAc composites with a ZT of ~0.2 at RT by possibly filtering low energy carriers at the carbon-polymer junctions.[28] Further, See et al presented Te nanowire/PEDOT:PSS composites with increased thermopower, indicating the potential of energy filtering at inorganic semiconductor-polymer junctions.[29] However, the improvements achieved so far are based on a possibility of the energy filtering effects involved and a systematic study thereof is still lacking. To date, only He et al have assigned the enhanced TE performance of their samples (Bi_2Te_3/P3HT composites in this case) to energy filtering at the inorganic semiconductor-polymer interfaces.[30] Therefore, a more systematic understanding of the energy filtering effect at organic-organic or organic-inorganic interfaces is desirable to improve the performance of organic composites for potential applications in flexible TE devices.

In this chapter, as a proof of concept, we prepared a simple SWCNT-doped inorganic semiconductor hybrid film with, for the first time, a rationally engineered SWCNT work function, to systematically tune the energy filtering at the carbon-inorganic semiconductor interfaces. Tellurium nanowire (TeNW) as a 1-dimensional inorganic semiconductor and SWCNT were selected due to their high thermopower and electrical conductivity, respectively. The SWCNT work function was controlled by acid treatment, lowering the interfacial barrier between the SWCNTs and TeNWs from 0.82 to 0.23 eV, to selectively scatter low-energy carriers at the interface. The power factor of the film with a low interfacial barrier energy of 0.23 eV was enhanced to 3.40 $\mu W \cdot m^{-1} \cdot K^{-2}$ at RT, several times higher than that of either pure TeNW or hybrid film with a larger interfacial barrier energy of 0.82 eV. In addition, the energy filtering effect at the SWCNT-TeNW interfaces was quantitatively characterized by measuring and calculating carrier transport characteristics such as the carrier concentration, carrier mobility, thermopower and scattering time.

4.2 Experimental

4.2.1 Preparation of Te nanowires

TeNWs were synthesized as reported previously in the literature.[31] All chemicals were purchased from Sigma-Aldrich and used without further purification. Ascorbic acid ($C_6H_8O_6$, 10 g) and cetyltrimethylammonium bromide (CTAB, 1 g) were dissolved in distilled water (400 mL). Sodium tellurite (Na_2TeO_3, 0.52 g) was added to the solution under vigorous stirring, forming a white suspension. The suspension was heated to 90 ℃ and reacted for 20 h. After reaction, the mixture was cooled down to room temperature and then washed with distilled water and ethanol to remove the excess CTAB. The synthesized TeNWs were dried overnight in an oven.

4.2.2 Controlling the work function of the SWCNT

The work function of the SWCNTs was controlled by acid treatment. SWCNTs (10 mg, AST-100F grade, Hanwa nanotech.) were added to a nitric acid solution (60 vol%, 30 mL), and the mixture was subjected to bath sonication at RT for 2, 4 and 8 h to control the degree of oxidation. Then, the acid-treated SWCNTs were washed with distilled water and ethanol several times until the pH of the SWCNT suspension in distilled water reached ~7. The final SWCNT concentration in distilled

water was adjusted to 1 $mg \cdot mL^{-1}$. All the SWCNT films used in this study were prepared by vacuum filtration and dried overnight in a vacuum oven.

4.2.3 Preparation of Te nanowire/SWCNT hybrid film

For the preparation of the hybrid films, TeNWs (10 mg) were re-dispersed in ethanol and added into separate a-SWCNT solutions (1 mg/mL in distilled water). The mixture was then slightly sonicated in a bath for 10 min, vacuum filtered through a 0.22 μm polyvinylidene fluoride membrane, and the resulting films were dried in a vacuum oven overnight.

4.2.4 Characterizations

The morphology of the hybrid films was characterized by field emission scanning electron microscopy (FE-SEM) (JSM-6701F, JEOL) and high-resolution transmission electron microscopy (HR-TEM) (Tecnai F20, FEI). The distribution of SWCNTs in the TeNW matrix was characterized by Raman microscopy (inVia Raman microscope, Reinshaw) with a 633 nm He-Ne laser source. The work functions of each sample were measured by ultraviolet photoelectron spectroscopy (UPS), and the degree of SWCNT oxidation was characterized by X-ray photoelectron spectroscopy (XPS). The electrical conductivity of the films was measured using a four-point probe system consisting of a four-point cylindrical probe head (JANDEL Engineering), a

direct current precision power source (Model 6220, Keithley), and a nanovoltmeter (Model 2182A, Keithley). The thermopower was measured using a Seebeck instrument (Model TEP 600, Seepel) at room temperature. The carrier concentration and mobility in the films were determined by Hall measurements (Ecopia HMS-3000), with the mean of at least five measurements. The in-plane thermal conductivity of the sample was obtained from the thermal diffusivity measured by laser flash system (LFA 457 NanoFlash, Netzsch), the specific heat measured by DSC (DSC7, PerkinElmer) and the density of the sample. The thickness of films was obtained by micrometer (Mitutoyo, 1 μm accuracy) with the mean of more than 5 times measurements. As shown in the supporting information (Fig. 4.1), the film thickness looks uniform over the sample area.

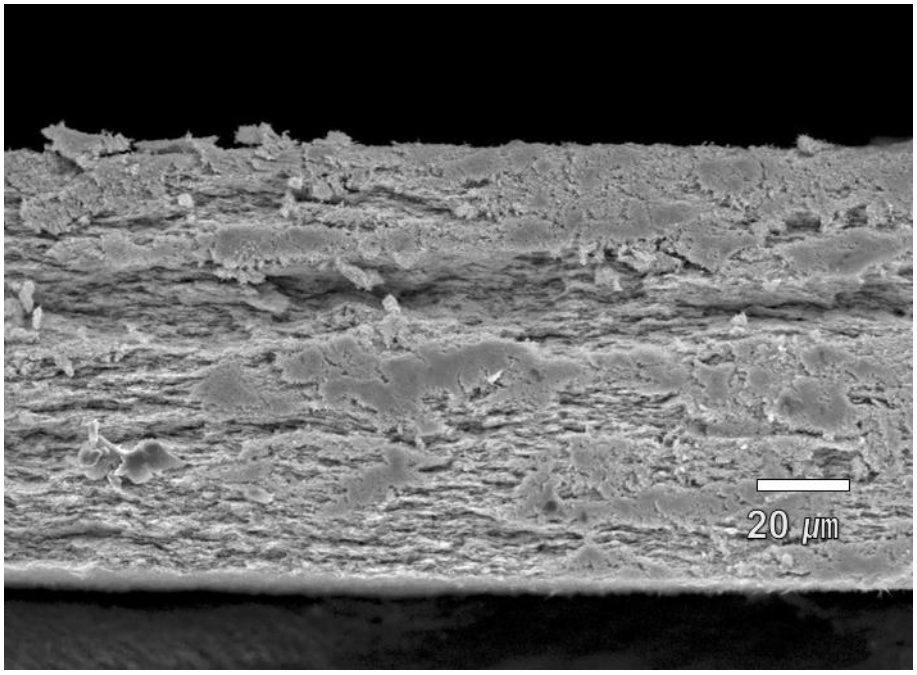

Fig. 4.1. FE-SEM image of 2 wt% a-SWCNT/TeNW hybrid film (cross-sectional view)

4.3 Results and discussion

4.3.1 Preparation of Te nanowire/SWCNT hybrid film

Tellurium nanowires were selected as a matrix for the flexible thermoelectric hybrid film due to their high thermopower. The quantum confinement effect of the 1-D nanostructures means that TeNWs have higher thermopowers than Te nanoparticles.[32] The TeNWs were synthesized as reported previously in the literature, using ascorbic acid as a reducing agent, sodium tellurite as a tellurium source and a cationic surfactant, CTAB, as a structure-directing agent.[31,33] As shown in the scanning and transmission electron micrographs in Fig. 4.2a, the synthesized TeNWs are 30 nm in diameter and 3 μm long on average. Fig. 4.2b shows the HR-TEM image and selected area electron diffraction (SAED) pattern obtained from a single TeNW to identify the crystal structure of the as-synthesized nanowires. The clear lattice fringes in the micrograph indicate that the nanowire is structurally uniform and single-crystalline. The interplanar spacing of ~5.9 Å corresponds to the distance between (001) lattice planes in hexagonal Te, as reported previously in the literature.[33] The X-ray diffraction patterns in Fig. 4.2c also indicate that the synthesized TeNWs consist of hexagonal Te, with all the peaks matching those in the reference JCPDS card (no. 36-1452). These data confirm the formation of high purity hexagonal TeNWs. The as-synthesized TeNWs have a low electrical conductivity of 4 S/m, so a small amount of acid-treated SWCNTs (a-

SWCNTs) with a high electrical conductivity was doped into the TeNW matrix. While the as-received SWCNT shows poor dispersibility in water, the acid-treated SWCNTs

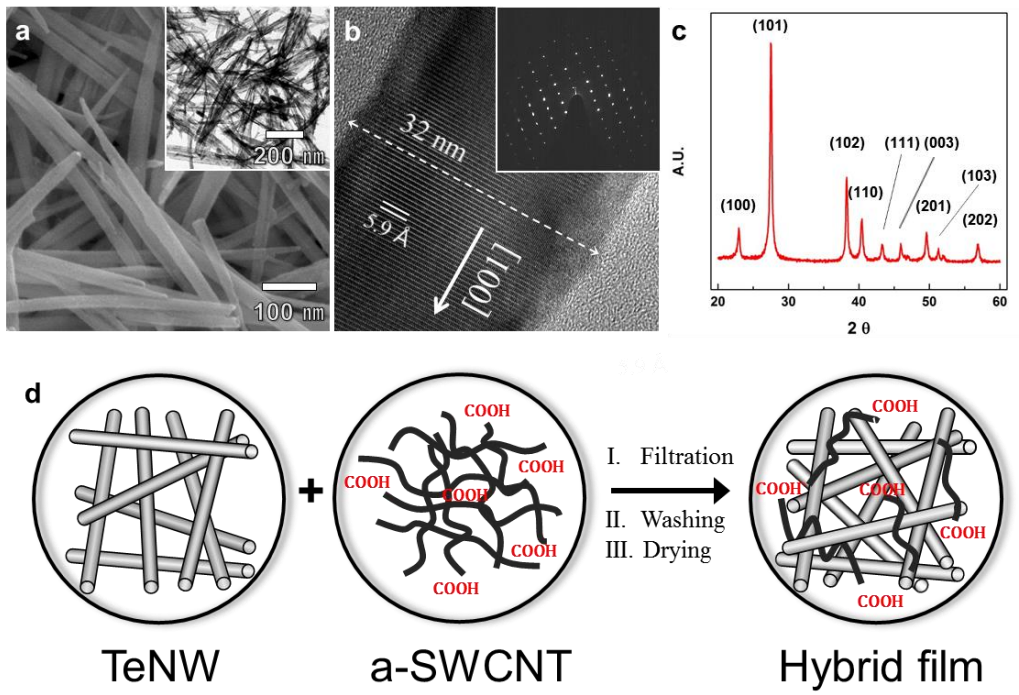

Fig. 4.2. (a) FE-SEM (inserted image: TEM), (b) HR-TEM (inserted pattern: SAED) and (c) XRD spectrum of synthesized TeNW, and (d) schematic illustration of the preparation of a-SWCNT/TeNW hybrid film

are well dispersed in water, thereby leading to a homogeneous mixture of a-SWCNTs with TeNW (Fig. 4.3). The synthesized TeNWs were mixed with a-SWCNTs well dispersed in water by sonication, then vacuum filtered, washed, and dried to obtain a uniform hybrid film. Fig. 4.2d illustrates the different steps involved in the preparation of flexible TeNW films hybridized with a-SWCNTs. For each characterization, the TeNWs should be mixed with a-SWCNTs right after the synthesis of TeNW. It is because the TeNWs are oxidized and recrystallized under ambient condition, thus leading to a decrease in the thermopower (Fig. 4.4 and 4.5)

The microstructural morphology of the prepared hybrid films was characterized by TEM and FE-SEM. Fig. 4.6a, b shows that the carrier transport network is formed by the rigid TeNWs with a small number of a-SWCNTs doped into the matrix. The distribution of a-SWCNTs in the TeNW matrix was characterized in more detail using Raman mapping at the characteristic G band wavenumber (1580 cm^{-1}) of a-SWCNTs (Fig. 4.6c) and Raman spectra (Fig. 4.7). The a-SWCNTs seem well distributed in the TeNW matrix, ensuring that carriers are added uniformly throughout the matrix. Fig. 4.6d shows a photograph of a typical hybrid film. While the TeNW films without a-SWCNTs are very brittle, the hybrid films are flexible because the mechanical strength and high aspect ratio of the a-SWCNTs support the TeNW network.

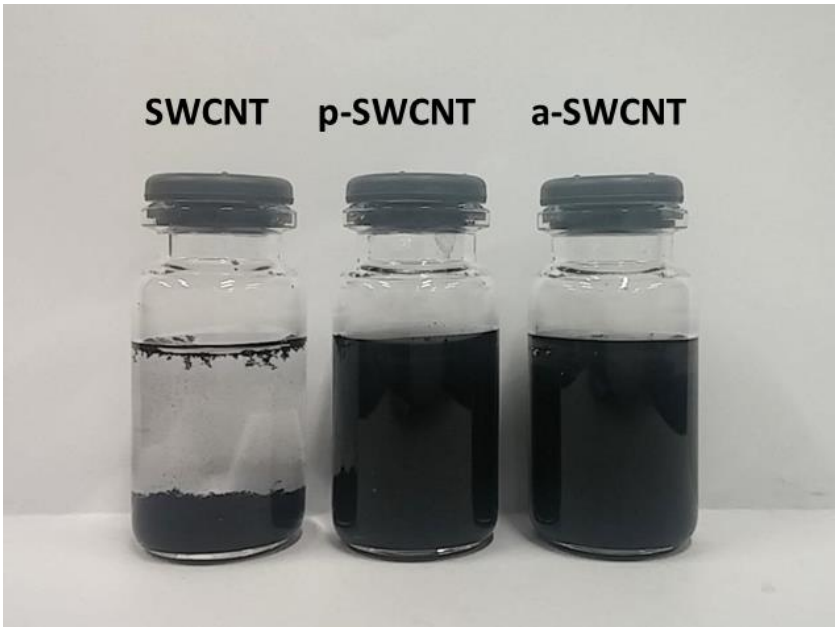

Fig. 4.3 Photographs of as-received SWCNT, p-SWCNT, and a-SWCNT in water after 3 h

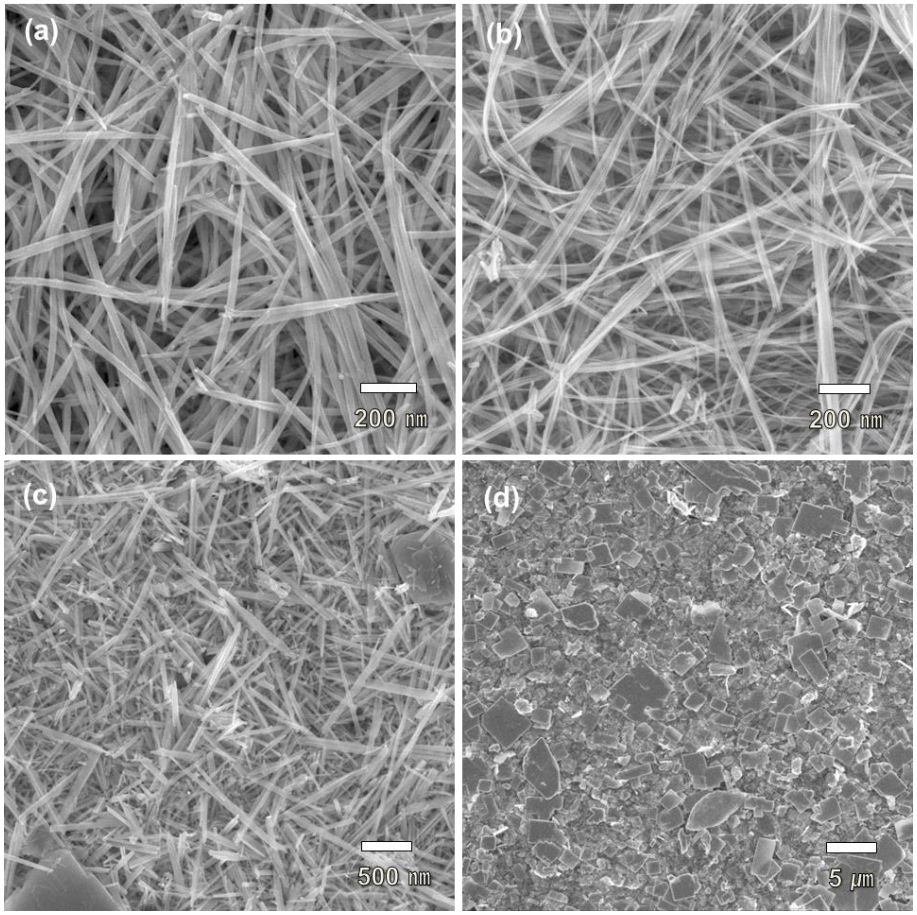

Fig. 4.4. FE-SEM images of (a) as-prepared TeNW, (b) TeNW film after one week under ambient condition, (c) TeNW film after one month under ambient condition, and (d) TeNW film after three months under ambient condition.

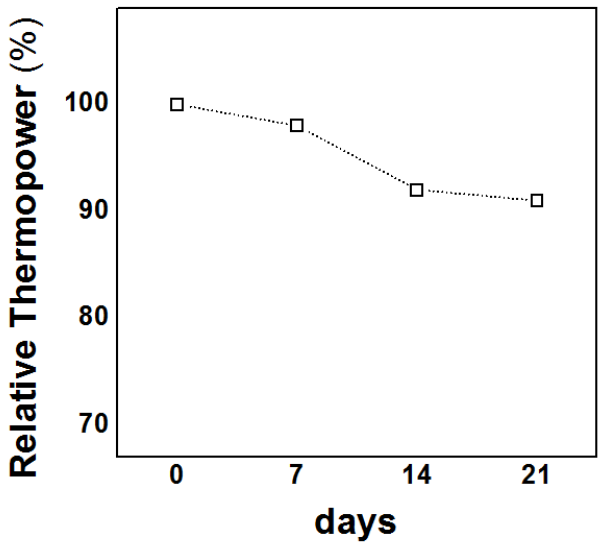

Fig. 4.5. Relative thermopower of the pure TeNW film as a function of days

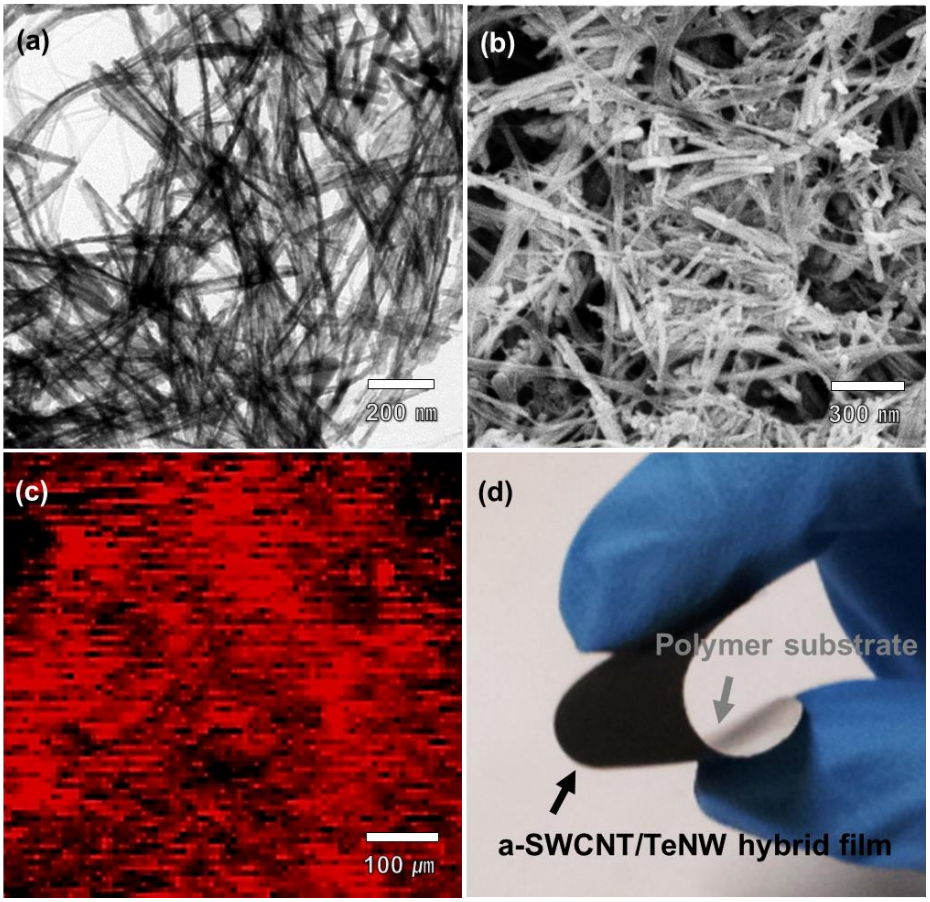

Fig. 4.6. (a) TEM, (b) FE-SEM, and (c) Raman mapping images of TeNW hybrid film with 2 wt% of a-SWCNT (Red dots in (c) indicate the intensity of G band peak at 1580 cm^{-1}). And (d) optical image of the hybrid film showing the flexibility

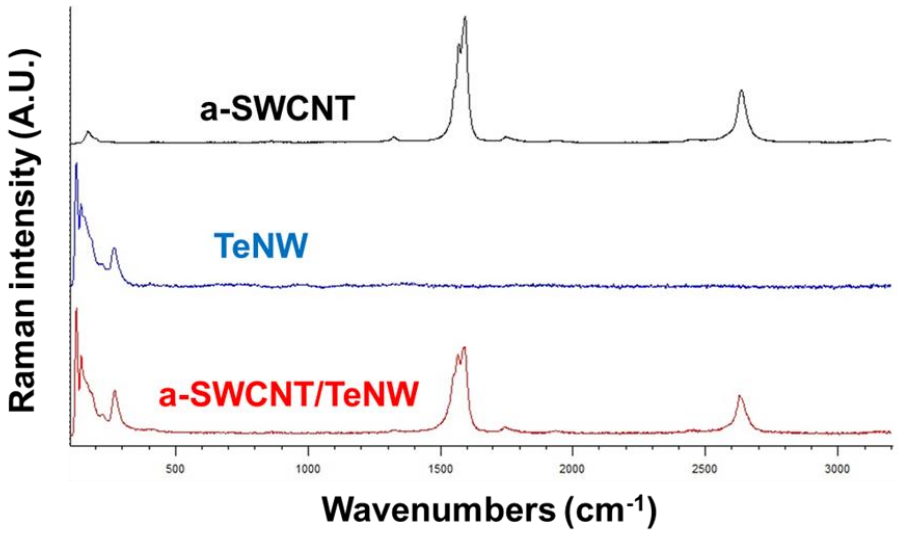

Fig. 4.7. Raman spectra of a-SWCNT, TeNW, and a-SWCNT/TeNW hybrid film

4.3.2 Work function control of SWCNT

In TE composites, the interfacial energy barrier between the two materials governs the transport of carriers across the interface. Shakouri and Bowers introduced the concept of carrier filtering in 1997, whereby the selective emission of hot electrons over interfacial barriers enhances the TE performance of inorganic semiconductor heterostructures.[34] This ensures that low energy carriers are filtered out within the narrow energy barrier, increasing the average potential energy of the carriers and thereby the thermopower of the material, with only a small decrease in its electrical conductivity. Several previous studies have shown how nanostructured interfaces can be introduced in organic-inorganic or organic-organic composites to possibly filter low-energy carriers.[28-30] In the present study, we controlled the height of the interfacial energy barrier between the SWCNTs and TeNWs by adjusting the work function of the SWCNTs via acid treatment. The acid treatment also provided well-dispersed SWCNT suspensions. Indeed, because of strong van der Waals interactions, pristine SWCNTs tend to agglomerate and do not disperse well in solvents, making hybridization with the TeNWs difficult.

Table 4.1 shows the electrical conductivity of SWCNTs prepared under different conditions with nitric acid. Because strong acids such as nitric/sulfuric mixture lead to the extensive formation of defects,[35] they

dramatically decrease the electrical conductivity of the SWCNTs; however, nitric acid by itself allows the electrical conductivity, work function, and dispersibility of the SWCNTs to be controlled as a function of the sonication time at RT. Short treatment time (2 h) with nitric acid

Samples	Electrical conductivity (S/m)	Thermopower (μV/K)	Carrier concentration (10^{20}/cm^3)	Carrier Mobility (cm^{2}v^{-1}s^{-1})	Work Function (eV)
p-SWCNT	5836	27	2.48	1.35	4.13
a-SWCNT (4h)	27596	20	2.67	6.42	4.72
a-SWCNT (8h)	3558	20	2.53	0.68	4.67

Table 4.1. Carrier transport characteristics of the purified SWCNT and acid-treated SWCNTs prepared under different conditions with nitric acid at room temperature.

ensures that oxide impurities on the surface of the bare SWCNTs are removed, leading to the purified SWCNTs (p-SWCNT). The electrical conductivity of the SWCNT treated with nitric acid for 4 h (a-SWCNT) is 4 times higher than that of p-SWCNT, because the acid treatment drastically reduces the junction resistance between individual tubes and bundles, thereby increasing hole mobility.[36] The carrier concentrations of a-SWCNT and p-SWCNT are similar, at 2.67×10^{20} and 2.48×10^{20} cm^{-3}, but the mobility in the former - and therefore the electrical conductivity - is 4 times higher than that of p-SWCNT. In accordance with these results, the O/C content ratio of a-SWCNT increases as shown in Fig. 4.8a. (The O/C content ratios were calculated from XPS data, based on the ratio of the integrated areas of the corresponding peaks corrected for sensitivity factors). However, further oxidation (8 h) with nitric acid leads to a decrease in the electrical conductivity, probably due to the formation of defects. Fig. 4.8b shows the UPS data recorded for the p-SWCNT and a-SWCNT, in order to investigate the influence of acid treatment on their work functions, as shown in Fig. 4.8c. The work function of p-SWCNT is 4.13 eV, leading to energy barriers of 0.82 eV with the TeNWs. On the other hand, a higher work function, 4.72 eV, is recorded for the a-SWCNT, which is ascribed to the presence of oxygen functional groups on their surface. Indeed, surface functional groups are known to disrupt π-conjugation and

introduce surface dipole moments, leading to higher work functions.[37-38] These results show first, that the SWCNT work function can be optimized by adjusting the duration and conditions of the acid treatment, and second, that the energy barrier between the TeNWs and SWCNTs can be reduced from 0.82 to 0.23 eV by reaction with nitric acid for 4 h.

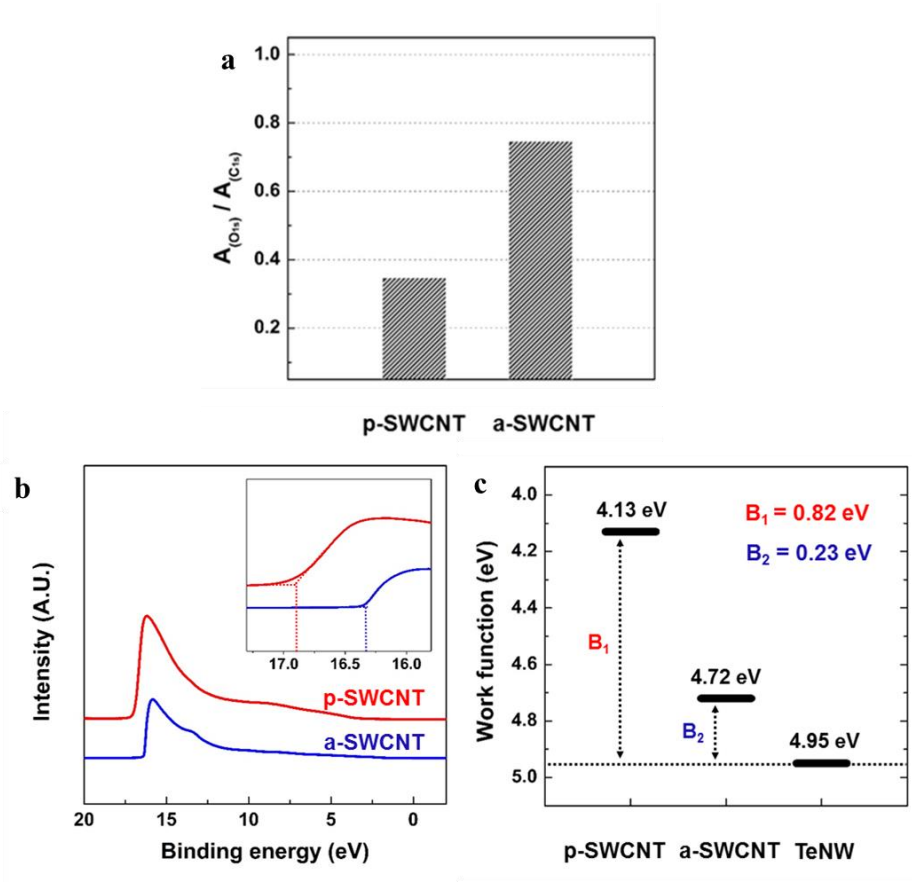

Fig. 4.8. (a) O/C area ratios, (b) UPS spectra, and (c) calculated work functions of the p-SWCNT and a-SWCNT

4.3.3 Thermoelectric properties of binary hybrid film

In order to study the effect of a-SWCNT doped into the TeNW matrix on TE properties of the hybrid film, we prepared the pure TeNW film as a control and a-SWCNT/TeNW hybrid film with the interfacial barrier energy of 0.23 eV. Fig. 4.9 shows the electrical conductivity, thermopower, and power factor of a-SWCNT/TeNW hybrid films as a function of their a-SWCNT content. The electrical conductivity and thermopower of the TeNW film without a-SWCNT are 4 S/m and 560 μV/K, respectively, in agreement with values reported in the literature.[29] The electrical conductivity of the films increases with the a-SWCNT content of the TeNW matrix, but their thermopower decreases. This behavior is typical of TE materials.[2] The thermopower is inversely proportional to the carrier concentration, which is directly proportional to the electrical conductivity, such that increasing the electrical conductivity decreases the thermopower. The power factor, $S^2\sigma$ (see equation 1), is the key to identify the optimum a-SWCNT content of the films. Fig. 4b shows the higher power factor of a-SWCNT/TeNW hybrid film than that of pure TeNWs in the range of 0.5 ~ 3 wt% a-SWCNT content, which is consistent with the results reported in the previous literature.[39] As the a-SWCNT content increases up to 10 wt%, more electrical paths among the SWCNTs form, thereby taking after TE properties of pure a-SWCNT. The maximum power factor, 3.40 $\mu W \cdot m^{-1} \cdot K^{-2}$ at RT, obtained for the hybrid film

containing 2 wt% of a-SWCNT, is approximately 3 times higher than the power factor of pure TeNWs. This enhanced power factor of the hybrid film is due to the doping

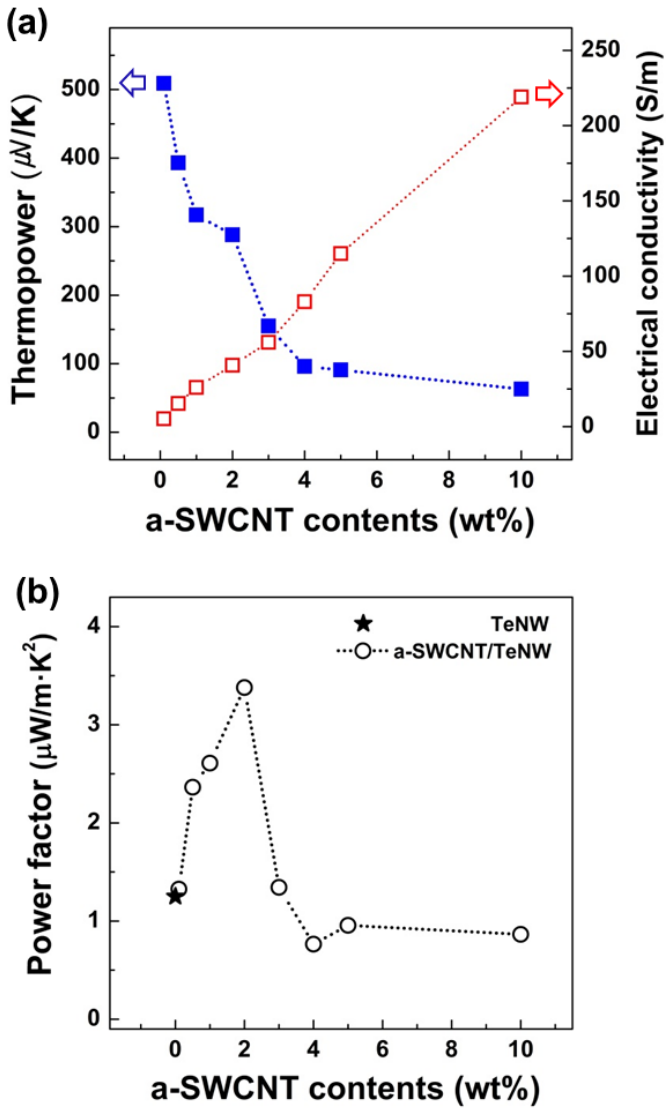

Fig. 4.9. (a) Electrical conductivity and thermopower, and (b) Power factor of a-SWCNT/TeNW hybrid films as a function of a-SWCNT content.

with the optimum a-SWCNT content. Furthermore, this enhancement may contain the synergetic effect, which is an energy filtering at the a-SWCNT-TeNW interfaces. Since the origin of the drastic power factor of the a-SWCNT/TeNW films is of great interest, we investigated the transport characteristics of the hybrid films to demonstrate this energy filtering effect. In addition, the mechanical stability of the hybrid film was characterized for practical application. Fig. 4.10 shows the relative power factor of the films as a function of bending cycles. While the pure TeNW film shows 70% decrease after 1000 bending cycles, the 2 wt% a-SWCNT/TeNW hybrid films shows much less decrease of 30%. It is because of the mechanical strength and high aspect ratio of the a-SWCNT that support the TeNW network.

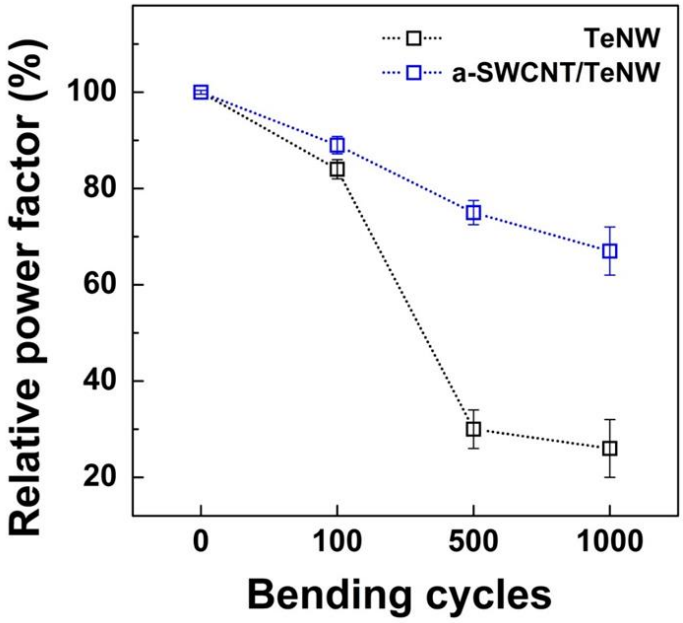

Fig. 4.10. Relative power factor of the films as a function of bending cycles

4.3.4 Demonstration of carrier filtering at hybrid interfaces

We used Hall measurements of the carrier concentration and mobility in the TeNW and a-SWCNT/TeNW hybrid films to understand the link between the thermopower and electrical conductivity. Table 4.2 shows the transport parameters of pure TeNW and TeNW hybrid films with 2 wt% a-SWCNT. Pure TeNWs have a low electrical conductivity and a high thermopower based on low carrier concentration of 2.01×10^{18} cm^{-3} and mobility of 0.46 $cm^2v^{-1}s^{-1}$. On the other hand, a-SWCNT/TeNW hybrid films show the higher electrical conductivity and lower thermopower than those of the pure TeNW, which is ascribed to the higher carrier concentration of 6.35×10^{18} cm^{-3}. In the energy filtering effect, low-energy carriers are preferentially scattered by the potential barrier at the interface between the two materials, whereas high-energy carriers readily cross the barrier.[40] Basically, high-energy carriers can transfer more heat than low-energy carriers, thereby resulting in the increase of thermopower.[30,34] Therefore, it is of much importance to consider a scattering time and carrier mobility to demonstrate the energy filtering at the a-SWCNT-TeNW interfaces. We calculated the scattering time (defined as $\tau = \mu \cdot m^*/e$, where τ, μ and m^* is the scattering time, carrier mobility and effective mass of the carrier, respectively) from the measured carrier mobility. The hybrid films show shorter scattering time (0.58×10^{-16} s) and lower mobility (0.23 $cm^2v^{-1}s^{-1}$) than those of the pure TeNW (1.17×10^{-16} s and 0.46

$cm^2v^{-1}s^{-1}$, respectively), indicating that more scattering events are occurred in the hybrid film. These decreased carrier mobility and scattering time of the hybrid film can be an evidence of the energy

Transport parameters	TeNW	a-SWCNT/TeNW
Electrical conductivity (S/m)	4	41
Thermopower (μV/K)	559	288
Power factor ($\mu W/m \cdot K^2$)	1.25	3.40
Thermal conductivity ($W\ m^{-1}K^{-1}$)	0.28	0.26
Figure of merit, ZT at RT (10^{-3})	1.34	3.92
Carrier concentration ($10^{18}/cm^3$)	2.01	6.35
Carrier Mobility ($cm^2v^{-1}s^{-1}$)	0.46	0.23
Hall coefficient ($10^{-6}m^3k^{-1}$)	3.13	0.99
Scattering time (10^{-16}s)	1.17	0.58
Work function barrier (eV)	-	0.23

Table 4.2. Transport parameters of the pure TeNW and a-SWCNT/TeNW hybrid films

filtering at the a-SWCNT-TeNW interfaces with the interfacial barrier energy of 0.23 eV.

For more quantitative interpretation of our TE data, we calculated the thermopower according to the Drude model. The thermopower is described by equation 2.

$$S = \frac{8\pi^2 {K_B}^2}{3eh^2} \cdot m^* \cdot T \cdot \left(\frac{\pi}{3n}\right)^{2/3} \qquad (2)$$

where K_B, h, n, m* and T is the Boltzmann constant, Plank constant, carrier concentration, effective mass of the carrier and absolute temperature, respectively. The calculated thermopower (S_c) relates to the carrier concentration without considering the energy filtering effect, whereas the measured thermopower (S_m) includes the enhancement arising from energy-dependent carrier scattering. Therefore, the ratio of these two parameters allows the energy filtering effect to be quantified. Table 4.3 shows the measured and calculated thermopower of the pure TeNW and hybrid films. The S_c and S_m values of the pure TeNW are very similar, thus showing only 1 % difference, which means that there is no synergetic effect. On the other hand, the S_m of the hybrid film is 12 % higher than S_c. This enhanced thermopower provides a solid evidence for synergetic energy filtering effect at the a-SWCNT-TeNW interfaces.

Samples	S (μV/K)		$(\frac{Sm-Sc}{Sc})$	Power factor
	Measured	Calculated	$\times 100$	($\mu W/m \cdot K^2$)
TeNW	559	555	1 %	1.25
a-SWCNT/TeNW	288	258	12 %	3.40
p-SWCNT/TeNW	378	423	-11 %	0.86

Table 4.3. Measured and calculated thermopower of the pure TeNW, a-SWCNT/TeNW and p-SWCNT/TeNW hybrid films

4.3.5 Effect of barrier height at the interfaces on TE properties

Although we confim the energy filtering effect at the a-SWCNT-TeNW interfaces with the interfacial barrier energy of 0.23 eV as mentioned above, it still needs further discussion about the degree of synergetic effect as a function of the barrier height between the SWCNTs and TeNWs. We hybridized the TeNWs with the purified SWCNT (p-SWCNT) to get a higher barrier height of 0.82 eV, and compared them with a-SWCNT/TeNW film with the 0.23 eV barrier height. As shown in Fig. 4.11a, the a-SWCNT/TeNW hybrid film has a higher electrical conductivity than the p-SWCNT/TeNW film with the same SWCNT content. This is probably due to the higher electrical conductivity of the as-prepared a-SWCNT. As expected, Fig. 4.11b shows that the thermopower of the a-SWCNT/TeNW film is slightly lower than that of the film prepared with the same concentration of p-SWCNT. As a result, the a-SWCNT/TeNW hybrid film has a higher power factor than the p-SWCNT/TeNW film at the same SWCNT content (Fig. 4.11c). It is because the a-SWCNT/TeNW film has the relatively high thermopower with increasing electrical conductivity compared with the p-SWCNT/TeNW film. Fig. 4.11d shows the thermopower of the two hybrid films as a function of their electrical conductivity. It is noteworthy that for electrical conductivities ranging from 10 to 50 S/m, the a-SWCNT/TeNW hybrid films show a significant higher thermopower than those prepared with p-SWCNT. This points toward more effective energy filtering at the a-SWCNT-TeNW interfaces due to lower energy barrier of 0.23 eV.

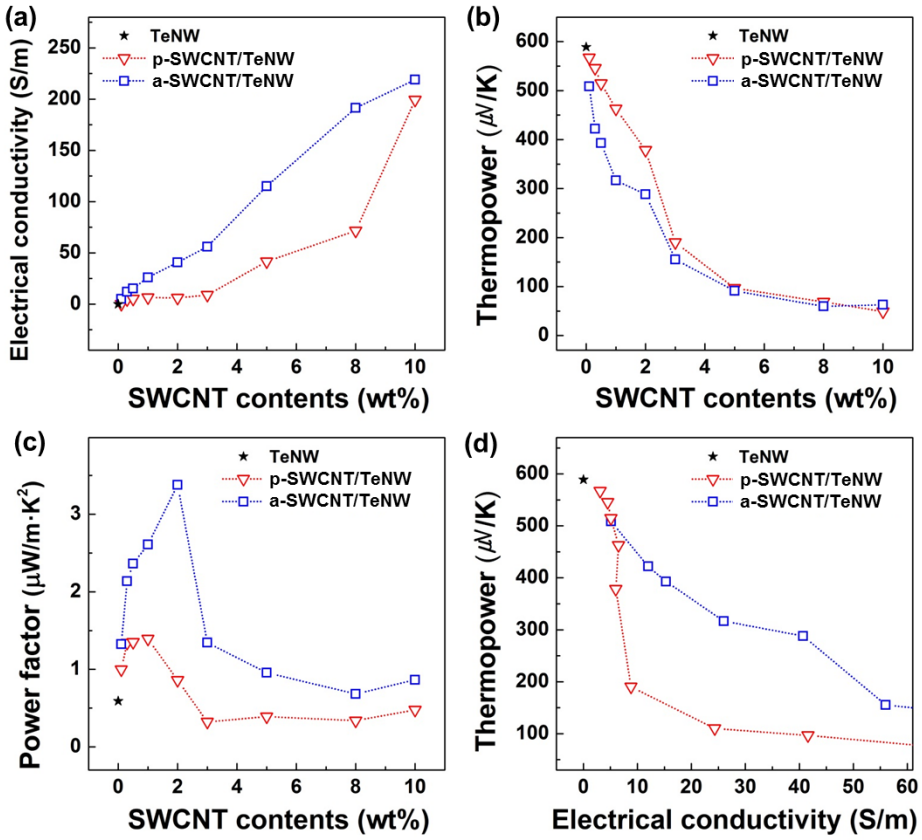

Fig. 4.11. (a) Electrical conductivity, (b) Thermopower, and (c) Power factor of SWCNT/TeNW hybrid films as a function of SWCNT content, and (d) Thermopower of the hybrid film as a function of electrical conductivity

The alignment of the SWCNT and TeNW bands is illustrated in Fig. 4.12. TeNWs form a degenerate semiconductor with a narrow band gap of 0.33 eV in which the Fermi level is positioned close to the valence band.[41] The work function of these TeNWs is assumed to be the same as that of bulk Te.[41] Moreover, the Fermi level of doped SWCNTs is known to be within the valence band.[42] The equilibrium band diagram in Fig. 6a for the p-SWCNT/TeNW hybrid film indicates that the 0.82 eV energy barrier scatters most charge carriers, reducing carrier transfer, the thermopower, and the power factor of this composite. For the a-SWCNT/TeNW hybrid film in contrast, Fig. 6b shows that low-energy carriers are filtered out by the 0.23 eV potential barrier while high-energy carriers readily cross the interface. The 4-fold enhancement of the power factor for the a-SWCNT/TeNW composite are therefore attributed to effective energy filtering at the a-SWCNT-TeNW interfaces. It is worth mentioning that a more precise control of the SWCNT work function and more precise measurements thereof could allow the energy filtering effect to be exploited at other carbon-inorganic semiconductor interfaces. Furthermore, although the TeNWs used in this study to fabricate the hybrid films were introduced immediately after synthesis, an oxide layer may have formed on their surface, increasing the energy barrier for charge transfer in the a-SWCNT/TeNW hybrid films. For further improvements therefore, one should look to increase the work function of the SWCNTs beyond 4.72 eV to lower the energy barrier at the SWCNT-TeNW interfaces, to develop a passivation layer to protect the TeNWs

from oxidation, and to increase the thermoelectric properties of the TeNWs themselves.

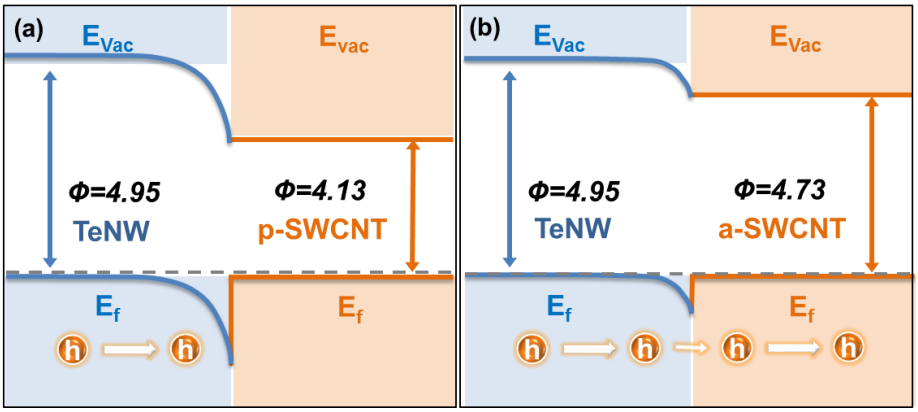

Fig. 4.12. Energy diagrams of (a) p-SWCNT/TeNW and (b) a-SWCNT/TeNW hybrid films

4.4 Conclusions

In summary, we have prepared flexible SWCNT-doped TeNW hybrid films and demonstrated how optimizing the SWCNT work function affords significant improvements in their thermopowers and power factors. The SWCNT work function was controlled by acid treatment, the duration of which was optimized to lower the interfacial energy barrier between the SWCNTs and TeNWs. The power factor (3.40 $\mu W \cdot m^{-1} \cdot K^{-2}$ at RT) of the a-SWCNT/TeNW film with the interfacial barrier energy of 0.23 eV is increased 3-fold, due to the doping of optimum a-SWCNT content into the TeNW matrix, compared to the pure TeNW film. Furthermore, this enhancement is also attributed to 12 % enhanced energy filtering at the a-SWCNT-TeNW interfaces, where low-energy carriers are filtered out leaving only high-energy carriers to cross the barrier. Because high-energy carriers transfer more heat than low-energy ones, this filtering increases the measured thermopower of the material. However, the relatively large energy barrier (0.82 eV) in the p-SWCNT/TeNW hybrid film leads to reduced carrier transfer and therefore to a low thermopower and power factor. We believe that the strategy proposed here to improve the performance of flexible thermoelectric materials by optimizing carrier transfer at the carbon-inorganic semiconductor interfaces shows a great potential for other applications, notably for the preparation of flexible/or wearable power conversion devices.

4.5 References

1. Bell LE. Cooling, heating, generating power, and recovering waste heat with thermoelectric systems. *Science* **321**, 1457-1461 (2008).
2. Snyder GJ*, et al.* Complex thermoelectric materials. *Nat. Mater.* **7**, 105-114 (2008).
3. Yang J*, et al.* Rational Design of Advanced Thermoelectric Materials. *Adv. Energy Mater.* **3**, 549-565 (2013).
4. Bux SK*, et al.* Nanostructured materials for thermoelectric applications. *Chem. Commun. (Camb.)* **46**, 8311-8324 (2010).
5. Sootsman JR*, et al.* New and old concepts in thermoelectric materials. *Angew. Chem. Int. Ed. Engl.* **48**, 8616-8639 (2009).
6. Zebarjadi M*, et al.* Perspectives on thermoelectrics: from fundamentals to device applications. *Energy & Environ. Sci.* **5**, 5147-5162 (2012).
7. Hicks L*, et al.* Effect of quantum-well structures on the thermoelectric figure of merit. *Phys. Rev. B* **47**, 12727-12731 (1993).
8. Dresselhaus MS*, et al.* New Directions for Low-Dimensional Thermoelectric Materials. *Adv. Mater.* **19**, 1043-1053 (2007).
9. Poudel B*, et al.* High-thermoelectric performance of nanostructured bismuth antimony telluride bulk alloys. *Science* **320**, 634-638

(2008).

10. Minnich AJ, *et al.* Bulk nanostructured thermoelectric materials: current research and future prospects. *Energy & Environ. Sci.* **2**, 466-479 (2009).

11. Zide J, *et al.* Demonstration of electron filtering to increase the Seebeck coefficient in In0.53Ga0.47As/In0.53Ga0.28Al0.19As superlattices. *Phys. Rev. B* **74**, 205335 (2006).

12. Zebarjadi M, *et al.* Power Factor Enhancement by Modulation Doping in Bulk Nanocomposites. *Nano Letters* **11**, 2225-2230 (2011).

13. Yadav A, *et al.* Fiber-based flexible thermoelectric power generator. *J. Power Sources* **175**, 909-913 (2008).

14. Francioso L, *et al.* Flexible thermoelectric generator for ambient assisted living wearable biometric sensors. *J. Power Sources* **196**, 3239-3243 (2011).

15. Dubey N, *et al.* Conducting polymers: Efficient thermoelectric materials. *J. Polym. Sci., Part B: Polym. Phys.* **49**, 467-475 (2011).

16. Zhang K, *et al.* Enhancing thermoelectric properties of organic composites through hierarchical nanostructures. *Sci. Rep.* **3**, 3448 (2013).

17. Bubnova O, *et al.* Optimization of the thermoelectric figure of merit in the conducting polymer poly(3,4-ethylenedioxythiophene). *Nat.*

Mater. **10**, 429-433 (2011).

18. Hone J*, et al.* Thermoelectric power of single-walled carbon nanotubes. *Phys. Rev. Lett.* **80**, 1042 (1998).
19. Zuev YM*, et al.* Thermoelectric and Magnetothermoelectric Transport Measurements of Graphene. *Phys. Rev. Lett.* **102**, 096807 (2009).
20. Tan X*, et al.* Thermoelectric properties of small diameter carbon nanowires. *Carbon* **53**, 286-291 (2013).
21. Kim SL*, et al.* Flexible Power Fabrics Made of Carbon Nanotubes for Harvesting Thermoelectricity. *Acs Nano* **8**, 2377-2386 (2014).
22. Bubnova O*, et al.* Towards polymer-based organic thermoelectric generators. *Energy & Environ. Sci.* **5**, 9345-9362 (2012).
23. Yu C*, et al.* Thermoelectric behavior of segregated-network polymer nanocomposites. *Nano letters* **8**, 4428-4432 (2008).
24. Kim D*, et al.* Improved Thermoelectric Behavior of Nanotube-Filled Polymer Composites with Poly(3,4-ethylenedioxythiophene) Poly(styrenesulfonate). *Acs Nano* **4**, 513-523 (2009).
25. Hewitt CA*, et al.* Multilayered carbon nanotube/polymer composite based thermoelectric fabrics. *Nano letters* **12**, 1307-1310 (2012).
26. Zhang B*, et al.* Promising thermoelectric properties of commercial PEDOT: PSS materials and their Bi_2Te_3 powder composites. *ACS applied materials & interfaces* **2**, 3170-3178 (2010).

27. Du Y, *et al.* Research progress on polymer–inorganic thermoelectric nanocomposite materials. *Prog. Polym. Sci.* **37**, 820-841 (2012).

28. Yu C, *et al.* Light-Weight Flexible Carbon Nanotube Based Organic Composites with Large Thermoelectric Power Factors. *Acs Nano* **5**, 7885-7892 (2011).

29. See KC, *et al.* Water-processable polymer-nanocrystal hybrids for thermoelectrics. *Nano Lett.* **10**, 4664-4667 (2010).

30. He M, *et al.* Thermopower enhancement in conducting polymer nanocomposites via carrier energy scattering at the organic–inorganic semiconductor interface. *Energy & Environ. Sci.* **5**, 8351 (2012).

31. Xi GC, *et al.* Large-scale synthesis, growth mechanism, and photoluminescence of ultrathin Te nanowires. *Cryst. Growth Des.* **6**, 2567-2570 (2006).

32. Wang Q, *et al.* Low-Dimensional Te-Based Nanostructures. *Adv. Mater.*, **25**, 15-21 (2013).

33. Ma J, *et al.* Growth of tellurium nanowire bundles from an ionic liquid precursor. *Cryst. Eng. Comm.* **13**, 2774-2778 (2011).

34. Shakouri A, *et al.* Heterostructure integrated thermionic coolers. *Appl. Phys. Lett.* **71**, 1234 (1997).

35. Datsyuk V, *et al.* Chemical oxidation of multiwalled carbon nanotubes. *Carbon* **46**, 833-840 (2008).

36. Nirmalraj PN, *et al.* Electrical connectivity in single-walled carbon nanotube networks. *Nano letters* **9**, 3890-3895 (2009).

37. Ago H, *et al.* Work Functions and Surface Functional Groups of Multiwall Carbon Nanotubes. *The Journal of Physical Chemistry B* **103**, 8116-8121 (1999).

38. Tey J, *et al.* Effect of doping on single-walled carbon nanotubes network of different metallicity. *Nanoscale Res Lett* **7**, 1-7 (2012).

39. Choi J, *et al.* Enhanced thermoelectric properties of the flexible tellurium nanowire film hybridized with single-walled carbon nanotube. *Synth. Met.* **198**, 340-344 (2014).

40. Narducci D, *et al.* Impact of energy filtering and carrier localization on the thermoelectric properties of granular semiconductors. *J. Solid State Chem.* **193**, 19-25 (2012).

41. Niles DW, *et al.* A photoemission determination of the band diagram of the Te/CdTe interface. *J. Appl. Phys.* **77**, 4489-4493 (1995).

42. Kim KK, *et al.* Fermi level engineering of single-walled carbon nanotubes by AuCl3 doping. *J. Am. Chem. Soc.* **130**, 12757-12761 (2008).

Chapter 5. Designing the work functions of Te nanowire / PEDOT:PSS /graphene ternary hybrid for effective mobility engineering at hybrid interfaces

5.1 Research backgrounds

Thermoelectric (TE) materials, harvesting electrical energy directly from temperature gradients, have attracted tremendous attention due to their potentials for realizing next-generation power generators and waste-heat-recovery systems[1-3]. Many attempts have been made to improve the TE materials' efficiency[4-6], which is quantified by the dimensionless figure-of-merit, $ZT = S^2\sigma T/\kappa$, where S, σ, κ, and T are, respectively, the thermopower, the electrical conductivity, the thermal conductivity, and the absolute temperature[1]. In particular, inorganic semiconductors with narrow band-gap for a large S, for example, the bismuth-tellurium-antimony-selenium (Bi-Te-Sb-Se) alloy family[7], and state-of-the-art nanostructures, including superlattices[8], quantum dots[9], and nano-inclusions[10], have been thoroughly investigated. In the engineered structures, interfacial phonon scattering and energy-dependent carrier scattering have been useful for reducing κ and increasing S, respectively,

thus enhancing ZT to values exceeding 1 at 300 K[11-13]. However, the mechanical endurance of TE modules based on inorganic semiconductors cannot be guaranteed owing to their brittleness, and with their energy-intensive process, exquisite or large-area flexible TE device are inconceivable[14]. As possible candidate for flexible TE materials, conducting polymers, carbon nanotubes, and their hybrid composites have been recently investigated because of their unique advantages including facile processability, scalability, and flexibility as well as low cost and weight[15, 16]. Although the performance of flexible TE materials has significantly improved, the high performance has mainly been due to polymers with high electrical conductivity such as PEDOT:PSS[17-19]. However, TE materials based on PEDOT:PSS are sensitive to humidity in ambient conditions, resulting in a limitation for practical applications.

In this study, we demonstrate for the first time a rationally designed graphene/polymer/inorganic nanocrystal free-standing paper with high-TE performance, high-flexibility, and mechanical/chemical durability. A hybrid design employing high-*S* inorganic and high-σ conducting constituents could be a potential facile strategy for improving both *S* and σ of the hybrid material[14, 20], but unfortunately, the power factor ($S^2\sigma$) of typical hybrids does not exceed those of the individual constituents[21, 22]. Interestingly, carrier-energy filtering at hybrid heterojunctions has been considered as a remedy to mitigate this

limitation[6, 23]. The energy filtering effect was originally proposed for superlattices where alternate energy barrier layers could act as energy filters[24, 25]. It has been successfully extended to bulk inorganics with nanoparticles[26, 27] and organic-inorganic hybrids[28, 29]. In this study, we rationally design the ternary hybrid paper of reduced graphene oxide (rGO)/PEDOT:PSS/tellurium nanowire (TeNW): It consists of two heterojunctions at rGO/PEDOT:PSS and PEDOT:PSS/TeNW, and demonstrates that the two interfaces could act as energy filters to scatter low-energy carriers. TE hybrids with two heterojunctions with controlled interfacial energy barriers show a significantly increased σ without a major decrease in *S*, thus leading to an enhanced power factor of 143 $\mu W \cdot m^{-1} \cdot K^{-1}$ and the maximum ZT of 0.2 at 300 K, which could be attributed to the double energy filtering at two junctions. These energy filtering effects are also systematically analyzed by carrier transport characteristics such as carrier concentration, carrier mobility, and scattering time. Furthermore, owing to outstanding mechanical and barrier properties of rGO, the hybrids exhibit not only high flexibility but also excellent mechanical and chemical durability. Using this hybrid paper and polyethyleneimine (PEI)-doped single-walled carbon nanotube (SWCNT) as p-type and n-type TE unit, respectively, we prepared a prototype flexible TE device and obtained a power density of 650 $nW \cdot cm^{-2}$ at the temperature difference (ΔT) of 50 K.

5.2 Experimental

5.2.1 Synthesis of PEDOT:PSS coated Te nanowires

TeNW was synthesized by using a previously reported surfactant-assisted chemical reduction method.[30] In the typical procedure, 57 mmol L-ascorbic acid and 2 mmol CTAB were dissolved in 400 ml distilled water for 1 h to form a clear solution, followed by addition of 2.5 mmol Na_2TeO_3 under vigorous stirring. The obtained white suspension was heated to 90 °C and maintained at this temperature for 20 h. Then, the resulting reaction mixture was cooled down to 25 °C naturally, and the precipitate was retrieved by centrifugation. The product was washed several times with distilled water and absolute ethanol in order to remove side products and residual reagents, and then freeze-dried for 2 days. To obtain DTe, 5 ml of 1 wt% PEDOT:PSS solution instead of CTAB was added into the reaction mixture containing 5 vol% of dimethyl sulfoxide during the synthesis procedure of TeNW. To control the amount of PEDOT:PSS in DTe, the loading content of the 1 wt% PEDOT:PSS solution was varied from 1 to 6 ml. After washing with distilled water several times, the as-prepared DTe hybrid film was freeze-dried for 2 days.

5.2.2 Preparation of ternary hybrid film

GO was synthesized from natural graphite powder (Bay Carbon, SP-1 graphite) through a previously reported with an oxidation procedure by using $KMnO_4$ and a 9:1 mixture of concentrated H_2SO_4/H_3PO_4.[31] HI (57 wt% in water, Sigma-Aldrich) was used as a reducing agent for chemical graphitization of GO-based films.

As-prepared GO suspension and DTe were re-dispersed in water by a sonication process to obtain 0.05 wt% GO and DTe aqueous solutions, respectively. Both GO and DTe solutions were mixed together, followed by sonication for 0.5 h and vigorous agitation for several hours to get a homogeneous GO-DTe suspension. The GO-DTe films were then prepared by vacuum-filtering the mixed suspensions through anodic membrane filters (Whatman) with 45 mm diameter and 0.2 μm average pore size. The resulting films were carefully peeled off from the filter membrane, and then dried in air for 24 h and in vacuum for 6 h. To fabricate GDTe hybrid papers, the free-standing GO-DTe films were treated with vapor-phase HI at 40 °C for chemical graphitization of the GO phase in hybrids.[32] After treatment with HI vapor, the resulting GDTe paper with a thickness of about 20 μm was rinsed with a small amount of methanol, saturated sodium bicarbonate, and then water, followed by drying overnight in ambient conditions.

5.2.3 Preparation of flexible thermoelectric generator

The TE device was fabricated using the $G_{0.1}DTe_{0.9}$ paper and PEI-doped SWCNT film as the p-type and n-type components, respectively. Five pairs of as-prepared GDTe paper and PEI-SWCNT film with a dimension of 2 × 1 cm were alternated with insulating layers as shown in Figure S11a. Each unit was electrically connected in series by Au paste. The power density of the device was measured by using a hand-made system.

5.2.4 Characterizations

The microstructure morphology of the as-prepared samples was identified by FE-SEM (JSM-6701F, JEOL), TEM (CM-30, Philips) with energy dispersive X-ray spectroscopy (EDS), and HR-TEM (Tecnai F20, FEI) with SAED patterns. XRD (D8 ADVANCE, Bruker) patterns of the samples were recorded using Cu-Kα radiation and then compared with the SAED patterns. X-ray photoelectron spectroscopy (XPS) and UPS (PHI-5000 VersaProbe, ULVAC-PHI**)** using a monochromatic Al-Kα and He source, respectively, were performed in order to obtain the chemical information and work function of the as-prepared samples. The TE properties of the as-prepared films deposited on glass substrates with a dimension of 2 × 2 cm were analyzed by measuring σ, *S*, and thermal conductivity at room temperature. The in-plane σ and *S* of the samples were simultaneously measured using a four-point probe SEEPEL TE

measurement system (TEP 600, Seepel instrument), and the average of at least ten measurements results was calculated. The measured σ was compared with the values obtained using a semi-automatic four-point probe surface resistance meter (Cresbox, Napson). The average of at least five measurement results for the carrier concentration and mobility determined by Hall measurements (HMS-3000, Ecopia) with 0.55 T and 1 mA, was calculated. The in-plane thermal conductivity of the sample was obtained from the thermal diffusivity measured using a laser flash system (LFA 457 NanoFlash, Netzsch), the specific heat measured using differential scanning calorimetry (DSC) (DSC7, PerkinElmer) and the density of the sample. The thickness of films was determined using a micrometer (Mitutoyo, 1 μm accuracy), and the average of more than five measurement results was calculated. The mechanical stability was evaluated by studying the TE properties as a function of the bending angle by observing change in σ and *S* values before and after bending at different angles. The performance durability on the bending cycle was measured by repeatedly bending the sample at the rate of one cycle per second, by using a home-made two-point-bending holder: the sample was bent to the maximum angle of 86° and then released in each cycle. In order to ensure reliability in performance durability test, the average performance of each sample was obtained from three random measurements.

5.3 Results and discussion

5.3.1 Preparation of ternary hybrid film

Hybrid systems designed to exploit the advantages of each component have led to enhanced TE performances. In this study, TeNW with high *S* was passivated by PEDOT:PSS with high σ, thus resulting in a power factor higher than that of either the nanowire or polymer thin film due to the possibility of energy filtering at the interfaces between PEDOT:PSS and TeNW[28, 33]. However, this hybrid film was brittle, so we introduced a 2-D graphene derivative as a frame for stable flexibility. Additionally, the introduction of a graphene derivative has the potential benefit of further energy-dependent carrier filtering at the interfaces between PEDOT:PSS and the graphene derivative. Our rationally designed concept of flexible TE paper is illustrated in Fig. 5.1. First, we synthesized PEDOT:PSS-coated TeNWs (DTe) using the reported procedure and characterized its structural morphology (Fig. 5.2)[34, 35]. In the synthesis of DTe, the loading amount of 1 wt% PEDOT:PSS solution was varied from 1 to 6 ml in order to control the composition of the conductive PEDOT:PSS layer in the DTe. The weight fractions of PEDOT:PSS layers in DTe were linearly controlled in the range from 1.8 to 9.7 wt%, as determined by thermogravimetric analysis (TGA) measurement, with increases in the PEDOT:PSS loading content, and the optimized fraction was determined to be

8.1 wt% based on the TE properties of DTe. The synthesized DTe is 30-50 nm in diameter and 3 μm long on average, and the surface is

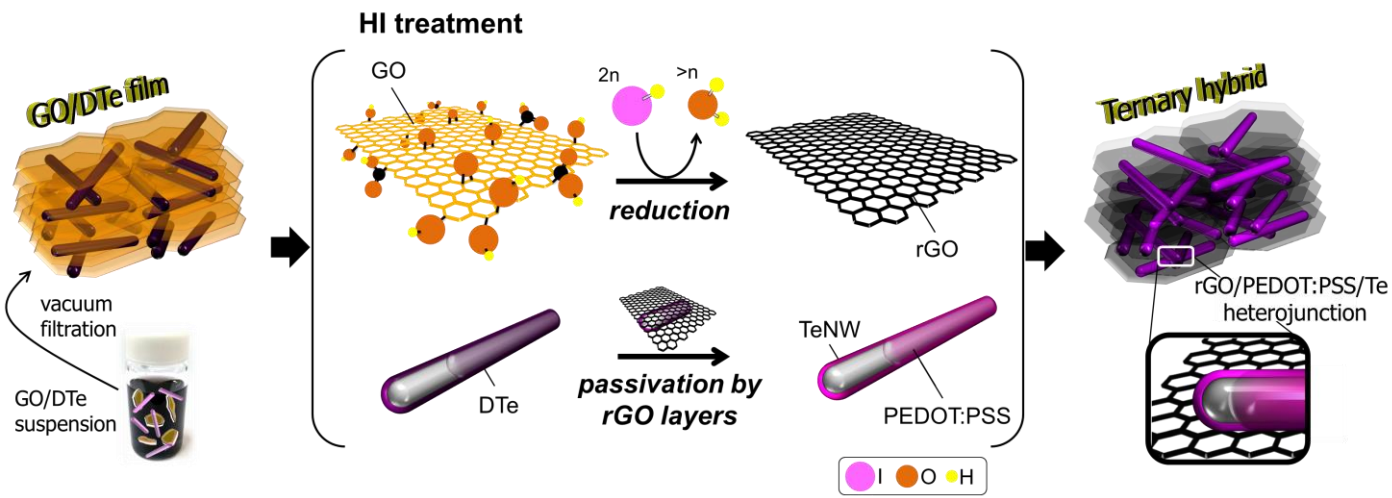

Fig. 5.1. Schematic illustration of our rationally designed TE hybrid paper

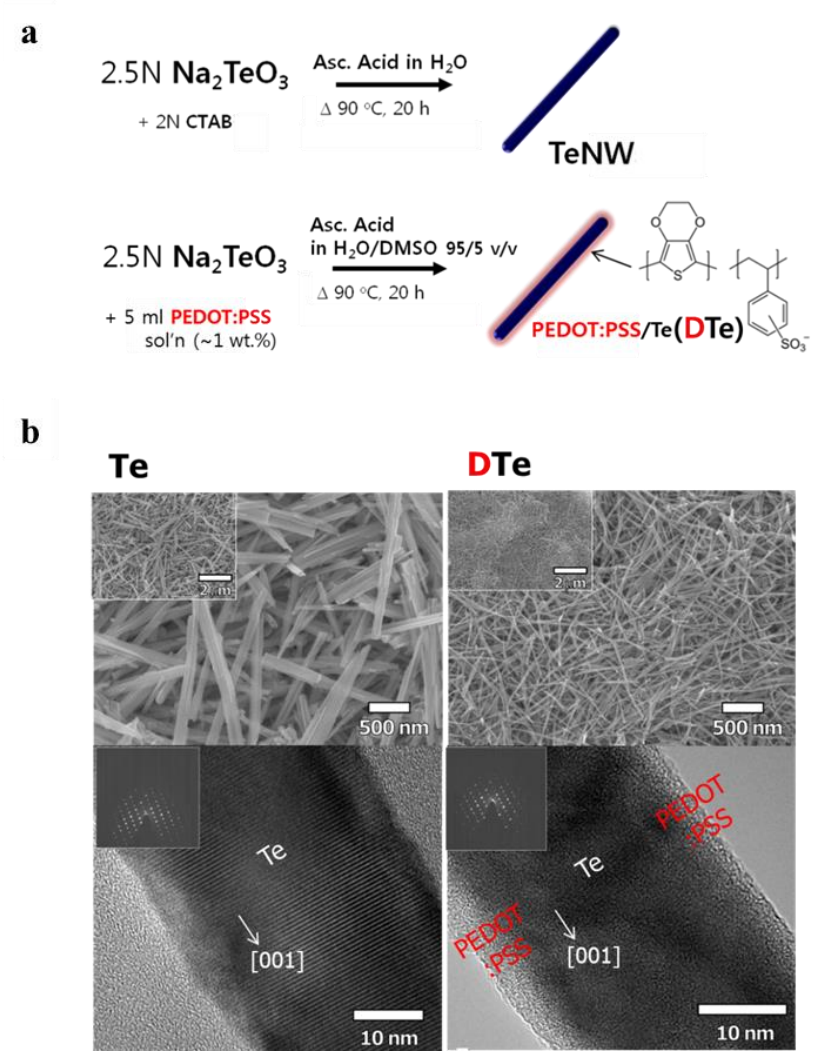

Fig. 5.2. (a) Synthesis of TeNWs and PEDOT:PSS passivated TeNWs (DTe) and (b) FE-SEM and TEM images (inset: SAED patterns) of TeNW and DTe

covered with a few-nanometer-thick PEDOT:PSS layer. Well-dispersed DTe in water was mixed with a graphene oxide (GO) aqueous solution and vacuum filtered. The as-prepared GO-DTe hybrid paper is 50 μm in thickness on average and shows great flexibility due to the mechanical strength of 2-D GO sheets. The GO-DTe paper constructed with GO layers and DTe shows porous microstructure (Fig. 5.3). The flexibility of the hybrid paper is strongly affected by the GO content in hybrid and more than 10 wt% of GO content ensures a high flexibility (Fig. 5.4). The GO-DTe paper with less than 10 wt% of GO is very brittle, so it is easily broken into small segments by bending or twisting.

After film formation, the GO-DTe paper should be reduced in order to enhance the TE properties because GO itself is an electronic insulator. Among various reduction methods, chemical reduction by the HI vapor was the most appropriate for our purpose. The GO film reduced by the HI vapor at 40°C shows a higher σ and relatively smoother surface without deformation than that reduced by hydrazine vapor (Fig. 5.5)[36]. However, as a very strong acid, HI is extremely harsh to inorganic materials such as a TeNW during the reduction process. As shown in Fig. 5.6, the electrical conductivity and thermopower of TeNW and DTe drastically decrease owing to exposure to the HI vapor, but the TE properties of GDTe hybrid paper remain almost unchanged. The rGO layers in the hybrid could effectively act as a sacrificial barrier to prevent the deformation of DTe from the HI vapor during the reduction process.

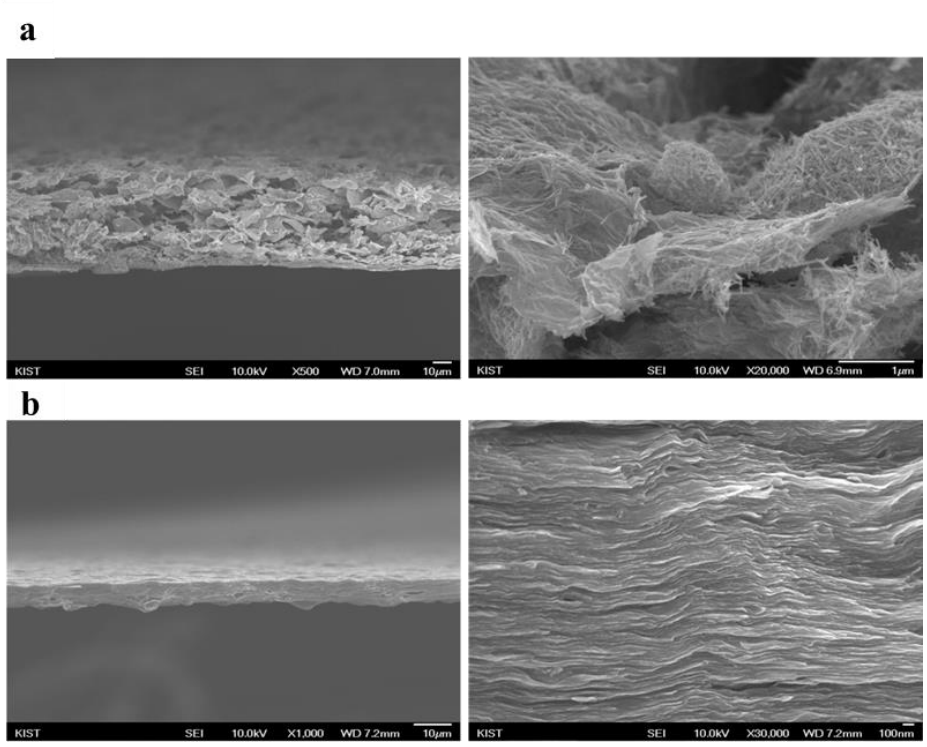

Fig. 5.3. Cross-sectional FE-SEM images of (a) $GO_{0.1}$-$DTe_{0.9}$ hybrid film and (b) rGO film

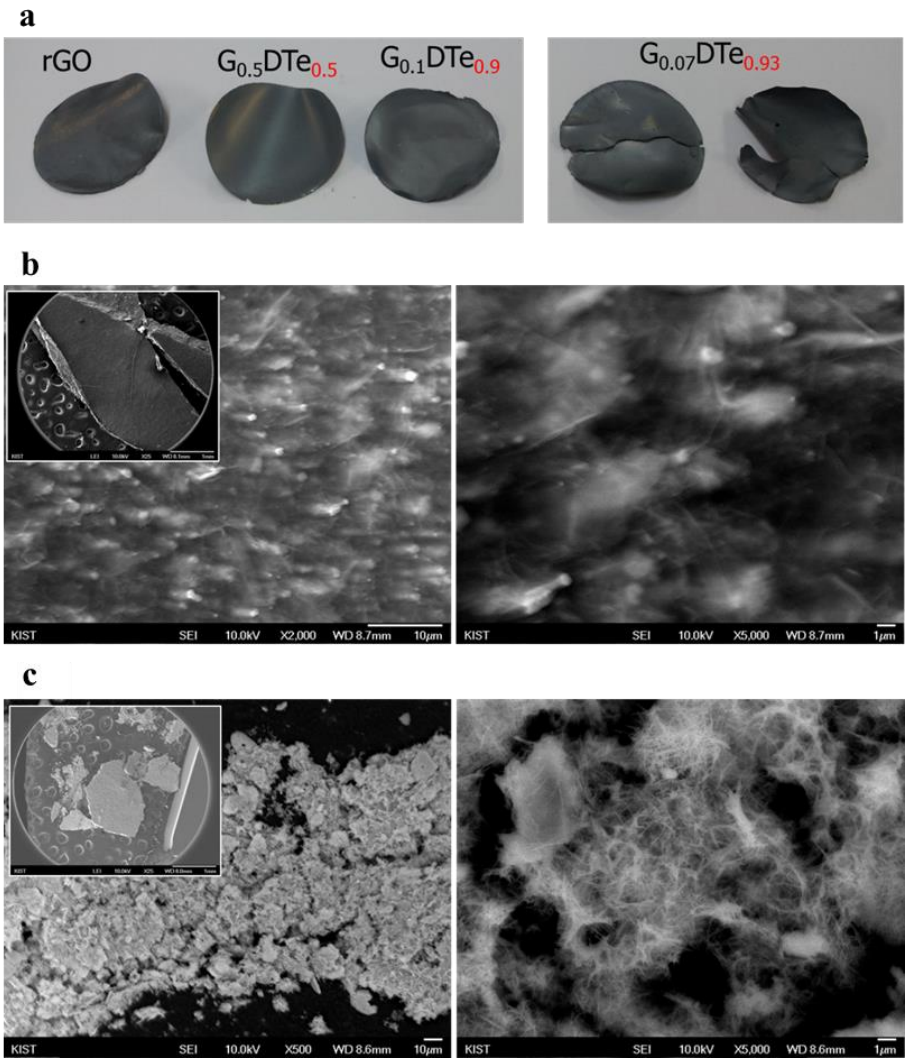

Fig. 5.4. (a) Photographs of G_xDTe_{1-x} hybrid paper with different rGO and DTe content. Note that x in G_xDTe_{1-x} is defined as mass fraction of GO loading content to total weight of hybrid constituents. (b) Surface SEM images of the $G_{0.1}DTe_{0.9}$ hybrid paper. (c) Surface SEM images of a cracked $G_{0.05}DTe_{0.95}$ hybrid paper

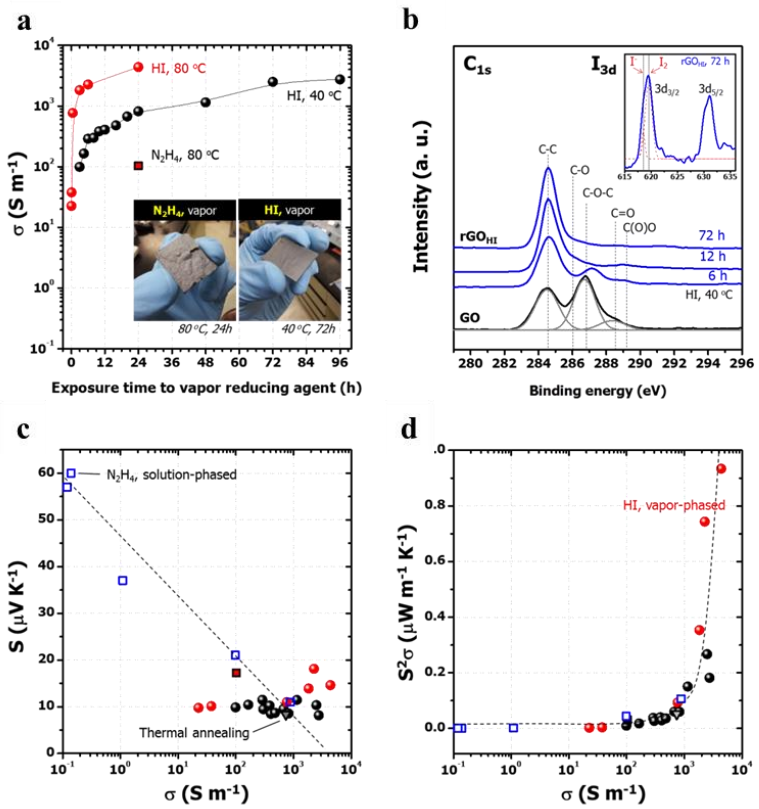

Fig. 5.5. (a) Electrical conductivity of rGO films reduced by HI vapor at 40 °C and 80 °C as a function of exposure time, compared with the rGO film reduced by hydrazine (N_2H_4) vapor at 80 °C for 24 h. (Inset: Photographs of the rGO films reduced by HI (40 °C, 72 h) and N_2H_4 (80 °C, 24 h), respectively). (b) XPS C_{1s} and (insert) I_{3d} peaks of GO and rGO films reduced by HI at 40 °C for various time. (c, d) Thermopower and power factor of rGO films reduced by various methods as a function of electrical conductivity. (Red circle: HI vapor at 80 °C, black circle: HI vapor at 40 °C, closed square: N_2H_4 vapor at 80 °C, open square: N_2H_4 solution with different contents of N_2H_4, open triangle: thermal reduction at 800 °C under nitrogen for 1 h)

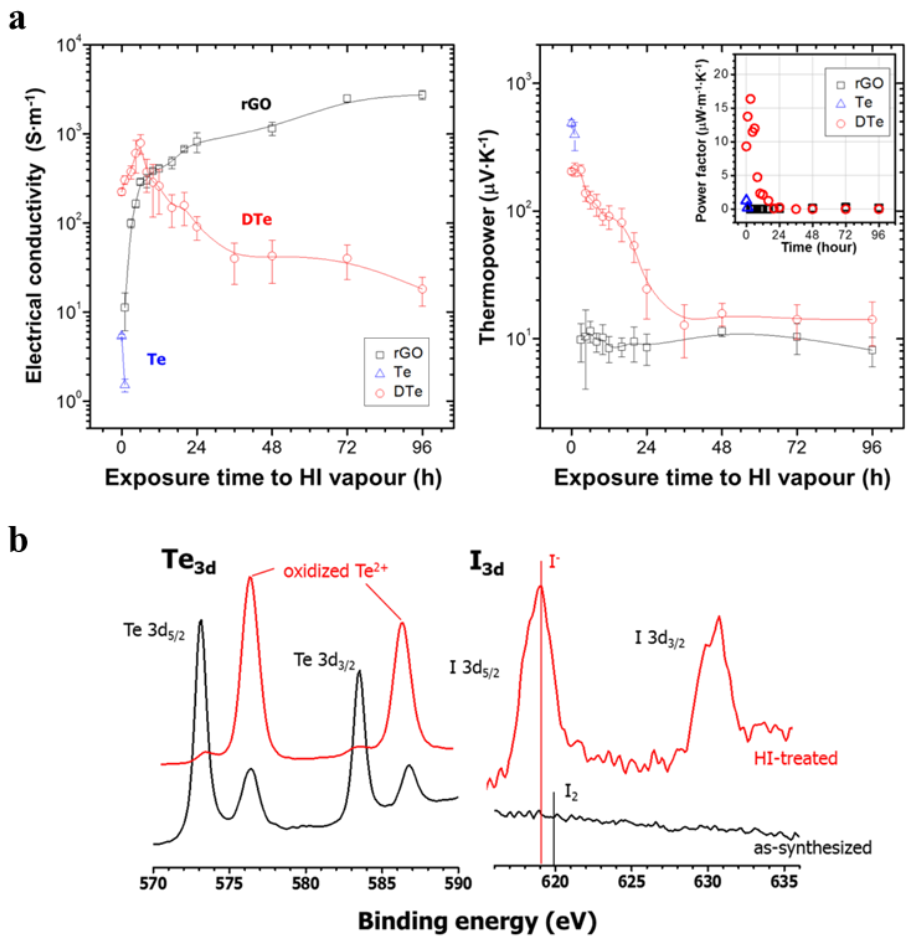

Fig. 5.6. (a, b) Electrical conductivity and thermopower of rGO, TeNW and DTe as a function of exposure time to HI vapor at 40 °C during reduction. (c) XPS Te_{3d} and I_{3d} peaks of the as-synthesized and HI-treated DTe at 40 °C for 12 h

Figure 5.7a shows the great flexibility of the GDTe hybrid paper and Figures 5.7b and c show the cross-sectional and surface scanning electron microscopy (SEM) images of the hybrid paper. These results indicate that the GDTe hybrid paper has a porous microstructure and hierarchically layered morphology composed of a few rGO layers with DTe randomly distributed between the layers. Additionally, these figures show that a few rGO layers effectively cover the DTe. Fig. 5.7d, e and f show the high-resolution transmission electron microscopy (HR-TEM) images of the GDTe paper and selected-area electron diffraction (SAED) pattern with X-ray diffraction (XRD) spectrum of the as-prepared DTe to identify the crystal structure of Te, respectively. The clear lattice fringes in the micrograph indicate that the nanowire is structurally uniform and single-crystalline. The interplanar spacing of ~5.9 Å corresponds to the distance between (001) lattice planes in hexagonal Te, as reported previously in the literature[35]. (More detailed morphology data of GDTe hybrid paper are given in Fig. 5.8)

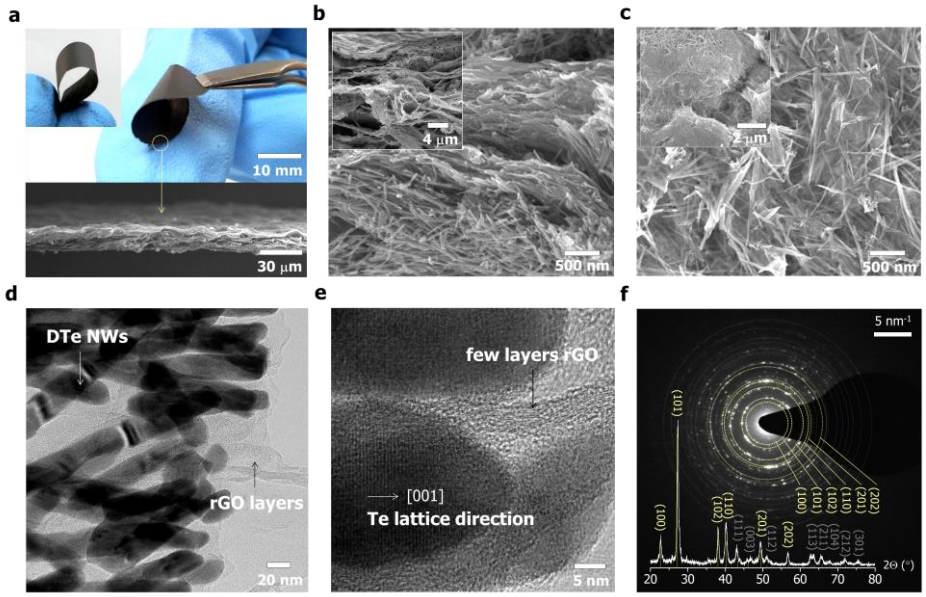

Fig. 5.7. (a) Photographs of flexible $G_{0.1}DTe_{0.9}$ hybrid paper prepared with HI reduction at 40 ℃ for 72 h. (b, c) Cross-sectional and surface SEM images of the $G_{0.1}DTe_{0.9}$ hybrid paper. (d, e) HR-TEM images of the $G_{0.1}DTe_{0.9}$ hybrid showing hybrid heterojunction between few rGO layers and several DTe nanowires. (f) SAED pattern obtained from TEM image and XRD spectrum of the as-prepared DTe nanowire

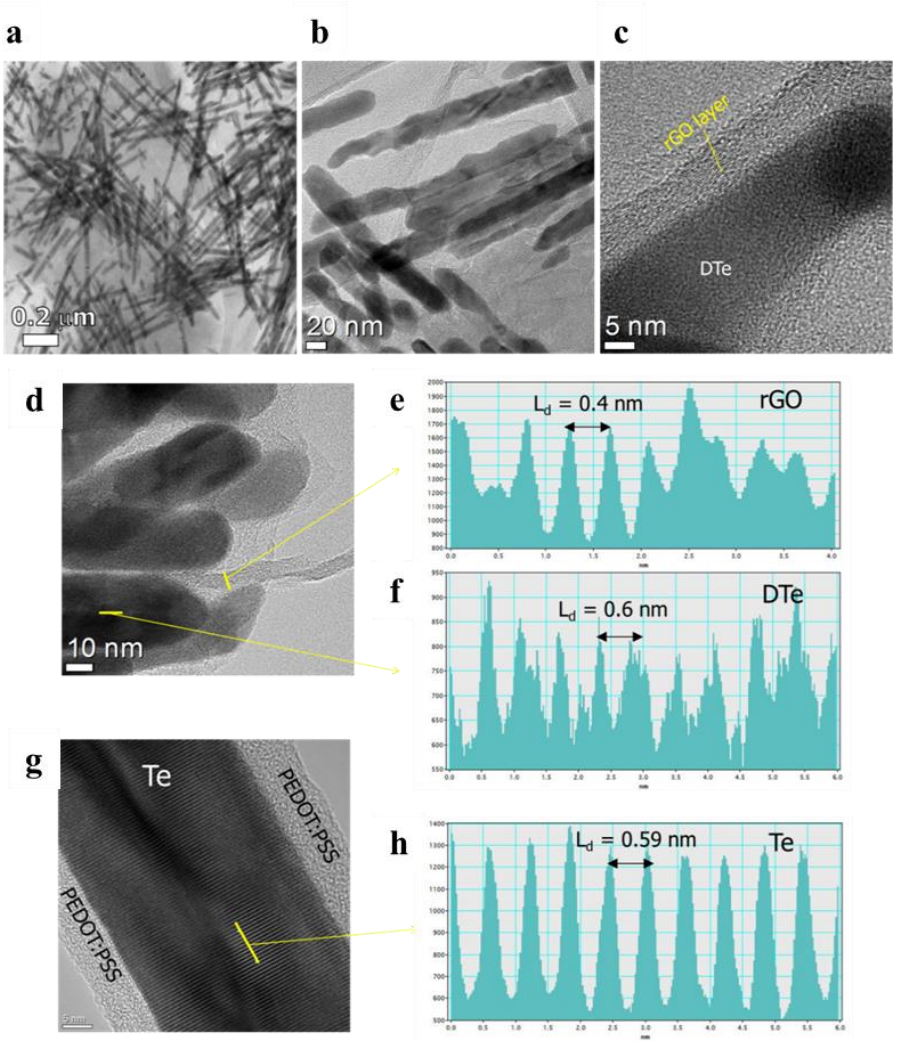

Fig. 5.8. (a, b, c, d) HR-TEM images of the $G_{0.1}DTe_{0.9}$ hybrid paper prepared with HI reduction at 40 ℃ for 72 h. (e, f) Line profiles of lattice planes of rGO layers and a single TeNW in the hybrid, obtained from (d). (g, h) HR-TEM image and line profile of tellurium lattice plane of the as-prepared DTe nanowire

5.3.2 Thermoelectric properties of ternary hybrid film

The TE properties of the as-prepared GDTe hybrid paper are critically changed by the hybrid composition and HI treatment time. With enough reduction time, i.e. 72 h, the electrical conductivity of the hybrid paper remains almost the same irrespective of the DTe content because the fully reduced rGO layers efficiently cover the DTe. However, its thermopower is drastically enhanced to 202 $\mu V \cdot K^{-1}$ as the DTe content increases to 90 wt%, thus leading to an increase in the power factor. The power factor reaches the maximum for a hybrid composition of $G_{0.1}DTe_{0.9}$, and, as we mentioned above, the hybrid paper with less than 10 wt% of GO content is not flexible. Therefore, we fixed the DTe content in the hybrid to 90 wt% and evaluated the TE properties of the hybrid paper as a function of the HI treatment time (Fig. 5.9). As expected, the TE properties of $G_{0.1}DTe_{0.9}$ hybrid paper show opposite trends compared to those from hybrid composition with increasing HI treatment time. The electrical conductivity of the hybrid paper drastically increases with the HI treatment time owing to the graphitization of GO to rGO (Fig. 5.9a)[36, 37]. However, interestingly, the thermopower of the hybrid paper is rarely changed with HI treatment time, thereby leading to an increase in the power factor to 143 $\mu W \cdot m^{-1} \cdot K^{-2}$, which is significantly higher than those of single-component (TeNW, PEDOT:PSS and rGO) and binary hybrid materials (rGO/TeNW hybrid ($G_{0.1}Te_{0.9}$),

PEDOT:PSS/TeNW hybrid ($D_{0.08}Te_{0.92}$)) (Figure 5.9b,c and d). The exact values of σ, *S*, and power factor are summarized in Table 5.1.

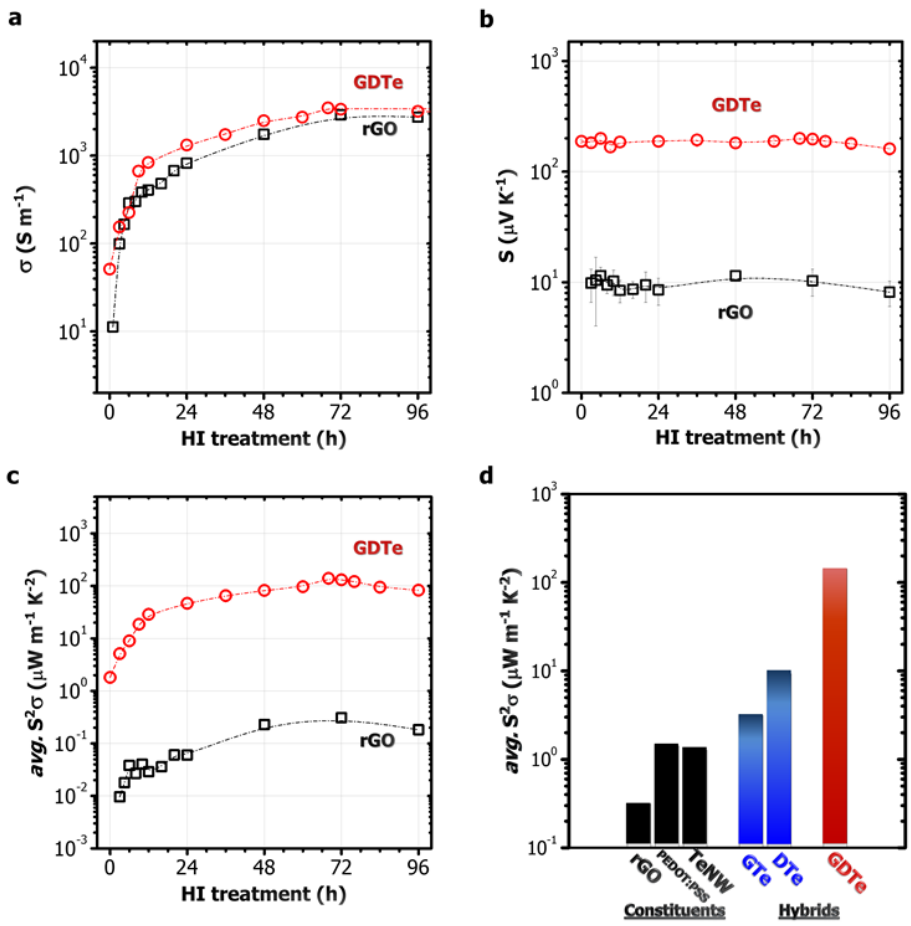

Fig. 5.9. (a) Electrical conductivities, (b) thermopowers, and (c) power factors of the $G_{0.1}DTe_{0.9}$ hybrid papers and rGO films as a function of HI treatment time at 40 ℃. (d) power factors of single components (TeNW, PEDOT:PSS, and rGO) and hybrids (rGO/TeNW hybrid ($G_{0.1}Te_{0.9}$), PEDOT:PSS/TeNW hybrid ($D_{0.08}Te_{0.92}$), and $G_{0.1}DTe_{0.9}$)

Material information			S	σ	$S^2\sigma$	n	u
Sample	Conditions	t_{HI} (h)	($\mu V \cdot K^{-1}$)	($S \cdot m^{-1}$)	($\mu W \cdot m^{-1} \cdot K^{-2}$)	($10^{20} \cdot cm^{-3}$)	($m^2 \cdot v^{-1} \cdot s^{-1}$)
Single component materials							
TeNW		0	487	5.34	1.26	0.029	0.46
PEDOT:PSS		0	45	696	1.41	0.44	0.46
rGO		72	10	2920	0.29	1.05	1.47
Hybrid materials							
DTe	PEDOT:PSS/TeNW	0	204	224	9.33	0.37	0.38
GTe	rGO/Te	72	11	241	0.03	0.35	0.49
GDTe	rGO/PEDOT:PSS/TeNW	72	202	3496	143	1.41	1.46

Table 5.1. Electrical conductivities, thermopowers, power factors, carrier concentrations and carrier mobilities of single components (TeNW, PEDOT:PSS, and rGO) and hybrids ($G_{0.1}Te_{0.9}$, $D_{0.08}Te_{0.92}$, and $G_{0.1}DTe_{0.9}$).

The thermal diffusivity of pelletized GDTe sample with the thickness of more than 1 mm was measured through the film because porous GDTe paper showed a low reliability in the measurement of thermal diffusivity, and thus the thermal conductivity was calculated to 0.21 $W \cdot m^{-1} \cdot K^{-1}$. Through-plane thermal diffusivity (α) is measured by laser flash method, and the thermal conductivity (k) is calculated as follows, $k = \alpha \cdot \rho \cdot C_p$, where ρ and C_p are the density and specific heat of the sample, respectively. Although the thermal conductivity through plane is higher than that in plane due to an anisotropy in the film, GDTe ternary paper with porous microstructure could have a lower thermal conductivity than above pelletized sample. Based on the through-plane thermal conductivity of pelletized GDTe sample, the maximum thermoelectric figure-of-merit was expected to be ca. 0.21 at 300 K for the $G_{0.1}DTe_{0.9}$ porous hybrid paper. It is 1-3 orders of magnitude higher than those of the constituents and binary hybrids because the ZT values of rGO, PEDOT:PSS, TeNW, $G_{0.1}Te_{0.9}$, and $D_{0.08}Te_{0.92}$ are very small in the range of 10^{-2} to 10^{-4}.

5.3.3 Mechanical and chemical stability of ternary hybrid film

For practical use of the flexible TE paper, the mechanical and chemical durability should be confirmed. We first controlled the bending angle of $G_{0.1}DTe_{0.9}$ paper, as shown in Fig. 5.10a. The TE properties are directly measured in bent and flat states (Fig. 5.10b). The resistance of the GDTe paper remains almost unchanged up to a bending angle of 45° and changes by less than 10 % even at 90° (Fig. 5.11). When we characterized σ, *S*, and power factor of the GDTe paper as a function of the number of bending cycles, we observed a slight decrease (~ 10 %) in the power factor without any serious decrease in performance after 1000 bending cycles: this was due to the small decrease in σ and due to the stable *S* (Fig. 5.12). These results demonstrate that the GDTe hybrid paper shows not only high flexibility but also good mechanical durability owing to the excellent mechanical strength and flexibility of the rGO layers.

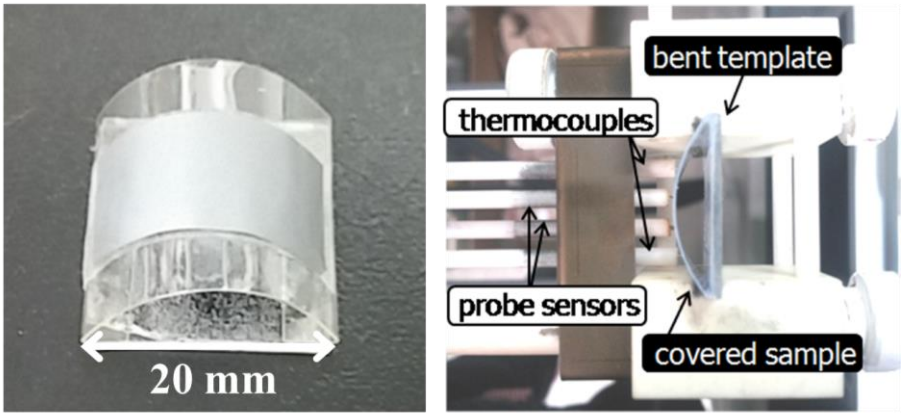

Fig. 5.10. (a, b) Photographs of an as-prepared specimen deposited on a template bent at Θ ~ 86° and the experimental setup for TE bending test

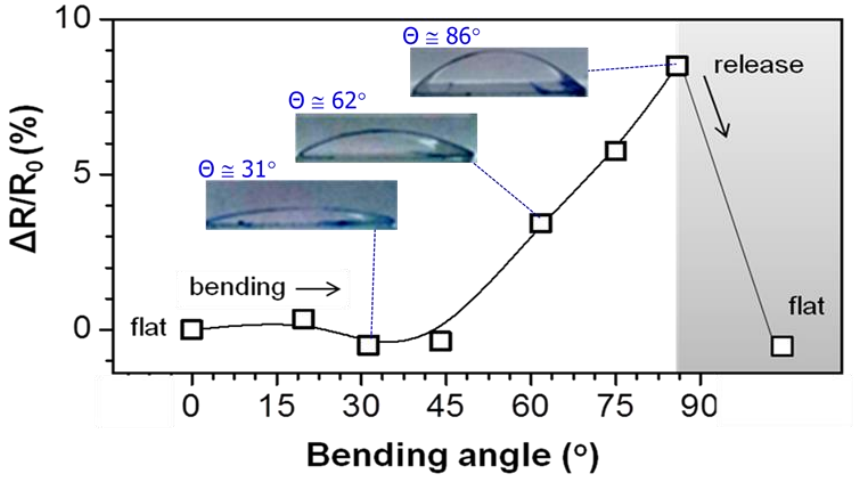

Fig. 5.11. Ratio of resistance variation (ΔR) to initial resistance (R_0) of the $G_{0.1}DTe_{0.9}$ paper as a function of bending angle

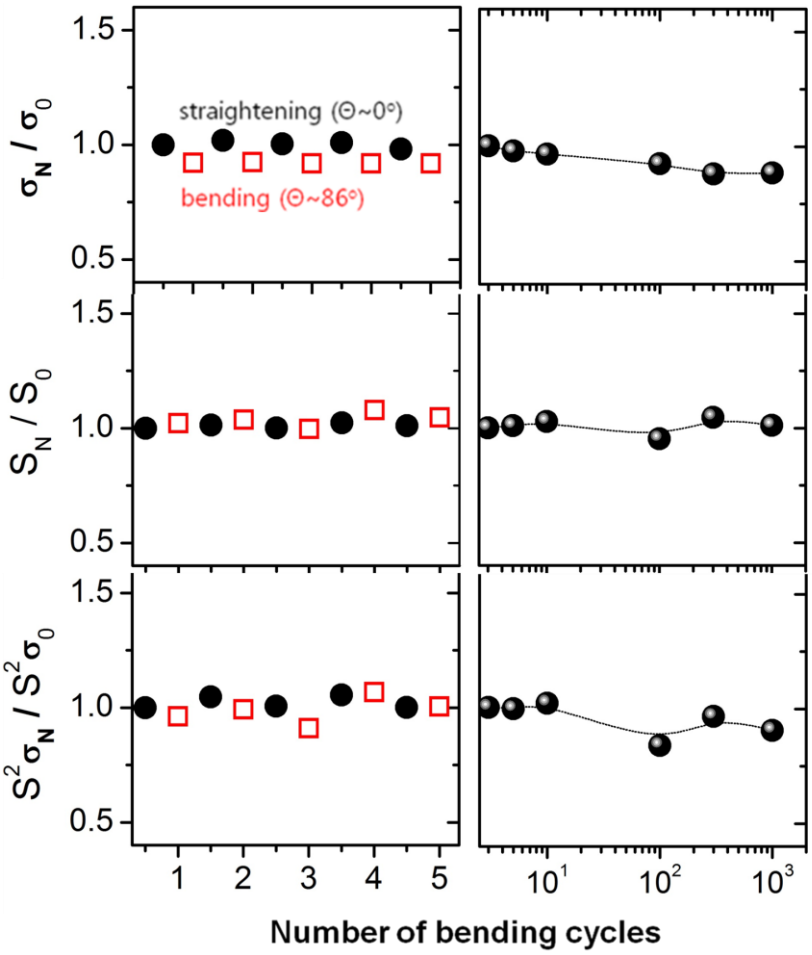

Fig. 5.12. Ratios of electrical conductivity (σ_N), thermopower (S_N), and power factor ($S^2\sigma_N$) of the $G_{0.1}DTe_{0.9}$ paper to their initial values as a function of the number of bending cycles

It is well-known that inorganic materials such as a tellurium are very sensitive to oxidation[38] and PEDOT:PSS is also sensitive to humidity, thus reducing its TE performance[39]. The TeNWs used in our study also have the problem of oxidation, resulting in morphological deformation (Fig. 5.13). Therefore, we tested the chemical durability of TeNW, DTe and GDTe paper under the 85 °C/85 % humidity condition. After 7 days in this condition, while TeNW and DTe films show a decrease in the power factor by the three orders of magnitude, the GDTe paper shows a much higher chemical durability than TeNW and DTe films (Fig. 5.14). This could be attributed to the chemical stability of the rGO layers that cover DTe nanowires effectively and act as a barrier to prevent the oxidation of TeNW.

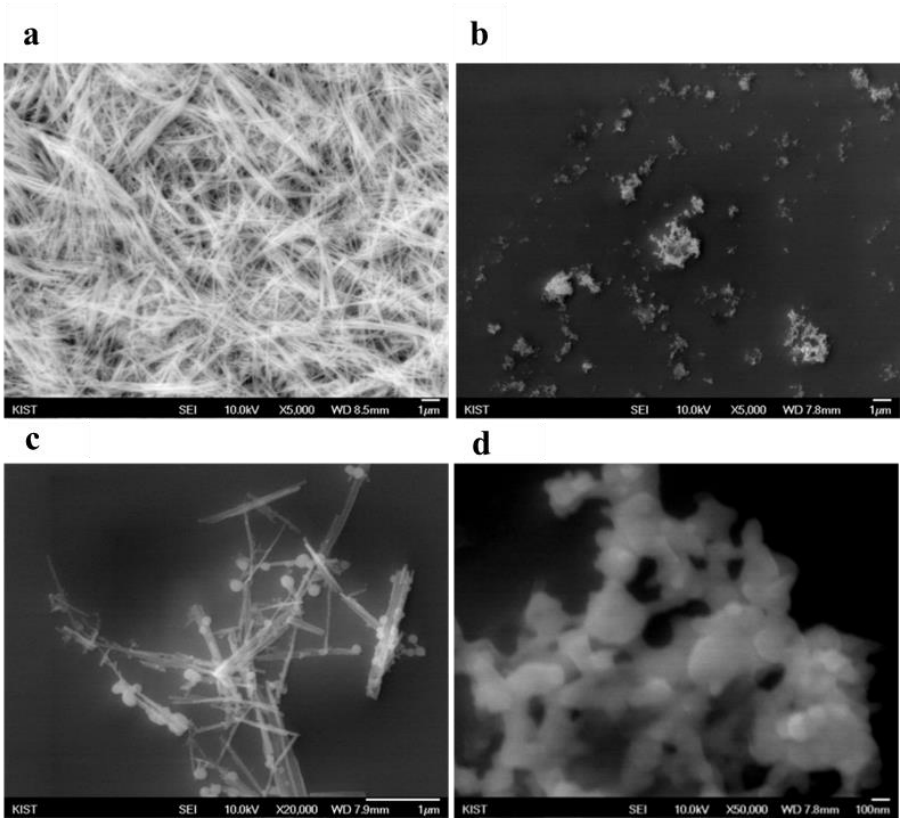

Fig. 5.13. SEM images of (a) as-synthesized TeNW and (b-d) oxidized TeNW after immersion in water at room temperature for 12 h

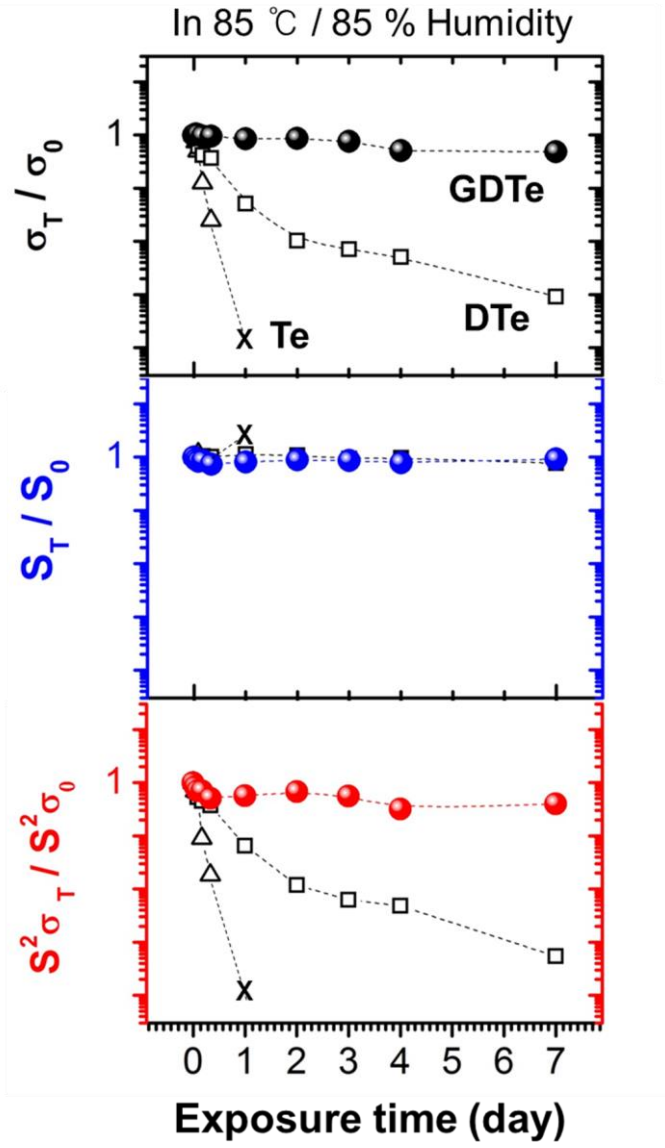

Fig. 5.14. Ratios of electrical conductivity (σ_T), thermopower (S_T), and power factor ($S^2\sigma_T$) of the $G_{0.1}DTe_{0.9}$ paper to their initial values as a function of exposure time in the 85 ℃/85 % humidity condition

5.3.4 Study on synergetic double carrier filtering at heterojunctions

Our rationally designed GDTe paper shows the significant enhancement in the TE performance as well as the mechanical and chemical durability as mentioned above. In order to systematically analyze the enhanced TE performance of the GDTe paper, we used Hall measurements of the carrier concentration and mobility in the pure TeNW, DTe, and GDTe hybrid. Table 5.2 shows the transport parameters of the pure TeNW, $D_{0.08}Te_{0.92}$, and $G_{0.1}DTe_{0.9}$. Pure TeNW film has a low σ and a high *S* based on low carrier concentration of 2.9×10^{18} cm^{-3} and mobility of 0.46 $cm^2 \cdot v^{-1} \cdot s^{-1}$. On the other hand, the binary DTe hybrid shows the higher σ of 224 $S \cdot m^{-1}$ and a lower *S* of 204 $\mu V \cdot K^{-1}$, which are attributed to the higher carrier concentration of 3.7×10^{19} cm^{-3}. However, the degree of decrease in the *S* is relatively low compared to the increase in the carrier concentration owing to the energy filtering at the interfaces between PEDOT:PSS and TeNW. In the energy filtering effect, low-energy carriers are preferentially scattered by the potential barrier at the interface between the two materials, whereas high-energy carriers readily cross the barrier[27, 29]. High-energy carriers can transfer more heat than low-energy carriers, thereby leading to the increase in *S*.[40]

Transport parameters	TeNW	PEDOT:PSS/TeNW	rGO/PEDOT:PSS/TeNW
Electrical conductivity ($S \cdot m^{-1}$)	5.34	224	3496
Thermopower ($\mu V \cdot K^{-1}$)	487	204	202
Power factor ($\mu W \cdot m^{-1} \cdot K^{-2}$)	1.26	9.33	143
Thermal conductivity ($W \cdot m^{-1}K^{-1}$)	0.28	0.27	0.21
Carrier concentration ($10^{20} \cdot cm^3$)	0.029	0.37	1.41
Carrier mobility ($m^2 \cdot v^{-1} \cdot s^{-1}$)	0.46	0.38	1.46
Hall coefficient ($10^{-6} m^3 \cdot k^{-1}$)	2.8	0.17	0.06
Scattering time (10^{-16}s)	1.18	0.97	3.74
Work function barrier (eV)	-	0.24	0.20 / 0.24

Table 5.2. Transport parameters of the pure TeNW, binary PEDOT:PSS/TeNW hybrid, and ternary rGO/PEDOT:PSS/TeNW hybrid films.

It is important to consider the scattering time and carrier mobility to demonstrate the energy filtering at the junctions. We calculated the scattering time (defined as $\tau = \mu \cdot m^*/e$, where τ, μ and m^* are the scattering time, carrier mobility, and effective mass of the carrier, respectively) from the measured carrier mobility. The DTe film shows a shorter scattering time of 0.97×10^{-16} s and a lower mobility of 0.38 $cm^2 \cdot v^{-1} \cdot s^{-1}$ than pure TeNW (1.78×10^{-16} s and 0.46 $cm^2 \cdot v^{-1} \cdot s^{-1}$, respectively), indicating that more scattering events could have occurred in the DTe film. The ternary GDTe paper also shows the same trend as that of binary DTe film. The carrier concentration and mobility of the ternary hybrid are one order of magnitude higher than those of the DTe films, thus increasing σ to 3496 $S \cdot m^{-1}$ with little difference in *S* (202 $\mu V \cdot K^{-1}$) compared to that of the binary DTe film. Further, although the high *S* of the ternary paper indicates energy filtering at the interfaces between rGO and PEDOT:PSS of DTe, the scattering time calculated from the measured carrier mobility is still higher than that of the DTe film. This can be attributed to the drastic increase in the high carrier mobility of rGO itself during reduction[36].

For more quantitative interpretation of our TE data, we compared the measured *S* of the pure TeNW, DTe, and GDTe hybrid with the calculated (theoretical) ones according to the Drude model (Table 5.3)[1]. While the pure TeNW shows a measured *S* value similar to the calculated one, the binary and ternary hybrids show remarkably higher measured values (204 $\mu V \cdot K^{-1}$ for DTe and 202 $\mu V \cdot K^{-1}$ for GDTe) than calculated ones (80 $\mu V \cdot K^{-1}$ for DTe and 33 $\mu V \cdot K^{-1}$ for GDTe). These enhanced thermopowers provide evidence of synergetic energy filtering effects at the two interfaces of PEDOT:PSS/TeNW and rGO/DTe. Based on increased σ without a major decrease in the *S*, the GDTe hybrid shows a power factor that is 1-2 orders of magnitude higher (143 $\mu W \cdot m^{-1} \cdot K^{-1}$) than those of pure TeNW or binary DTe hybrid and the maximum ZT of 0.2 at 300 K, which is comparable to the highest values reported for CNT composites.[41, 42] The energy diagram of the rGO/PEDOT:PSS/TeNW heterojunctions in Fig. 5.15 shows the energy filtering at two junctions of PEDOT:PSS/TeNW and rGO/PEDOT:PSS of DTe. Bulk Te forms a degenerate semiconductor with a narrow bandgap of 0.33 eV in which the Fermi level is positioned close to the valence band.[43] The work function of the TeNW is assumed to be the same as that of bulk Te.[44] The work functions of PEDOT:PSS and rGO were measured using ultraviolet photoelectron spectroscopy (UPS), and they are consistent with the values from the previous reports in the literature (Fig. 5.16)[39, 45]. The equilibrium band diagram for the ternary GDTe hybrid indicates that the energy barriers of 0.24 and 0.31 eV at the PEDOT:PSS/TeNW and rGO/PEDOT:PSS

Samples	S (μV/K)		$\left(\frac{Sm - Sc}{Sc}\right) \times 100$	Power factor (μW/m·K²)
	Measured	Calculated		
TeNW	487	493	-1.2 %	1.26
PEDOT:PSS/TeNW	204	80	156 %	9.33
rGO/PEDOT:PSS/TeNW	202	33	512 %	143

Table. 5.3. Measured and calculated thermopowers and power factors of the pure TeNW, PEDOT:PSS/TeNW hybrid, and rGO/PEDOT:PSS/TeNW hybrid films

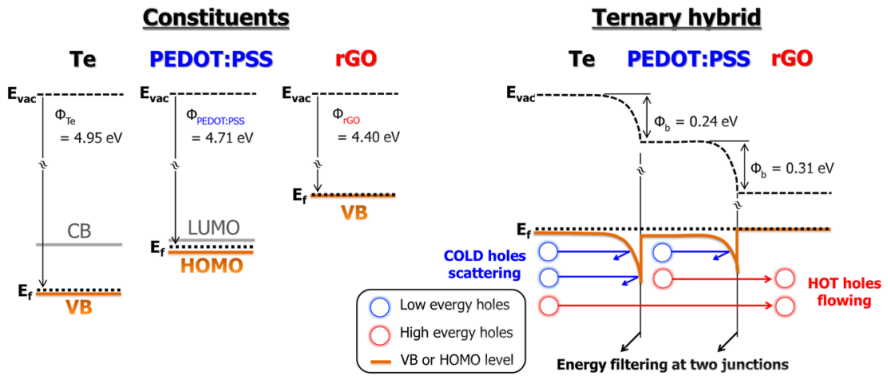

Fig. 5.15. Energy diagram of the rGO/PEDOT:PSS/TeNW (bulk Te) heterojunctions showing energy filtering at two junctions, i.e., PEDOT:PSS/TeNW and rGO/PEDOT:PSS of DTe.

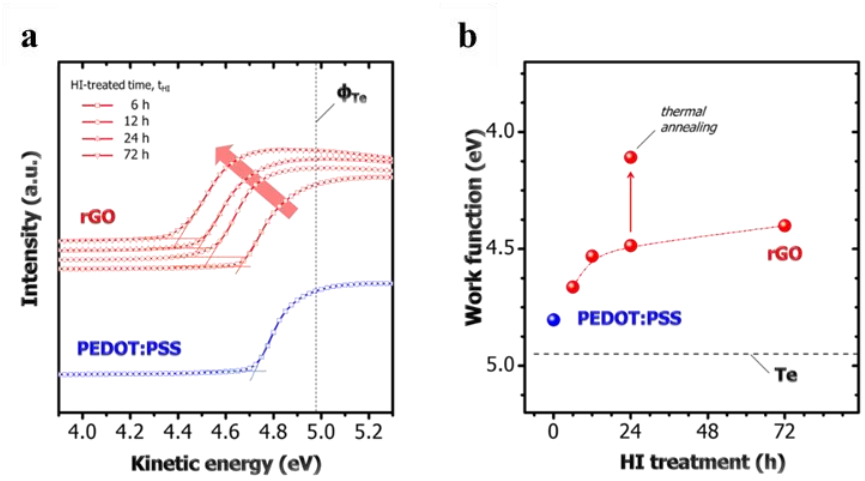

Fig. 5.16. (a, b) UPS data and work function of PEDOT:PSS and rGO as a function of HI-treatment time

interfaces, respectively, filter out low-energy carriers while they allow high-energy carriers to cross over the interfaces, thus enhancing TE performance. Notably, the binary hybrid ($G_{0.1}Te_{0.9}$) without PEDOT:PSS has a high energy barrier of 0.55 eV, but it has a low power factor of 0.03 $\mu W \cdot m^{-1} \cdot K^{-1}$ as mentioned above (Fig. 5.9d). Therefore, this seems to be the optimum energy barrier value for efficient carrier filtering. It is worth mentioning that the precise work function of TeNW is helpful to better illustrate the energy filtering effect at organic-inorganic semiconductor interface although we used the work function of bulk Te instead of that of TeNW. In addition, further experimental evidence, especially by performing direct measurement of the energy-dependent scattering rate, are required to prove conclusively the energy-filtering effect in the ternary hybrid paper.

5.3.5 Flexible thermoelectric generator based on ternary hybrid film

The TE device was fabricated using the $G_{0.1}DTe_{0.9}$ paper and PEI-doped SWCNT film as the p-type and n-type components, respectively. Five pairs of the $G_{0.1}DTe_{0.9}$ paper and PEI-SWCNT film were electrically connected in series, and a temperature difference was applied between the two ends of the devices in the in-plane direction (Fig. 5.17). Since the thermopower of the GDTe paper and the PEI-SWCNT film is approximately 200 and -40 $\mu V \cdot K^{-1}$, respectively, the ideal voltage per ΔT of the device is 1.2 mV. Fig. 5.18a shows the output voltage of the device as a function of the temperature difference. While the ideal voltage of the device at ΔT = 50 K is 60 mV, the measured output voltage is 58 mV, i.e., slightly lower than the ideal value. At ΔT = 50 K, the output power density of the device was measured with varying load resistance, and the maximum value of 650 $nW \cdot cm^{-2}$ was obtained at 642 Ω of circuit resistance (Fig. 5.18b). Although the power density is lower than that of inorganic TE device, it is comparable to the highest values reported for a freestanding TE device based on CNT composites.[46] In case of multilayer devices, the temperature drop due to the thermal resistance of the device along the through-plane direction could reduce the output power of the device.[47] Furthermore, because the circuit resistance is the sum of material resistance and contact resistance at the junctions, it is important to reduce the contact resistance to realize higher power.

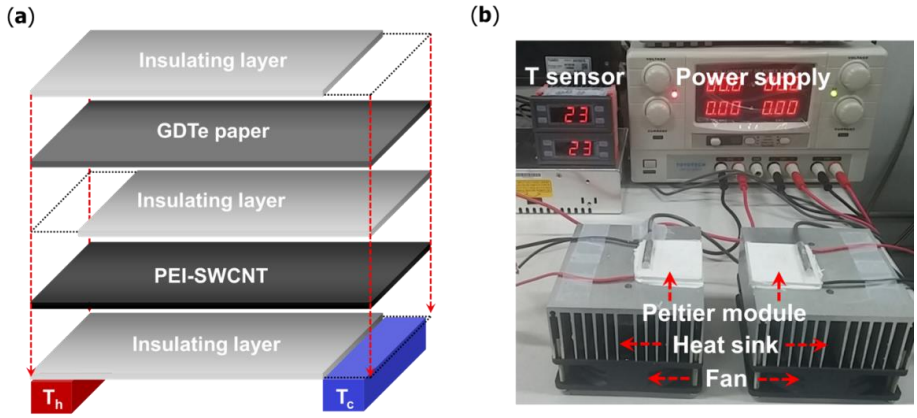

Fig. 5.17. (a) Schematic illustration of GDTe/PEI-SWCNT flexible device and (b) Photograph of hand-made system to apply a temperature difference across the device and measure the power at the both ends of the TE device

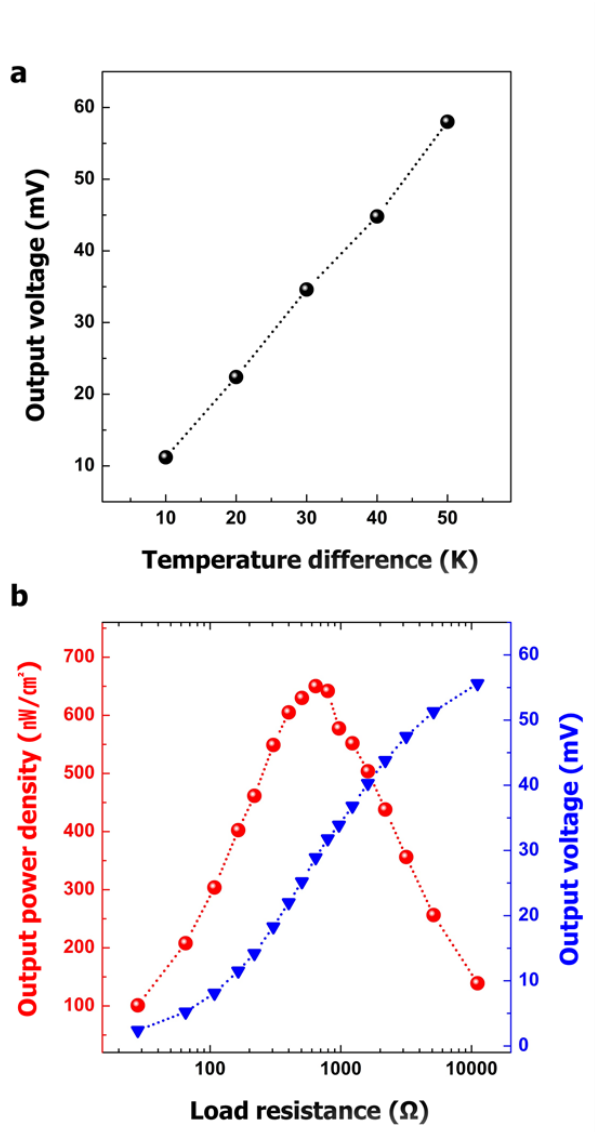

Fig. 5.18. (a) Output voltage of the device as a function of temperature differences and (b) output power density of the device as a function of load resistance

5.4 Conclusions

In conclusion, we have rationally designed the ternary hybrid paper composed of rGO, PEDOT:PSS, and TeNW to enhance the TE performance as well as to improve flexibility and mechanical and chemical durability. The PEDOT:PSS passivated TeNW shows an 8-fold enhancement in the power factor over that of pure TeNW, because of the energy-dependent filtering at the junction. Further, the introduction of rGO into this binary system results in a power factor 15-times higher than that of the binary film, and this could be attributed to the additional energy filtering at the interface between the rGO and PEDOT:PSS. Using this hybrid paper and PEI-doped SWCNT as p-type and n-type TE units, respectively, we prepared a prototype flexible TE module and obtained the maximum electrical power density of 650 $nW \cdot cm^{-2}$ at $\Delta T = 50$ K. We believe that the strategy proposed here to improve the performance of flexible TE materials by introducing more heterojunctions and optimizing carrier transfer at those junctions shows a great potential for the preparation of flexible/or wearable power-conversion devices.

5.5 References

1. Snyder GJ*, et al.* Complex thermoelectric materials. *Nat. Mater.* **7**, 105-114 (2008).
2. Chu S*, et al.* Opportunities and challenges for a sustainable energy future. *Nature* **488**, 294-303 (2012).
3. Bell LE. Cooling, heating, generating power, and recovering waste heat with thermoelectric systems. *Science* **321**, 1457-1461 (2008).
4. Liu W*, et al.* Recent advances in thermoelectric nanocomposites. *Nano Energy* **1**, 42-56 (2012).
5. Zebarjadi M*, et al.* Perspectives on thermoelectrics: from fundamentals to device applications. *Energy Environ. Sci.* **5**, 5147-5162 (2012).
6. Minnich AJ*, et al.* Bulk nanostructured thermoelectric materials: current research and future prospects. *Energy Environ. Sci.* **2**, 466-479 (2009).
7. Poudel B*, et al.* High-thermoelectric performance of nanostructured bismuth antimony telluride bulk alloys. *Science* **320**, 634-638 (2008).
8. Chowdhury I*, et al.* On-chip cooling by superlattice-based thin-film thermoelectrics. *Nat. Nanotechnol.* **4**, 235-238 (2009).

9. Harman TC, *et al.* Quantum Dot Superlattice Thermoelectric Materials and Devices. *Science* **297**, 2229-2232 (2002).

10. Ohta H, *et al.* Giant thermoelectric Seebeck coefficient of a two-dimensional electron gas in SrTiO3. *Nat. Mater.* **6**, 129-134 (2007).

11. Sootsman JR, *et al.* New and old concepts in thermoelectric materials. *Angew. Chem. Int. Ed. Engl.* **48**, 8616-8639 (2009).

12. Dresselhaus MS, *et al.* New Directions for Low-Dimensional Thermoelectric Materials. *Adv. Mater.* **19**, 1043-1053 (2007).

13. Yang J, *et al.* Rational Design of Advanced Thermoelectric Materials. *Adv. Energy Mater.* **3**, 549-565 (2013).

14. He M, *et al.* Towards high-performance polymer-based thermoelectric materials. *Energy Environ. Sci.* **6**, 1352-1361 (2013).

15. Poehler TO, *et al.* Prospects for polymer-based thermoelectrics: state of the art and theoretical analysis. *Energy Environ. Sci.* **5**, 8110-8115 (2012).

16. Bubnova O, *et al.* Towards polymer-based organic thermoelectric generators. *Energy Environ. Sci.* **5**, 9345-9362 (2012).

17. Bubnova O, *et al.* Optimization of the thermoelectric figure of merit in the conducting polymer poly(3,4-ethylenedioxythiophene). *Nat Mater* **10**, 429-433 (2011).

18. Chabinyc M. Thermoelectric polymers: Behind organics' thermopower. *Nat. Mater.* **13**, 119-121 (2014).

19. Kim GH, *et al.* Engineered doping of organic semiconductors for enhanced thermoelectric efficiency. *Nat. Mater.* **12**, 719-723 (2013).

20. Du Y, *et al.* Research progress on polymer–inorganic thermoelectric nanocomposite materials. *Prog. Polym. Sci.* **37**, 820-841 (2012).

21. Yao Q, *et al.* Enhanced Thermoelectric Performance of Single-Walled Carbon Nanotubes/Polyaniline Hybrid Nanocomposites. *ACS Nano* **4**, 2445-2451 (2010).

22. Kim KT, *et al.* The influence of CNTs on the thermoelectric properties of a CNT/Bi2Te3 composite. *Carbon* **52**, 541-549 (2013).

23. Szczech JR, *et al.* Enhancement of the thermoelectric properties in nanoscale and nanostructured materials. *J. Mater. Chem.* **21**, 4037-4055 (2011).

24. Shakouri A, *et al.* Heterostructure integrated thermionic coolers. *Appl. Phys. Lett.* **71**, 1234 (1997).

25. Zide J, *et al.* Demonstration of electron filtering to increase the Seebeck coefficient in In0.53Ga0.47As/In0.53Ga0.28Al0.19As superlattices. *Phys. Rev. B* **74**, 205335 (2006).

26. Liu M, *et al.* Enhanced thermoelectric performance through energy-filtering effects in nanocomposites dispersed with metallic particles. *Appl. Phys. Lett.* **101**, 132103 (2012).

27. Ko DK, *et al.* Enhanced thermopower via carrier energy filtering in solution-processable Pt-Sb2Te3 nanocomposites. *Nano Lett.* **11**,

2841-2844 (2011).

28. Coates NE, *et al.* Effect of interfacial properties on polymer-nanocrystal thermoelectric transport. *Adv. Mater.* **25**, 1629-1633 (2013).

29. He M, *et al.* Thermopower enhancement in conducting polymer nanocomposites via carrier energy scattering at the organic–inorganic semiconductor interface. *Energy & Environ. Sci.* **5**, 8351 (2012).

30. Xi GC, *et al.* Large-scale synthesis, growth mechanism, and photoluminescence of ultrathin Te nanowires. *Cryst. Growth Des.* **6**, 2567-2570 (2006).

31. Marcano DC, *et al.* Improved Synthesis of Graphene Oxide. *Acs Nano* **4**, 4806-4814 (2010).

32. Moon IK, *et al.* Reduced graphene oxide by chemical graphitization. *Nat. Commun.* **1**, 73 (2010).

33. See KC, *et al.* Water-processable polymer-nanocrystal hybrids for thermoelectrics. *Nano Lett.* **10**, 4664-4667 (2010).

34. Xi GC, *et al.* Large-scale synthesis, growth mechanism, and photoluminescence of ultrathin Te nanowires. *Cryst. Growth Des.* **6**, 2567-2570 (2006).

35. Hawley CJ, *et al.* Shape-Controlled Vapor-Transport Growth of Tellurium Nanowires. *Cryst. Growth Des.* **12**, 2789-2793 (2012).

36. Moon IK, *et al.* Reduced graphene oxide by chemical graphitization. *Nat. Commun.* **1**, 73 (2010).

37. Gao W, *et al.* New insights into the structure and reduction of graphite oxide. *Nat. Chem.* **1**, 403-408 (2009).

38. Lan W-J, *et al.* Dispersibility, Stabilization, and Chemical Stability of Ultrathin Tellurium Nanowires in Acetone: Morphology Change, Crystallization, and Transformation into TeO2 in Different Solvents. *Langmuir* **23**, 3409-3417 (2007).

39. Huang J, *et al.* Investigation of the Effects of Doping and Post-Deposition Treatments on the Conductivity, Morphology, and Work Function of Poly(3,4-ethylenedioxythiophene)/Poly(styrene sulfonate) Films. *Adv. Funct. Mater.* **15**, 290-296 (2005).

40. Zhang K, *et al.* Enhancing thermoelectric properties of organic composites through hierarchical nanostructures. *Sci. Rep.* **3**, 3448 (2013).

41. Yu C, *et al.* Light-Weight Flexible Carbon Nanotube Based Organic Composites with Large Thermoelectric Power Factors. *Acs Nano* **5**, 7885-7892 (2011).

42. Toshima N, *et al.* Novel Hybrid Organic Thermoelectric Materials:Three-Component Hybrid Films Consisting of a Nanoparticle Polymer Complex, Carbon Nanotubes, and Vinyl Polymer. *Adv. Mater.* **27**, 2246-2251 (2015).

43. Peng H*, et al.* Elemental tellurium as a chiral p-type thermoelectric material. *Phys. Rev. B* **89**, 195206 (2014).

44. Zhang G*, et al.* Design Principle of Telluride-Based Nanowire Heterostructures for Potential Thermoelectric Applications. *Nano Lett.* **12**, 3627-3633 (2012).

45. Sutar DS*, et al.* Electronic structure of graphene oxide and reduced graphene oxide monolayers. *Appl. Phys. Lett.* **101**, 103103 (2012).

46. Nonoguchi Y*, et al.* Systematic Conversion of Single Walled Carbon Nanotubes into n-type Thermoelectric Materials by Molecular Dopants. *Sci. Rep.* **3**, 3344 (2013).

47. Kim SL*, et al.* Flexible Power Fabrics Made of Carbon Nanotubes for Harvesting Thermoelectricity. *Acs Nano* **8**, 2377-2386 (2014).

PART III. Rational design of high-performance flexible thermoelectric generators based on nano-carbon materials

Chapter 6. Designing all-carbon nanotube thermoelectric generators without metal electrodes for minimizing contact resistance of circuit

6.1 Research backgrounds

Excellent TE properties of flexible materials are essential for high performance TEGs. However, for practical applications, many requirements including modular design, flexibility, portability, and facile fabrication must be considered.[1] While many previous reports on flexible TE materials show excellent TE properties, they lack facile module fabrication and performance, which do not move past characterization of the TE properties.[2-6]

One of main requirements in the design of a TE module is to determine the optimum module geometry, based upon available TE material and fabrication technology, which meets the given application specifications.[7-9] A typical multi-pair TE module is designed for through-plane thermal gradients. N and P-type TE elements are connected in series by highly conducting metal electrodes to form a thermocouple.[7, 8] The electrical contacts are formed at the interface between TE element and metal electrode, which is one of the critical factors to determine the

module performance. Since a TE generator is consisted of many TE pairs and electrical contacts, even tiny mismatch of an electrical contact may cause a high contact resistance of the whole module. That is why forming an ohmic contact between TE material and metal electrode is important. In this viewpoint, organic TE materials have disadvantage due to comparably bad compatibility with metals.[10] Therefore, to overcome this limitation, novel module design for maximizing the strengths of organic TE materials is urgently required. In this chapter, novel module designs based on all-CNT film and yarn without metal electrode which exhibit excellent power density are demonstrated. Because the flexible CNTs in this research shows not only the requisite mechanical strength but also shape advantages for modular fabrication, various types of flexible TEGs can be easily designed and fabricated.

6.2 Design of all-carbon nanotube film module

6.2.1 Preparation of all-carbon nanotube film module

CNT film (CNTF) was synthesized by a floating catalyst method as previously reported.[11] Ferrocene, thiophene, and methane were used as a catalyst precursor, promoter, and carbon source for CNT synthesis at 1200 ℃, respectively. CNTs are highly integrated into aerogel-like forms in a reactor. These aerogel forms can be continuously withdrawn from the reactor at the bottom without length limitations. The CNT film was prepared as an aerogel directly wound on a roller. As shown in Fig. 6.1, large size CNT film of over 1500×500 mm dimension with 50 μm thickness in average was prepared. The CNTF was p-doped with a $FeCl_3$ ethanol solution (Sigma-Aldrich, 2 mM) for 30 min, followed by well drying in ambient conditions. Additionally, the CNTF was n-doped with a polyethyleneimine ethanol solution (PEI (MW = 600), Sigma-Aldrich, 8 mM) for 30 min. The alternately n-and p-doped CNTY with undoped regions as electrodes was carefully assembled into polydimethylsiloxane (PDMS) supporting unit prepared by stainless steel/aluminium mold. (Fig. 6.2) Schematic image of module design based on all-CNT film is presented in Fig. 6.3, and a prototype of all-CNT film module is shown in Fig. 6.4.

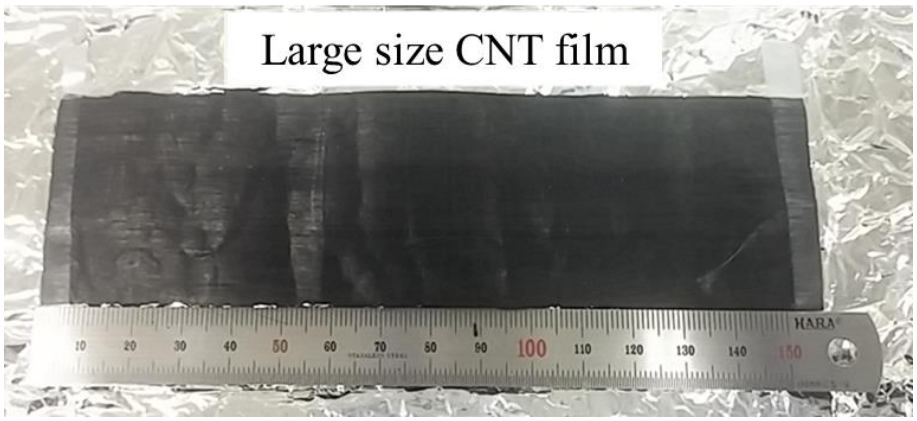

Fig. 6.1. Photograph of prepared CNT film

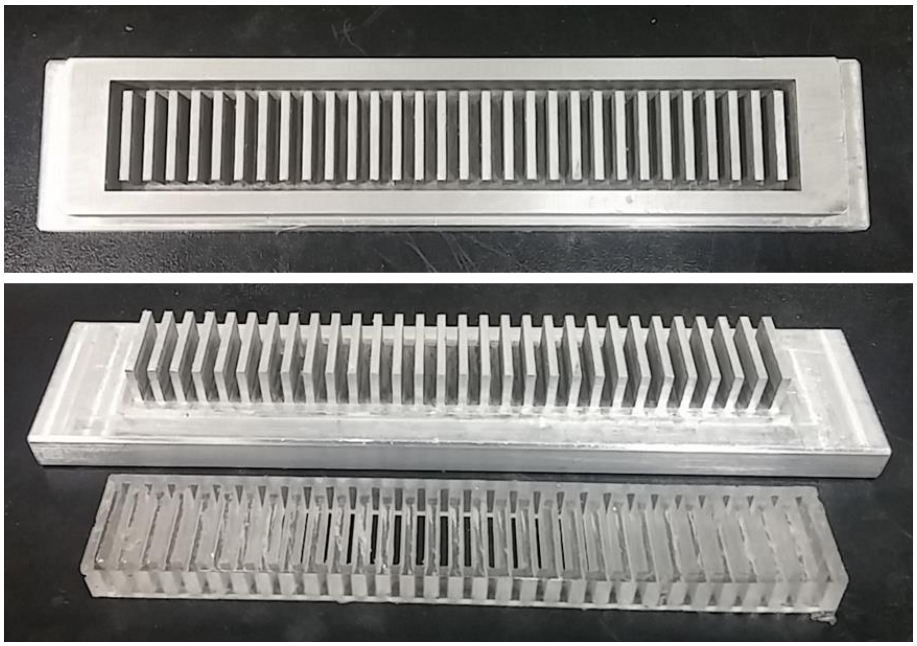

Fig. 6.2. Photographs of stainless steel/aluminium mold and fabricated PDMS supporting unit

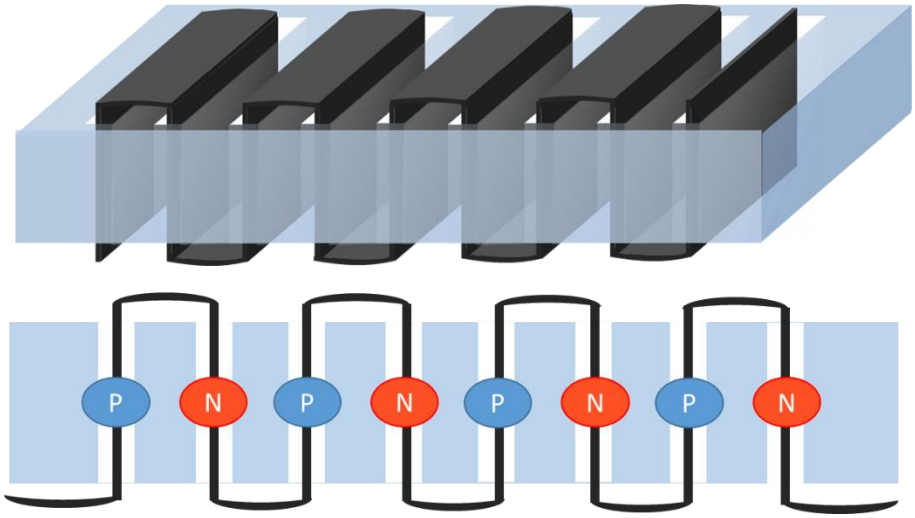

Fig. 6.3. Schematic image of module design based on all-CNT film

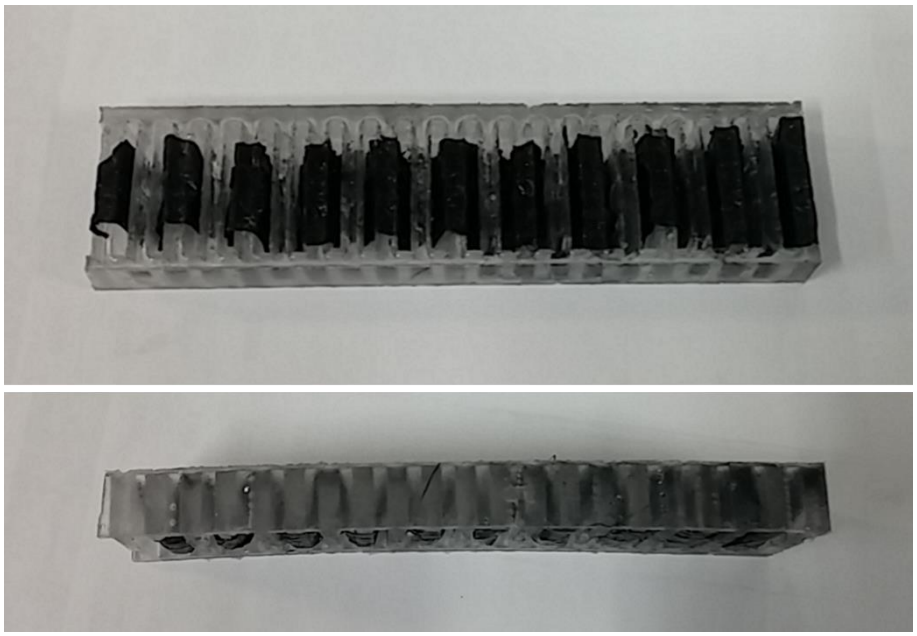

Fig. 6.4. Photograph of a prototype all-CNT film module without metal electrodes

6.2.2 Performance of all-carbon nanotube film TE generator

There are numerous works related with carbon TE materials and devices. However, nobody reports all-carbon TE module without additional metal electrodes. As shown in Fig. 6.5, previous typical TE modules is consisted of vertically and alternatively stacked N-, P-type CNT films with Ag or Au electrodes to connect the films. While they are restricted to energy conversion by in-plane thermal gradients, novel all-CNT film module in this research could be widely applied in various thermal sources including through-plane thermal gradients. In addition, the CNT film between the doped regions was used as electrodes to minimize the circuit resistance, thereby leading to the enhancement of TE performance. In table 6.1, 10 pairs of CNT film module without Ag electrodes shows lower circuit resistance and higher maximum generated power than with Ag electrodes. However, more systematic study is needed to demonstrate the effect of electrode-less module design.

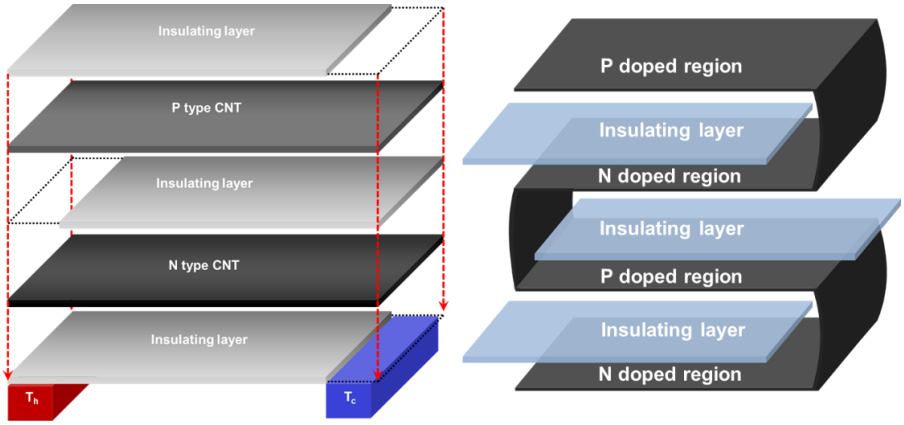

Fig. 6.5. Schematic illustrations of previous typical module and novel all-CNT film module

10 Pairs of N, P legs	Internal R (ohm)	Circuit R (ohm)	5K Open voltage (mV)	5K Max. Power (μW)	50K Open voltage (mV)	50K Max. Power (μW)
MF-TEG with Ag electrode	18	71	1.17	0.005	19.0	1.42
MF-TEG without Ag electrode	18	20	1.38	0.05	20.6	5.05

Table 6.1. Output voltage and power of CNT film module with and without Ag electrode

6.3 Design of all-carbon nanotube yarn module

6.3.1 Preparation of all-carbon nanotube yarn module

CNT yarn (CNTY) was synthesized by a floating catalyst method, which is same process of CNTF. As a proof of concept, all-CNT yarn based module like in Fig. 6.6, was designed and a prototype parallel-connected flexible TE generator using CNTYs (Fig. 6.7) was fabricated. The alternately n-and p-doped CNTY with undoped regions as electrodes was carefully wound around polydimethylsiloxane (PDMS) supporting unit having dimensions of 4×10×80 mm^3 without interconnection of CNTY. The dimensions of the PDMS unit were arbitrarily determined for ease of handling, and thus further work is needed to optimize the TE performance of this module in terms of shape and size. In addition, the CNTY can be woven onto fabric after doping, so facile module fabrication is available. A schematic of whole process of wearable TEG based on CNTY without metal electrodes is introduced in Fig. 6.8.

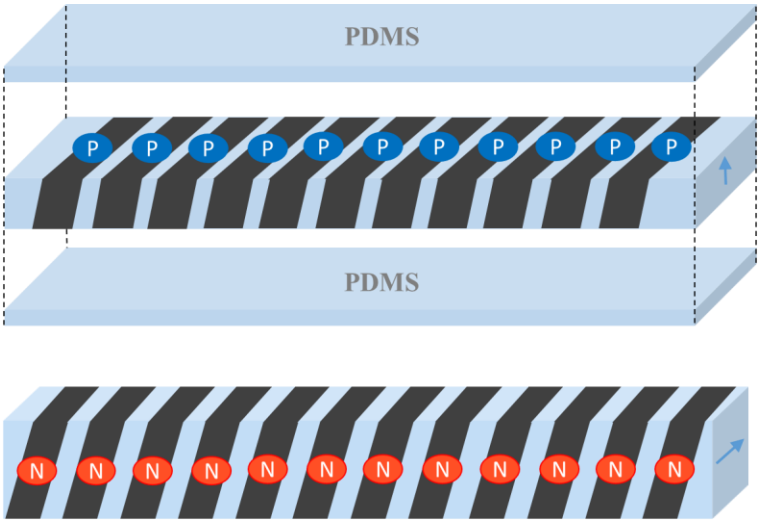

Fig. 6.6. Schematic illustration of flexible TE generator based on CNTY

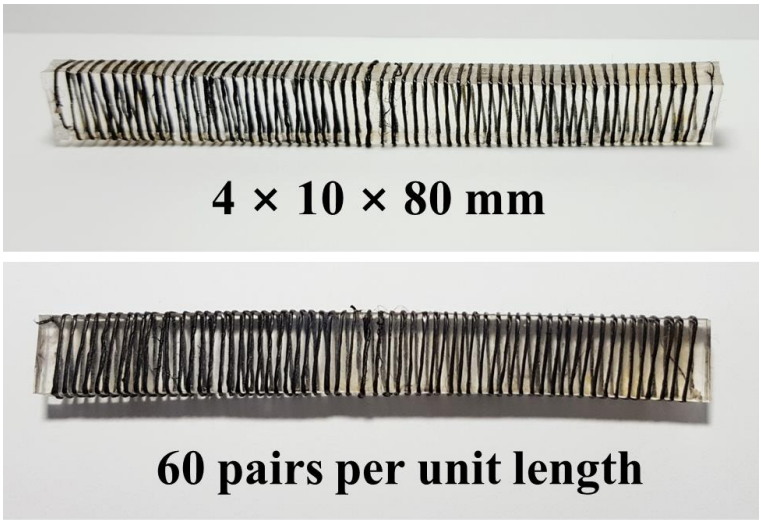

Fig. 6.7. Photograph of flexible TE generator with 60 PN pairs

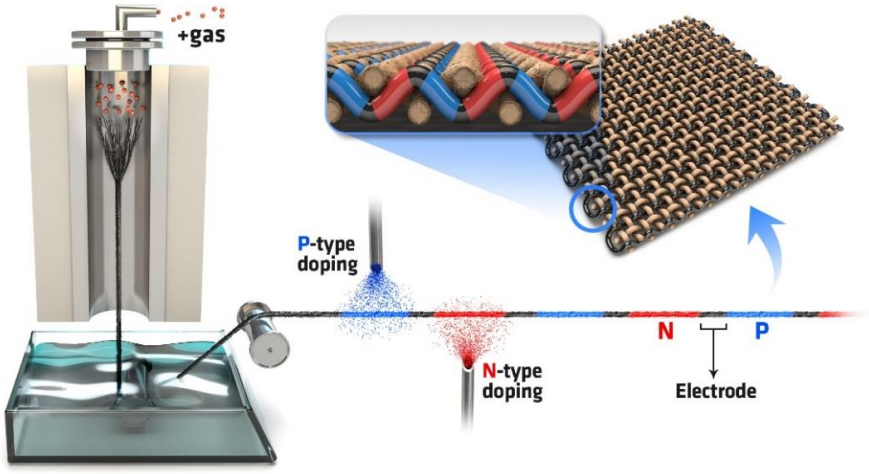

Fig. 6.8. Schematic illustration of whole fabrication process of the wearable TEG based on CNTY

6.3.2 Performance of all-carbon nanotube yarn TE generator

The TE generator composed of 60 PN pairs made by CNTY with 1.7 m in length was characterized using a hand-made instrument which can accurately control the temperature gradient by four commercial peltier modules (Fig. 6.9). As shown in Fig. 6.10b and c, the TEG with 60 PN pairs shows output voltage density of 0.15 and 1.2 V/g and maximum power density of 10.85 (0.42 $\mu W/cm^2$) and 697 $\mu W/g$ (26.8 $\mu W/cm^2$) at temperature differences (ΔT) of 5 and 40 K, respectively.

This excellent TE performance is mainly due to the high electrical conductivity of CNTY and minimized circuit resistance by excluding additional metal deposition steps (Fig. 6.11). In addition, we can easily enhance the generation power by increasing the CNTY length and the number of PN pairs in series. At $\Delta T = 5$ K, as the number of PN pairs increases from 60 to 240, the maximum power density of the TE generator increases from 1.3 to 4.2 μW (Fig. 6.12). The circuit resistance also linearly increases with an increasing number of PN pairs, while the average resistance per PN pair is nearly constant (Fig. 6.13). These results demonstrate that we can enhance the generation power of these modules by both minimizing the circuit resistance and expanding the number of PN pairs in series.

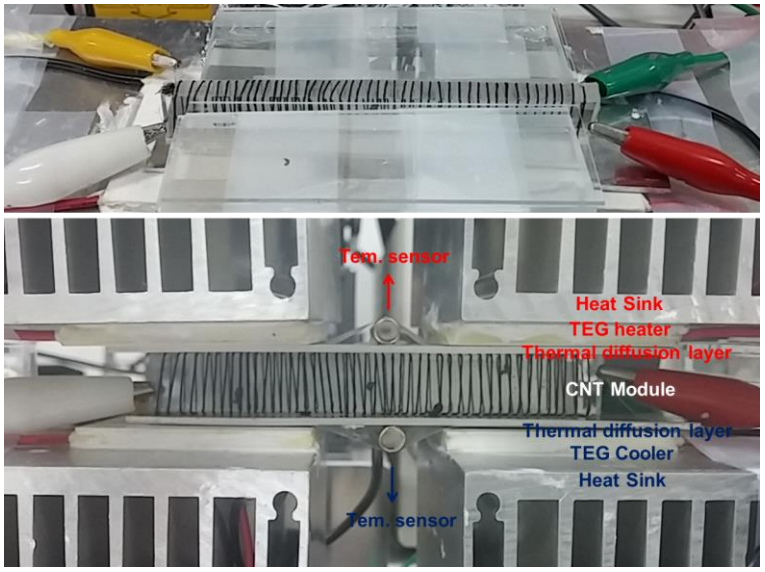

Fig. 6.9. Photograph of power measurement system

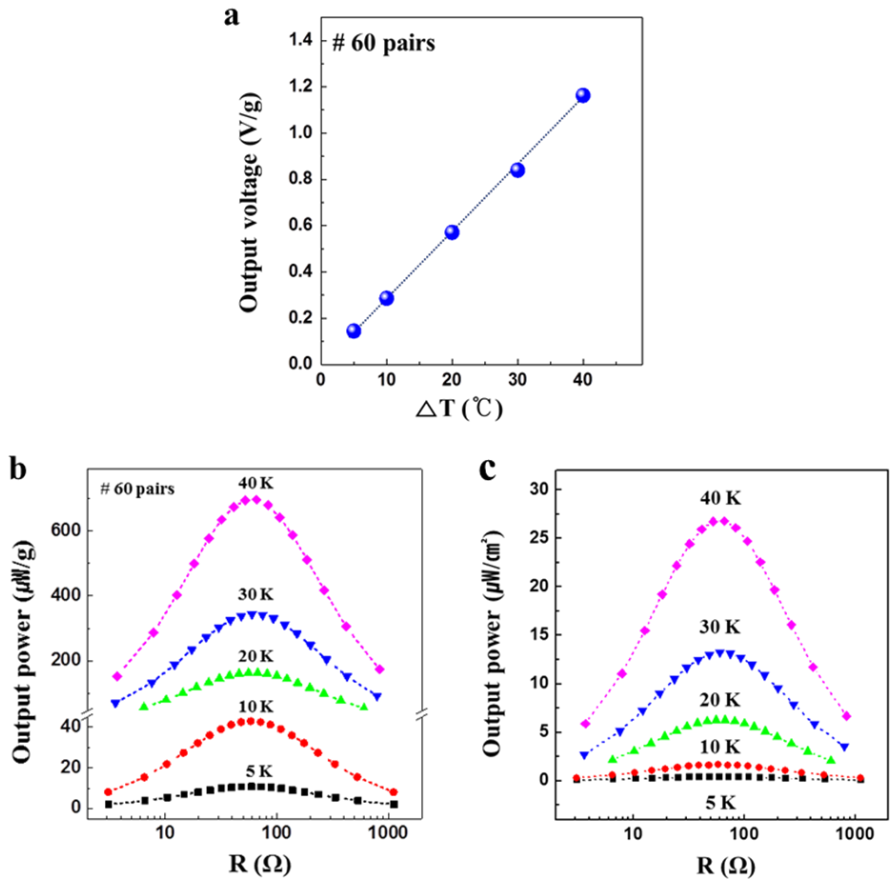

Fig. 6.10. (a) Output voltage density of flexible TE generator with 60 PN pairs as a function of temperature difference (b, c) Output power density of flexible TE generator with 60 PN pairs as a function of load resistance

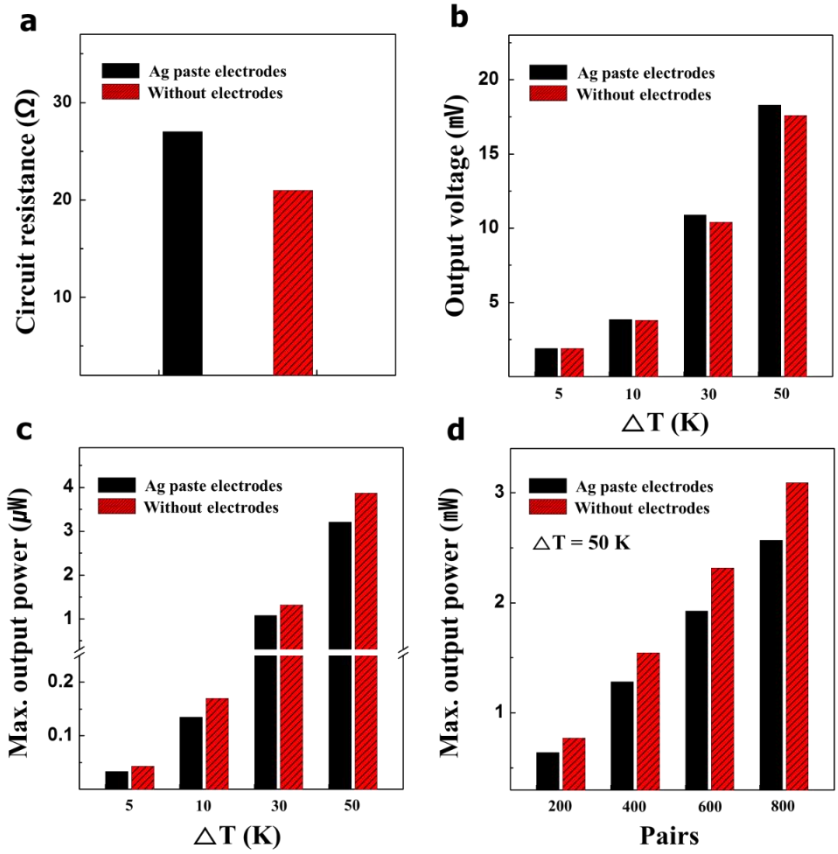

Fig. 6.11. Circuit resistance, output voltage, and output power of the TEG composed of 5 PN with and without metal electrodes.

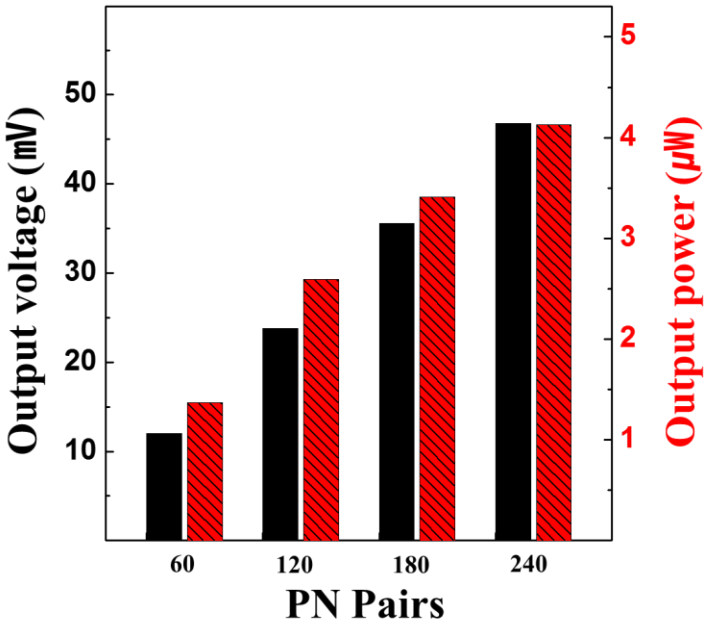

Fig. 6.12. Output voltage and power of flexible TE generator with different numbers of PN pairs at $\Delta T = 5$ K

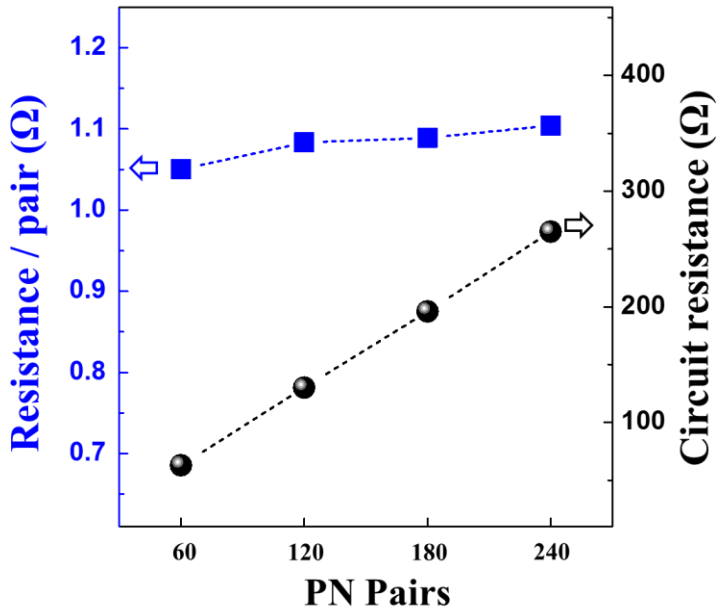

Fig. 6.13. Average resistance per PN pair and circuit resistance of flexible TE generator with different numbers of PN pairs at $\Delta T = 5$ K

For practical applications, flexible TE generator with 240 PN pairs was prepared, featuring high flexibility and mechanical stability (Fig. 6.14a). It can generate output voltage of approximately 54 mV when applied to the human arm at room temperature (Fig. 6.14b). Although the voltage of flexible TE generator generated from human heat is insufficient, we can successfully power a red LED using an energy harvesting circuit at ΔT = 50 K (Fig. 6.15), demonstrating CNTY's great potential as flexible power conversion devices. In addition to the prototype flexible TE generator above, we simply fabricated wearable TEGs woven into two types of fabrics to generate energy from body heat (Fig. 6.16).

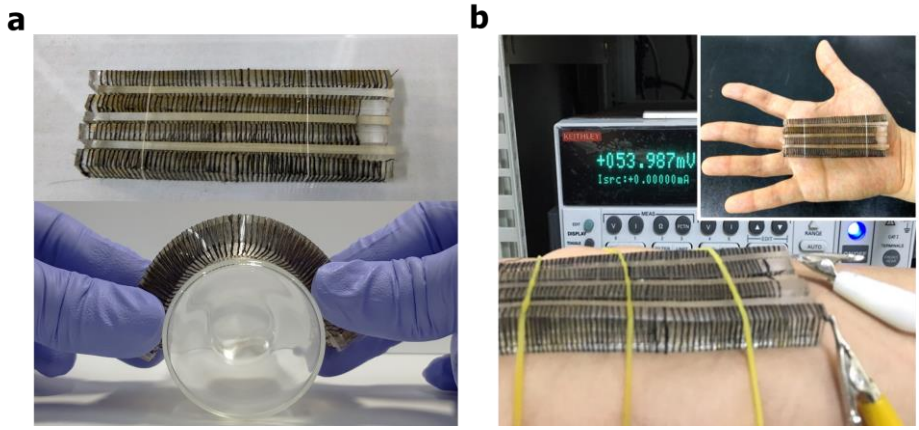

Fig. 6.14. (a) Photographs showing the flexible TE generator (**b)** Output voltage of flexible TE generator obtained from the temperature difference between body heat and atmosphere

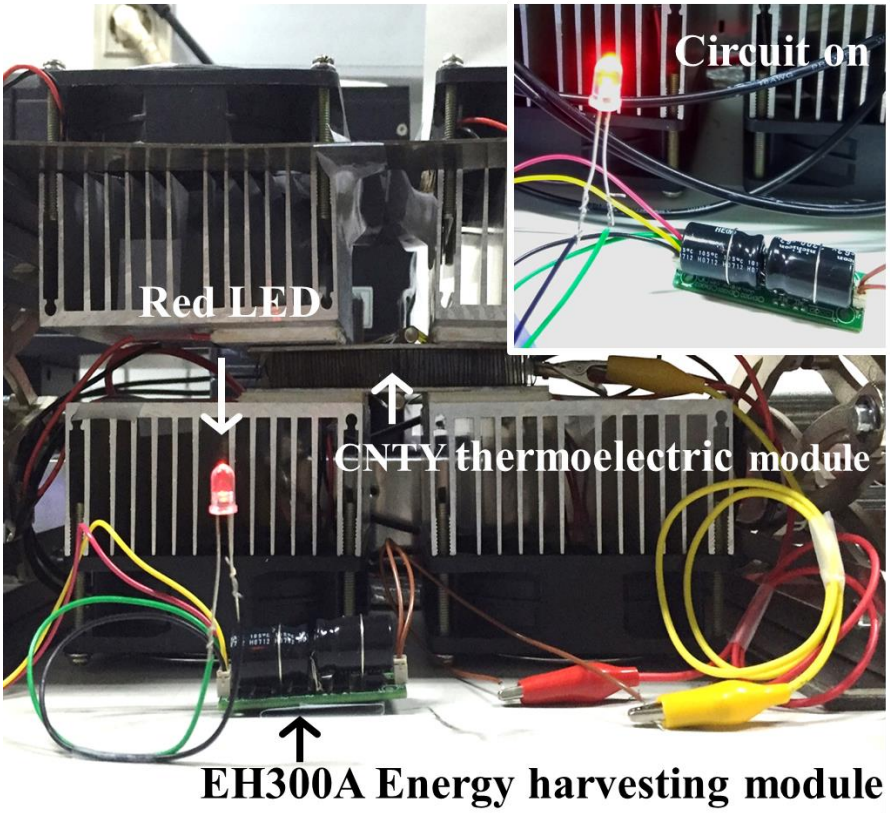

Fig. 6.15. Photograph showing a red LED powered using flexible TE generator at $\Delta T = 50$ K

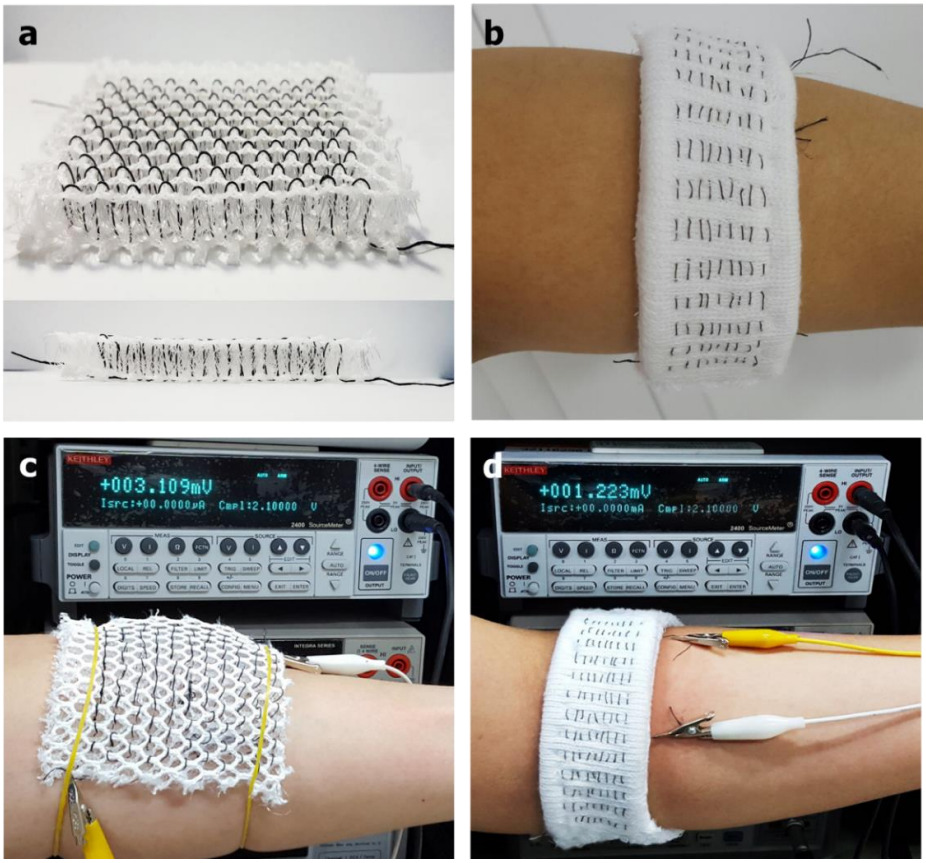

Fig. 6.16. Various types of wearable TE generators. (a,b) flexible TE generator with 120 PN pairs woven into two types of fabrics (c,d) Output voltages obtained from the temperature difference between body heat and atmosphere

6.4 Conclusions

In conclusion, I have for the first time demonstrated the novel flexible TE generator based on CNTY with excellent TE performance. CNTY was alternatively doped into n- and p-types, and the CNTY between doped regions was used as electrodes to minimize the circuit resistance. The flexible TE generator fabricated with 60 PN pairs shows maximum power density of 10.85 (0.42 $\mu W/cm^2$) and 697 $\mu W/g$ (26.8 $\mu W/cm^2$) at $\Delta T = 5$ and 40 K, respectively, which are the highest values among reported flexible TE generator. Furthermore, the flexible TE generator with 240 PN pairs can successfully power a red LED at $\Delta T = 50$ K. Our results provide a new direction for the preparation of flexible/or wearable power conversion devices.

6.5 References

1. Zebarjadi M*, et al.* Perspectives on thermoelectrics: from fundamentals to device applications. *Energy & Environ. Sci.* **5**, 5147-5162 (2012).
2. Avery AD*, et al.* Tailored semiconducting carbon nanotube networks with enhanced thermoelectric properties. *Nature Energy* **1**, 16033 (2016).
3. Bubnova O*, et al.* Optimization of the thermoelectric figure of merit in the conducting polymer poly(3,4-ethylenedioxythiophene). *Nat. Mater.* **10**, 429-433 (2011).
4. Nonoguchi Y*, et al.* Systematic Conversion of Single Walled Carbon Nanotubes into n-type Thermoelectric Materials by Molecular Dopants. *Sci. Rep.* **3**, 3344 (2013).
5. See KC*, et al.* Water-processable polymer-nanocrystal hybrids for thermoelectrics. *Nano Lett.* **10**, 4664-4667 (2010).
6. Zhou WB*, et al.* Ultrahigh-Power-Factor Carbon Nanotubes and an Ingenious Strategy for Thermoelectric Performance Evaluation. *Small* **12**, 3407-3415 (2016).
7. Rowe D*, et al.* Design theory of thermoelectric modules for electrical power generation. *IEE Proceedings-Science,*

Measurement and Technology **143**, 351-356 (1996).

8. He W*, et al.* Recent development and application of thermoelectric generator and cooler. *Applied Energy* **143**, 1-25 (2015).
9. Shinohara Y. The State of the Art on Thermoelectric Devices in Japan. *Materials Today: Proceedings* **2**, 877-885 (2015).
10. Bahk J-H*, et al.* Flexible thermoelectric materials and device optimization for wearable energy harvesting. *J. Mater. Chem. C* **3**, 10362-10374 (2015).
11. Jung Y*, et al.* Effect of polymer infiltration on structure and properties of carbon nanotube yarns. *Carbon* **88**, 60-69 (2015).

PART IV. Conclusion and outlook

One distinct advantage of TE generator is its flexibility, which makes it very effective to scavenge the low-grade waste heat to supply the electricity for small devices such as wearable electronics, wireless communication units and sensors. Nevertheless, this technology is still at the primitive stage. In recent years, as the new potential market for self-powered wearable mobile electronics is booming, researches on flexible TEG have drawn more attentions. Soft materials such as organics, hybrid composites, and paste-type materials are preferred to rigid inorganics. However, most of their performance could not satisfy the needs, yet.

Aim of this research is to design and fabrication of high performance flexible TE generators based on nano-carbons. To improve the TE performance of nano-carbons, the alignment of CNTs for high carrier mobility was manipulated. As intrinsic low thermopower of nano-carbons is a critical obstacle for TE applications, therefore, hybridization of nano-cabons and inorganic materials with high thermopower is one of the facile strategies. Via systematic study, simultaneous enhancement of both electrical conductivity and thermopower by carrier energy filtering at hybrid interfaces was demonstrated. Furthermore, tactical approaches with competitive TE materials are required for flexible TE generator to use in real life. Novel module designs based on all-CNT film and yarn without metal electrode and in excellent power density were

developed. Its maximum power density is the highest values among reported flexible TE generator based on organic TE materials. Despite the necessity of a boost converter to achieve sufficiently high voltages of 1–3 V, generated power is sufficient to power a red LED. This could be improved if a larger size of TE generator is used because both the voltage and power output are proportional to the module size.

In conclusion, this study has significant meaning in engineering research, because not only high performance nano-carbon based TE materials and modules was rationally designed, but also commercialization potential was realized by successfully fabricating prototype module. Furthermore, carrier mobility engineering strategies employed in this research can be a good guideline for researchers aiming to achieve high performance flexible TE generator. However, high thermal stress and precise doping techniques still remain as further works for use in real life. Thermal stability and optimized dimension of module are also important questions that need answering.

Abstract in Korean

본 연구는 나노 카본 재료를 기반으로 한 유연 열전 소자의 설계를 목적으로 수행되었다. 열전 재료는 온도 차이를 전기 에너지의 형태로 변환할 수 있는 재료로서, 폐열을 재활용하여 에너지를 생산해 낼 수 있는 차세대 에너지 변환 소자로 큰 기대를 받아 왔다. 지난 수십 년 동안 열전 재료의 변환 효율을 높이고자 하는 많은 연구들이 수행되어 왔고, 현재 반도체 재료를 기반으로 한 열전 소자들이 자동차, 우주선 등 다양한 영역에 상용화 되어 사용되고 있다. 그런데 최근에는 전자기기들이 첨단화, 소형화 되면서, 이에 맞추어 열전 소자가 본연의 에너지 변환 역할 뿐만 아니라 새로운 기능을 필요로 하게 되었다. 그 중 가장 주목받고 있는 분야가 바로 웨어러블 스마트 디바이스들에 지속적인 에너지를 공급할 수 있는 유연 열전 소자의 개발이며, 이를

달성하기 위해 다양한 재료들을 활용한 많은 연구들이 진행되고 있다.

높은 열전 성능을 얻을 수 있는 좁은 밴드 갭을 가진 무기 반도체 재료들, 특히 비스무스-텔러륨-안티몬-셀레늄 (Bi-Te-Sb-Se) 고용체 들은 우선적으로 널리 연구되었다. 그러나 이들의 우수한 열전 성능에도 불구하고, 여전히 반도체 재료의 깨지기 쉬운 특성에서 기인한 소자의 유연성 부족과 화학적 불안정성, 대면적 생산 공정의 어려움 등 상용화를 위해 해결해야할 문제점들이 아직 많이 남아있다. 유연 열전 재료의 다른 대안으로, 전도성 고분자 및 이들을 포함한 복합재료 등 다양한 유기 재료들이 고 유연성, 가벼운 무게, 가격 경쟁력, 생산 용이성 등 장점을 바탕으로 최근 많은 관심을 받고 있다. 하지만 대부분의 유기재료들은 아직 반도체 재료만큼의 충분한 성능을 보여주지 못하고 있을뿐더러, 성능이 개선되더라도 수분 등에 민감하여 상용화에 제한적인 실정이다.

따라서, 유연 열전 소자에 사용되기 위한 열전 재료는 성능, 유연성, 기계적, 화학적 안정성, 생산성 등의 다양한 요소들을 종합적으로 고려하여 선정되어야 한다. 또한, 효율적인 소자를 만들기 위해 N, P 타입의 재료가 모두 필요하고, 높은 열 효율을 얻을 수 있는 효율적인 소자 형태의 설계 및 제조 공정도 필수적으로 함께 고려되어야 한다.

우수한 기계적, 화학적, 전기적 물성을 바탕으로 한 나노 카본 재료들은 이러한 요구조건을 충족시킬 수 있는 유망한 열전 재료로서 연구되어 왔지만, 복합재료의 필러로 사용되어 전기 전도도를 보완하기 위한 목적으로 제한적으로 사용되어 왔을 뿐 열전 성능 자체를 획기적으로 높이기 위한 체계적인 연구는 거의 이루어 지지 못하고 있다. 그 이유는 열전 성능을 결정 짓는 전기전도도와 지벡 계수가 서로 반비례하는 관계에 놓여있기 때문에, 도핑 등을 통해 전기 전도도를 향상시키더라도 지벡 계수가

감소하여 효과적인 열전 성능의 개선이 이루어지지 않기 때문이다. 이러한 근본적인 문제를 해결하고 나노 카본 재료의 열전 성능을 획기적으로 향상시키기 위해서는, 에너지를 수송할 수 있는 입자의 농도가 아니라 이동도를 조절하는 것이 효과적인 방법이 될 수 있음을 전기전도도와 지벡 계수의 이론적 관계로부터 도출하였다. 이를 바탕으로 본 연구에서는, 나노 카본 재료의 근본적인 열전 성능 향상을 위해 이동도의 관점에서 어떤 재료적인 설계가 필요한지를 체계적으로 연구하였다.

챕터 1 에서는 열전 소자의 전반적인 이해와 함께 웨어러블 전자기기에 사용될 수 있는 유연 열전 소자의 필요성에 대해 소개될 것이다. 열전 현상을 열적, 전기적 관점에서 이해하기 위해 필요한 이론적 고찰 역시 포함하였다. 핵심적으로는. 유연 열전 소자 연구들의 동향 파악과 함께 이들이 지닌 의의와 한계에

대해서 논의하고, 이를 토대로 본 연구가 가지는 목표와 전략 그리고 연구 범위를 밝혔다.

챕터 2 에서는 본 연구에서 열전 재료와 소자의 성능을 측정한 장비에 대해서 소개하였다. 여기에는 기성품과는 다른 고안된 장비의 설계 차이점과 이러한 시스템이 유연 열전 소자 연구에 적합한 이유들도 포함하였다.

챕터 3 에서는 제조 방법에 따라 다른 배향도를 가진 카본나노튜브 필름들과 섬유를 제조하고 배향도 차이가 열전 성능에 미치는 영향에 대해 고찰하였다. 고도로 배향된 카본나노튜브 섬유의 경우 높은 이동도를 바탕으로 매우 우수한 전기 전도도를 가지면서도 상대적으로 높은 지벡 계수를 가짐으로써 기존의 반비례 관계를 벗어나 획기적인 열전 성능 향상이 가능함을 확인하였다.

챕터 4, 5 에서는 나노 카본 재료와 무기 재료의 하이브리드를 통해 전기전도도와 지벡 계수를 동시에 높이고자 하는 연구들에 대해

논의하였다. 단순한 하이브리드를 통해서는 전기전도도와 지벡 계수 사이의 의존적 한계를 극복할 수 없지만, 나노 카본의 일함수 조절을 통해 효율적인 에너지 구조를 갖는 2 원 및 3 원계 나노 카본 / 무기 재료 복합재료들을 설계하였고, 이들 내부의 이종 계면에서 일어나는 에너지 필터링에 의해 열전 성능이 향상될 수 있음을 확인하였다. 에너지 필터링이 일어나면 복합 재료 계면에서의 이동도는 소폭 감소하지만 입자의 에너지 수송 효율이 증가되어 향상된 열전 성능을 얻을 수 있다. 이러한 재료적 설계 역시 이동도의 효과적인 조절이라는 측면에서 우수한 열전 성능을 확보하기 위한 좋은 전략이 될 수 있음을 보였다.

챕터 6 에서는 재료적 연구뿐만 아니라, 나노 카본 재료를 기반으로 하여 우수한 성능을 가진 새로운 형태의 유연 열전 소자를 제안하였다. 재료 자체의 우수한 열전 성능도 중요하지만, 실제 상용화를 위해서는 소자 제작의 용이성 및 제작된 소자의 우수한

성능 또한 매우 중요하다. 소자의 설계 측면에서도 전류의 이동도가 높을수록 열 손실이 적고 생산 전력이 높아질 수 있으므로, 이에 착안하여 기존 소자에 사용되던 금속 전극 없이도 효율적인 열전 발전이 가능한 새로운 형태의 열전 발전 소자를 개발하고, 실제 체온으로부터 전력 생산이 가능함을 보였다.

종합해 보면, 본 연구에서 나노 카본 재료를 기반으로 하여 고성능의 유연 열전 재료와 소자를 설계하는데 그치지 않고 실제 제작하여 상용화 가능성까지 확인하였다는 점에서 공학적으로 큰 의의를 갖는다. 또한 입자의 이동도 조절이라는 전략을 통해 유연 열전 재료의 성능을 획기적으로 향상시킨 연구 결과들은 동일한 목표를 가진 연구자들에게 좋은 학문적 가이드라인이 될 것이다.

주요어: 유연 열전 소자, 재료 설계, 카본 나노튜브, 그래핀, 텔레늄 나노선, 복합 재료, 에너지 필터링

학번: 2013-30188

List of Publications

1. J. Y. Oh, Y. Jung, Y. S. Cho, **J. Choi**, J. H. Youk, N. Fechler, S. J. Yang, C. R. Park, "Metal-Phenolic Carbon Nanocomposites for Robust and Flexible Energy Storage Devices", *ChemSusChem,* 2017.

2. **J. Choi**, J. Y. Lee, S-S. Lee, C. R. Park, and H. Kim, "High-Performance Thermoelectric Paper Based on Double Carrier-Filtering Processes at Nanowire Heterojunctions", *Advanced Energy Materials*, 2016.

3. H. J. Lee, G. Anoop, H. J. Lee, C. Kim, J-W. Park, **J. Choi**, H. Kim, Y. J. Kim, E. J. Lee, S-G. Lee, Y-M. Kim, J-H. Lee and J. Y. Jo, "Enhanced thermoelectric performance of PEDOT:PSS/PANI-CSA polymer multilayer structures", *Energy & Environmental Science*, 2016.

4. H. Jang, H. Yoon, Y. Ko, **J. Choi**, S-S. Lee, I. Jeon, J-H. Kim, and H. Kim, "Enhanced performance in capacitive force sensors using carbon nanotube/polydimethylsiloxane nanocomposites with high dielectric properties", *Nanoscale*, 2016.

5. J. H. Kang, T. Kim, **J. Choi**, J. Park, Y. S. Kim, M. S. Chang, H. Jung, K. Park, S. J. Yang, and C. R. Park, "The Hidden Second Oxidation Step of Hummers Method", *Chemistry of Materials*, 2015.

6. **J. Choi**, K. Lee, C. R. Park, and H. Kim, "Enhanced thermopower in flexible tellurium nanowire films doped using single-walled carbon nanotubes with a rationally designed work function", *Carbon*, 2015.

7. N. D. Kha Tu, **J. Choi**, C. R. Park, H. Kim, “Remarkable Conversion Between n- and p Type Reduced Graphene Oxide on Varying the Thermal Annealing Temperature”, *Chemistry of Materials*, 2015.

8. **J. Choi**, J. Y. Lee, H. Lee, C. R. Park, and H. Kim, “Enhanced thermoelectric properties of the flexible tellurium nanowire film hybridized with single-walled carbon nanotube”, *Synthetic Metals*, 2014.

9. **J. Choi**, K. Tu, S-S. Lee, H. Lee, J-S. Kim, and H. Kim, “Controlled oxidation level of reduced graphene oxides and its effect on thermoelectric properties”, *Macromolecular Research*, 2014.

10. **J. Choi**, Y. Jung, S. J. Yang, J. Y. Oh, J. Oh, K. Jo, J. G. Son, J-S. Kim, C. R. Park, and H. Kim, “High-performance flexible thermoelectric generators based on all-carbon nanotube yarn without metal electrodes”, submitted, 2017.

11. K. Jo, **J. Choi**, H. Kim, “Simultaneous Exfoliation and n-doping of MoS2 Nanosheets by Benzyl Viologen via a Solution Process”, submitted, 2017.

12. J. Oh, H. Yoo, **J. Choi**, J. Y. Kim, D. S. Lee, M. J. Kim, J. Lee, W. N. Kim, J. Grossman, J. H. Park, S. Lee, H. Kim, J. G. Son, “Significantly reduced thermal conductivity and enhanced thermoelectric properties of single- and bi-layer graphene nanomeshes with sub 10 nm neck width”, submitted, 2017.

List of Patents

1. **J. Choi**, Y. S. Jung, H. Kim, C. R. Park, “Flexible thermoelement comprising carbon nanotube strand, preparation method thereof”, KR 2016-0149400 (2016)
2. H. Kim, J. Y. Lee, **J. Choi**, J.G. Son, “Highly flexible thermoelectric material comprising organic-inorganic hybrid composite and thermoelectirc device comprising the same”, KR 10-2013-0107189 (2015)